A THESIS
FOR THE DEGREE OF MASTER OF SCIENCE

Structural and functional delineation of two glutathione S-Transferases from Disk abalone (*Haliotis discus discus)*

AND

Two phospholipid scramblase 1–related proteins from Red lip mullet (*Liza haematocheila); deciphering their* transcriptional responses against immune stimulants

Wijamunige Gayashani Sandamalika

Department of Marine Life Sciences
GRADUATE SCHOOL
JEJU NATIONAL UNIVERSITY
REPUBLIC OF KOREA

February 2019

제주대학교 중앙도서관
JEJU NATIONAL UNIVERSITY LIBRARY

Structural and functional delineation of two glutathione S-Transferases from Disk abalone (*Haliotis discus discus*)

AND

Two phospholipid scramblase 1–related proteins from Red lip mullet (*Liza haematocheila*); deciphering their transcriptional responses against immune stimulants

Wijamunige Gayashani Sandamalika
(Supervised by Professor Jehee Lee)

A thesis submitted in partial fulfillment of the requirement for the degree of

MASTER OF SCIENCE

February 2019

The thesis has been examined and approved by

……………………………………………………………………………………

Thesis director, **Myoung-Jin Kim**, (PhD) - Research professor,
Fish Vaccine research Center, Jeju national university

…………………………………………………………………………………….

Qiang Wan, (PhD) -Research professor,
Fish Vaccine research Center, Jeju national university

………………………………………………………………………………………......

Jehee Lee, (PhD) -professor of Marine life sciences,
School of Marine Biomedical sciences, Jeju national university

2018/11/28
Date

Department of Marine Life Sciences
Graduate School
Jeju National University
Republic of Korea

Acknowledgement

Though the following dissertation is an individual work, I could never have researched the heights or explored the depths without the support, guidance and efforts lot of people.

First and foremost, I would like to express my deepest sincere gratitude to my supervisor Professor Jehee Lee, who gave me a precious opportunity to commence my post graduate studies at the Marine Molecular Genetics Lab in Jeju National University and directing me to the field of genetics. I am especially grateful to Dr. Thanthrige Thiunuwan priyathilaka for his systemic guidance and great effort he put into training me in the scientific field by improving my laboratory experiments and writings.

Beside my advisors, I would like to thank my thesis panel director Dr. Myoung-Jin Kim and Dr. Qiang Wan from Fish Vaccine Research Center, Jeju National University for being my thesis committee members. I sincerely thank all my lab members and faculty members for giving me various supports by instructing and providing laboratory facilities. And I am also thankful to my Korean and Sri Lankan friends for supporting me to fulfill my laboratory works and their kind co-operation to completion of my work.

My sincere thanks to National Fisheries Research and Development Institute for providing research grant to accomplish our studies.

I would like to express my eternal appreciation towards all my family members who always been with me and giving moral support to achieve my target.

Contents

Summary

Disk abalone (*Haliotis discus discus*) and redlip mullet (*Liza haematocheila*) are two species which are very important in the aquaculture industry, especially in South Korea. However, both these key species are highly vulnerable to the spreading of infectious diseases caused by bacteria, viruses and parasites. Relatively high stock densities and poor environmental conditions in the culture farms resulted with mass mortalities ending with financial losses. Therefore, understanding the immune responses against infectious diseases in abalones and redlip mullets is essential for a sustainable development of the aquaculture industry. Therefore, in this study we have identified and studied two types of genes: Glutathione S- transferases and phospholipid scramblases from disk abalone and redlip mullet for the understanding of their characteristic features and behaviors in line with innate immune system.

Glutathione *S*-transferases (GSTs) are a superfamily of detoxification enzymes that primarily catalyze the nucleophilic addition of reduced glutathione to both endogenous and exogenous electrophiles. GSTs can convert toxic substances into less reactive and more hydrophilic products to facilitate their excretion. Currently, based on their primary and tertiary structures, substrate/inhibitor specificity and immunological cross-reactivity, cytosolic GSTs have been grouped into more than ten classes, which have been designated as classes α, β, δ, ζ, θ, μ, ρ, π, σ, τ, ϕ, ε and Ω. In this study we are dealing with GST theta (θ) and kappa (κ) revealing their molecular and transcriptional properties. Characterization of AbGST-θ revealed with 226 amino acids, 26.6 kDa of predicted molecular mass and 8.9 of theoretical isoelectric point. As illustrated in the multiple sequence alignment, eight glutathione binding sites (G-sites) and ten substrate binding sites (H-sites) were identified in the well-distinct N-terminal and C-terminal domains of AbGST-θ, respectively. AbGST-θ exhibited its

highest sequence identity with *Mizuhopecten yessoensis* (59.1%) and the phylogenetic tree clearly positioned AbGST-θ with pre-defined GST-θ molluscan homologues. The *AbGST-θ* was highly expressed in digestive tract of un-challenged abalones. Upon challenge experiment, *AbGST-θ* showed significant modulations in their transcriptional levels depending on the time and the tissue type. The biochemical properties of AbGST-θ were identified to be 37 ℃ of optimum temperature and 7.5 of optimum pH. The determined enzyme kinetic parameters of AbGST-θ showed low affinity towards 1-Chloro-2,4-dinitrobenzene (CDNB) and glutathione (GSH) as substrates. Nonetheless with Cibacron blue, IC_{50} (half maximal inhibitory concentration) was calculated to be 0.08 μM while observing 100% inhibition with 100 μM. Furthermore, AbGST-θ resulted with significant protection ability towards H_2O_2, $CdCl_2$, $CuSO_4$ and $ZnCl_2$ in the disk diffusion assay.

The predicted AbGSTκ protein consists of 227 amino acids, with a predicted molecular weight of 25.6 kDa and a theoretical isoelectric point (pI) of 7.78. *In silico* analysis reveals that *AbGSTκ* is a disulfide bond formation protein A (DsbA), consisting of a thioredoxin domain, GSH binding sites (G-sites), and a catalytic residue. In contrast, no hydrophobic ligand binding site (H-site), or signal peptides, were detected. *AbGSTκ* showed the highest sequence identity with the orthologue from pufferfish (*Takifugu obscurus*) (60.0%). In a phylogenetic tree, AbGSTκ clustered closely together with other fish GSTκs, and was evolutionarily distanced from other cytosolic GSTs. The predicted three-dimensional structure clearly demonstrates that the dimer adopts a butterfly-like shape. A tissue distribution analysis revealed that *GSTκ* was highly expressed in the digestive tract, suggesting it has detoxification ability. Depending on the tissue and time, *AbGSTκ* showed different expression patterns, and levels of expression, following challenge of the abalone with

immune stimulants. Enzyme kinetics of the purified recombinant proteins demonstrated its conjugating ability using 1-Chloro-2,4-dinitrobenzene (CDNB) and glutathione (GSH) as substrates, and suggested it has a low affinity for both substrates. The optimum temperature and pH for the rAbGSTκ GSH: CDNB conjugating activity were found to be 35°C and pH 8, respectively indicating that the abalone is well adapted to a wide range of environmental conditions. Cibacron blue (100 μM) was capable of completely inhibiting rAbGSTκ (100%) with an IC_{50} (half maximal inhibitory concentration) of 0.05 μM. A disk diffusion assay revealed that rAbGSTκ could significantly protect cells from H_2O_2, $CdCl_2$, and $ZnCl_2$.

Phospholipid scramblases (PLSCRs) are a family of transmembrane proteins known to be responsible for Ca^{2+}-mediated bidirectional phospholipid translocation in the plasma membrane. Apart from the scrambling activity of PLSCRs, recent studies revealed their diverse other roles, including antiviral defense, tumorigenesis, protein–DNA interactions, apoptosis regulation, and cell activation. Nonetheless, the biological and transcriptional functions of PLSCRs in fish have not been discovered to date. Therefore, in this study, two new members related to the PLSCR1 family were identified in the red lip mullet (*Liza haematocheila*) as *MuPLSCR1like-a* and *MuPLSCR1like-b*, and their characteristics were studied at molecular and transcriptional levels.

Sequence analysis revealed that MuPLSCR1like-a and MuPLSCR1like-b are composed of 245 and 228 amino acid residues (aa) with the predicted molecular weights of 27.82 and 25.74 kDa, respectively. A constructed phylogenetic tree showed that MuPLSCR1like-a and MuPLSCR1like-b are clustered together with other known PLSCR1 and -2 orthologues, thus pointing to the relatedness to both PLSCR1 and PLSCR2 families. Two-dimensional (2D) and 3D graphical representations illustrated

제주대학교 중앙도서관
JEJU NATIONAL UNIVERSITY LIBRARY

the well-known 12-stranded β-barrel structure of MuPLSCR1like-a and MuPLSCR1like-b with transmembrane orientation toward the phospholipid bilayer. In analysis of tissue-specific expression, the highest expression of *MuPLSCR1like-a* was observed in the intestine, whereas *MuPLSCR1like-b* was highly expressed in the brain, indicating isoform specificity. Of note, we found that the transcription of *MuPLSCR1like-a* and *MuPLSCR1like-b* was significantly upregulated when the fish were stimulated with poly(I:C), suggesting that such immune responses target viral infections. Overall, this study provides the first experimental insight into the characteristics and immune-system relevance of *PLSCR1*-related genes in red lip mullets.

List of figures

List of Tables

CHAPTER 1:

Structural and functional delineation of two glutathione

S-Transferases from Disk abalone (*Haliotis discus discus*)

1. Introduction

The marine environment is a complex and dynamic environment filled with multiple stressors including chemical, physical and biological stresses, resulting from both natural and human anthropogenic activities (MURRAY et al., 2014). Marine organisms have inherited several mechanisms and adaptations to tolerate these challenges in order to survive (Guo et al., 2015). Cellular detoxification mechanisms are one such mechanism. Generally, a cellular detoxification mechanism consists of four distinct phases which are temporally and spatially distinct. Phase zero (0) includes the uptake of xenobiotics by membrane transport proteins; phase I includes enzymatic bio-activation of the parent compounds through oxidation-reduction reactions; phase II includes enzyme(s) mediated conjugation of phase I metabolites, or parent compounds, to water-soluble moieties; and finally, phase III involves the efflux of parent compounds, or metabolites, from cells by membrane transporters (Hodgson, 2010).

Glutathione S-transferases (GSTs; EC 2.5.1.18) are enzymes that are found in many organisms including microbes, insects, plants, fish, birds and mammals, and contribute to phase II detoxification in their respective species (Hayes and Pulford, 1995). In keeping with other detoxification enzymes, GSTs protect the organism by removing harmful substances by converting them into non-reactive water-soluble substances (Hayes and Pulford, 1995). These enzymes also have non-catalytic functions, including the binding of hydrophobic non-substrate ligands, modulation of signaling processes, regulation of stress-activated cell signaling pathways, biosynthesis of leukotriene and prostaglandins, and catabolism of aromatic amino acids (Hayes et al., 2005; Hayes and Pulford, 1995).

In most animals, the GST family of enzymes has been categorized as being cytosolic,

제주대학교 중앙도서관
JEJU NATIONAL UNIVERSITY LIBRARY

mitochondrial, or MAPEG (membrane associated proteins in eicosanoid and glutathione metabolism) subfamily members (Hayes et al., 2005). Based on their amino acid sequence, structure, immunological cross reactivity, evolutionary relationship, catalytic, and substrate specificity, cytosolic GSTs are further subdivided into several classes: alpha, beta, delta, epsilon, zeta, theta, mu, nu, pi, sigma, tau, phi, rho, kappa, omega, elongation factor 1 gamma, dehydroascorbate reductase, and tetrachlorohydroquinone dehalogenase (Frova, 2006). Microsomal GST and leukotriene C_4 synthase are categorized as belonging to the MAPEG group. The GSTs from each family have short regions of high identity in common, and share a common evolutionary pathway (Li et al., 2005). GSTs generally share greater than 60% sequence identity within a class, and less than 30% among distinct classes (Li et al., 2005). Over the past years the three-dimensional structures of soluble GSTs in several classes have been reported (Board et al., 2000; Cameron et al., 1995; Ji et al., 1992; Oakley et al., 2001; Polekhina et al., 2001; Rossjohn et al., 1998).

Cytosolic GSTs can be identified as homodimers or heterodimers consisting with two distinct domains of 23–30 kDa in each monomer as :a N-terminal thioredoxin-like domain and a C-terminal alpha helical domain (Kasthuri et al., 2013). The dimer interface may have variations as hydrophobic ball-and-socket (α, μ, π, ϕ classes) or hydrophilic nature (θ, σ, β, classes). The thioredoxin-like domain is responsible for GSH binding with the presence of specific substrate, hence termed as GSH-binding sites (G-site) (Allocati, 2018). The catalytic activity of these G-sites are controlled by tyrosine (Tyr), serine (Ser), or cysteine (Cyst) residues, considered as critical mediators of glutathione conjugation (Ji et al., 1992). The C-terminal domain together with N-terminal domain are involving in the shaping of hydrophobic substrate binding sites (H-site) (Allocati, 2018). Although the G-site sequences are highly conserved

3

among the GST classes, H-sites had exhibited significant variations in their sequences, which allows the diversification of the substrate specificity (Ji et al., 1992).

GST theta (θ) class was first identified and characterized using 1-menaphthyl sulphate and 1,2-epoxy-3-(ρ-nitrophenoxy) propane as substrates (Motoyama and Dauterman, 1977). However, GST-θ is considered as the most ancient group which consists with two different types: GST-θ1 and GST-θ2 sharing 55% sequence identity in their protein structure. According to the studies of rat, although GSTs are expressing an organ-specific pattern in their tissue distribution, most of the examined GST-θ were observed in liver, lung, blood, kidney, spleen, brain, testis, ovary, heart and small intestine (Hayes et al., 2005). In human studies, GST-θ1 and GST-θ2 have been identified, cloned and provided evidences for their ability to detoxify carcinogenic chemicals and chemotherapeutic agents (Landi, 2000). Considering about marine invertebrates, GST-θ has been characterized only from freshwater prawn (*Macrobrachium rosenbergii*) (Arockiaraj et al., 2014) manila clam (*Ruditapes philippinarum*) (Saranya Revathy et al., 2012) and sea cucumber (*Apostichopus japonicus*) (Shao et al., 2017), up to date. Out of them, only the studies of GST-θ from manila clam and sea cucumber are consisted with the recombinant protein expression and the functional studies. Moreover, apart from the xenobiotic detoxification of GSTs, these studies have further revealed the innate immune responses of GST-θ class by inducing the organisms with viral and bacterial pathogens.

However, among the cytosolic GSTs, kappa is the least studied (Harris et al., 1991). The GST kappa (GSTκ) proteins are an ancient protein family, with orthologues in bacteria and eukaryotes. The protein was identified and isolated for the first time from the mitochondrial matrix of rat liver (Harris et al., 1991). Recently, the structure of a kappa class GST from rat mitochondrion (rGSTκ) in complex with glutathione (GSH)

4

was reported, which shows a folding topology different from that of the other GST classes (Ladner et al., 2004). These enzymes have recently been demonstrated to localize in peroxisomes (Morel et al., 2004), and are proposed to be present in the endoplasmic reticulum in adipose tissue (Liu et al., 2008; Zhou et al., 2010). The kappa class GSTs possess peroxidase activity, which permits the detoxification of lipid peroxides and reactive oxygen species (ROS) generated from lipid metabolism and the respiratory chain (Bonekamp et al., 2009). GST kappa possesses a disulfide bond formation protein A (DsbA) domain, consisting of a thioredoxin domain and a protein disulfide isomerase from *Escherichia coli*, thus it is considered as orthologous to bacteria (Martin, 1995). The expression, purification, and crystal structure of human kappa class GST (hGSTκ) has been determined by the multiple-isomorphous replacement method (Li et al., 2005), and suggests that within the GST superfamily, the kappa class of GST is more closely related to the θ class of enzymes. Although many GST isoforms from several aquatic organisms have been previously studied, reports on GSTκ are very rarely available. GSTκ has been studied in *Macrobrachium rosenbergii*, and appears to possess a detoxification capability that can overcome various abiotic and biotic oxidative stressors (Chaurasia et al., 2016). In zebrafish, an overall study of GST superfamily has been conducted and showed the structural and functional characteristic features of GSTκ (Glisic et al., 2015). The effect of a cyanobacterial crude extract on the transcription of *GSTκ* has been studied in goldfish (*Carassius auratus*), with the result that there was differential expression in various tissues (Hao et al., 2008). However, to date there have been no detailed reports of GSTκ from mollusks.

Abalones are slow growing marine gastropods that live in the coastal intertidal zone, and are a key element in the marine ecosystem, as well as in the fisheries and

aquaculture industry. Because of the dynamic environmental and pathogenic conditions in the intertidal zone that create numerous environmental stresses, and the fact that abalone population is highly sensitive to environmental variations, this has led to a decrease in abalone survival (Elvitigala et al., 2015). In parallel, in the abalone farming industry, mass mortality has occurred because of poor water quality, critical climate changes, and unexpected disease outbreaks (Cook, 2014). In the present study, using a variety of molecular bioinformatics tools, we have characterized GST theta (*AbGSTθ*) and kappa (*AbGSTκ*) from the disk abalone (*Haliotis discus discus*), which is widely cultured in South Korea. Functional studies were carried out with the recombinant proteins to determine their enzymatic and antioxidant properties, and an analysis of the stress mediated response were also conducted. In addition, the transcriptional levels of *AbGSTs* were determined under normal physiological conditions and immunologically challenged conditions in order to evaluate the involvement of AbGSTθ and AbGSTκ in the abalone's immunity.

2. Materials and Methods

2.1 Experimental animals and tissue collection

Healthy disk abalones (*Haliotis discus discus*), with an average body weight of 50 ± 5 g, were obtained from a commercial abalone farm in Jeju Island, Republic of Korea. The abalones were acclimatized to the laboratory conditions by maintenance in 60 L flat-bottomed fiberglass tanks with aerated sea water at temperature of $20 \pm 1°C$ and 34 ± 0.6 psµ of salinity for a one-week period and fed with marine seaweed (*Undaria pinnatifida*).

2.2 Chemicals & reagents

SYBR Premix *Ex Taq* ™ was purchased from TaKaRa, Japan. Tri Reagent™ (Sigma - Aldrich, USA) was used for total RNA extraction. For the immune challenge experiments, polyinosinic: polycytidylic acid (poly (I: C)) (Sigma -Aldrich, USA) was used as an immune stimulant. Reduced glutathione (GSH), 1-chloro-2,4-dinitrobenzene (CDNB), 1,2-dichloro-4-nitrobenzene (DCNB), ethacrynic acid (ECA), 4-nitrobenzyl chloride (4-NBC) and 4-nitrophenethyl bromide (4-NPB) were purchased from Sigma-Aldrich. Cibacron blue (CB) and isopropyl-β-D-thiogalactopyranoside (IPTG) were purchased from Polyscience Inc. and Promega respectively.

2.3 Identification & sequence analysis of GSTs from Disk Abalone

The full length coding sequence of disk abalone glutathione S-transferase theta and kappa was identified from the abalone transcriptome database (Elvitigala et al., 2015), established in our laboratory, using a Roche 454 Genome sequencer FLX system (GS-FLX™) (Droege and Hill, 2008). Briefly, total RNA was extracted from healthy disk abalones with Tri Reagent™ (Sigma- Aldrich, Missouri, USA) and processed with a FastTrack 2.0 mRNA isolation kit (Invitrogen, USA). A Creator™ SMART™ cDNA

library construction kit (Clontech, USA) and a Trimmer cDNA normalization kit (Evrogen, Russia), were used to synthesize first strand cDNA and normalize it, respectively. The Basic Local Alignment Search Tool (BLAST) at the National Center for Biotechnology Information (NCBI) (http://www.ncbi.nlm.nih.gov/BLAST) was used to confirm the identity of the *AbGSTθ* and *AbGSTκ* genes. The open reading frames (ORF) and the amino acid sequences of the deduced proteins were determined using ORF finder (https://www.ncbi.nlm.nih.gov/orffinder). ExPASy prosite (Sigrist et al., 2013) and SignalP (Petersen et al., 2011) programs were used to scan for conserved domains and signal peptides within AbGSTθ and AbGSTκ, respectively. Characteristic signature domains were identified using the SMART online server (http://smartembl-heidelberg.de), and the NCBI-conserved domain database (CDD) (https://www.ncbi.nlm.nih.gov/Structure/cdd/cdd.shtml). The phylogenetic trees were constructed using the neighbor-joining method using MEGA 6 software (Tamura et al., 2011). The multiple sequence alignments were performed using Clustal omega (http://www.ebi.ac.uk/Tools/msa/clustalo) (Sievers et al., 2014) and Color align conservation (http://www.bioinformatics.org/sms2/color_align_cons.html) (Perry, 2002) web based software. The three-dimensional (3D) models of GSTθ and GSTκ were generated using the SWISS-MODEL (https://swissmodel.expasy.org) protein structure modelling server (Schwede et al., 2003), and then visualized using the PyMOL v1.5 software (DeLano, 2002).

2.4 Tissue isolation and immune challenge experiment

Tissue samples derived from the gills, mantle, digestive tract, muscles, and hepatopancreas were carefully isolated from four healthy abalones to analyze the tissue specific expression of *AbGSTs*. Hemolymph was collected from the pericardial cavity of each abalone using a sterile syringe and immediately centrifuged at $3000 \times g$ for 10 min at 4°C in order to isolate the hemocytes. All the tissue samples were snap-frozen and stored at −80°C until RNA extraction.

Healthy disk abalones were divided into four groups and maintained separately to determine their immune response to one pathogenic bacterial strain and two immune stimulants. For the bacterial challenge experiment, one group of abalones was injected with the gram-negative bacterial strain (*Vibrio parahaemolyticus*). To do this, live *V. parahaemolyticus* (100 µL, 1×10^4 CFU/µL) were suspended in saline (0.9% NaCl) and injected intramuscularly into each abalone. For the immune stimulation experiment, one group of abalone was injected with 100 µL of the double stranded RNA viral mimic poly I:C (5 µg/µL), while in one other group each abalone was injected intramuscularly with 100 µL of LPS (5 µg/µL, from *Escherichia coli* 055: B5; Sigma, St. Louis, MO, USA) in saline. The remaining group of abalones was injected with 100 µL saline and were treated as the control group. After the different immune challenges, the gill tissues and hemocytes were isolated at 3, 6, 12, 24, 48, 72, and 120 h post-injection (p.i.). All the collected samples were snap-frozen and stored at -80°C until RNA extraction.

2.5 RNA extraction and first-strand cDNA synthesis

Total RNA was extracted from the above-mentioned abalone tissues using TRIzol Reagent (Sigma) following the manufacture's protocol. The concentration of the extracted RNA was determined using its absorbance at 260 nm in a spectrophotometer

(BioRad, USA). Thereafter an aliquot (2.5 µg) of the total RNA was reverse transcribed using a Prime Script ^{TM} first-strand cDNA synthesis kit (TaKaRa, Japan) and stored at −20°C after being diluted 40-fold.

2.6 Transcriptional analysis –Quantitative real-time PCR

The transcriptional analysis of *AbGSTθ* and *AbGSTκ* in healthy and immune challenged disk abalones were performed by quantitative real time PCR (qPCR) using a Real Time System TP800 Thermal Cycler Dice ^{TM} (TaKaRa, Japan) with SYBR Green as the fluorescent agent. The gene specific primers were designed according to the MIQE guidelines (Sinton et al., 1999) (Table 1), and were used to amplify the *AbGSTθ* and *AbGSTκ* genes. For standardization, the abalone ribosomal protein L5 (GenBank accession: EF103443) was used as an internal reference with the appropriate primers (Table 1). The qPCR reaction mixture contained 3 µL of diluted cDNA from the respective tissue, 5 µL of 2 × TaKaRa Ex Taq™ SYBR premix, 0.5 µL of each primer (10 pmol/µL), and 1 µL of dH$_2$O (PCR grade) in a total volume of 10µL. The PCR program consisted of one cycle at 95°C for 10 s; followed by 45 cycles of 95°C for 5 s, 58°C for 20 s; and 72°C for 20 s; and a final single cycle of 95°C for 15 s, 60°C for 30 s, and 95°C for 15 s. The Livak ($2^{-\Delta\Delta CT}$) method (Livak and Schmittgen, 2001) was used to quantitatively analyze the relative mRNA expression levels of *AbGSTs*. All the challenged samples had normalized to the relevant saline control at each time point. Obtained results were represented as fold changes (mean +/- standard deviation) using the expression at 0 h un-injected control as the basal level reference.

Table 1. Sequences of primers used in this study

Primer name	Application	Sequence of primer (5'-3')
AbGSTκ _F	ORF	GAGAGAGGATCCATGTCGGCAAAGAAGAGAGTGGAGT
AbGSTκ _R	amplification	GAGAGAAAGCTTTCAGAGCTTAGCTTTGGCCATTTCTG
AbGSTκ_qF	qPCR-	GTTGACATGCAACAGCCTGACAAGAC
AbGSTκ_qR	amplification	TGCATCACTAAGACCAGCCTTCTTCC
AbGSTθ _F	ORF	GAGAGAGAATTCATGGCGTTGAAAGTGTACTATGATTTGATGTCTC
AbGSTθ_R	amplification	GAGAGAGTCGACTCAAAGATTAGATCCAAGTGAGGACTTGGTCA
AbGSTθ_qF	qPCR-	AACTGGCAGCACCTGAACACAAG
AbGSTθ_qR	amplification	TACCGGTGACAGCTTTACGAACCA
AbRib_F	qPCR-	TCACCAACAAGGACATCATTTGTC
AbRib_R	Internal control	CAGGAGGAGTCCAGTGCAGTATG

2.7 Cloning of GSTs into the pMAL-c5X expression vector

Primers were designed with appropriate restriction sites to allow for cloning of the coding region of *AbGSTθ* and *AbGSTκ* into the expression vector pMAL-c5X, as shown in Table 1. PCR amplification was performed using a TaKaRa thermal cycler (Japan), and the ExTaq™ DNA polymerase (TaKaRa, Bio Inc., Japan). The reaction was performed in a total volume of 50 µL, containing 5 U of Ex Taq polymerase, 5 µL of 10 Ex Taq buffer, 4 µL of 2.5 mM dNTPs, 50 ng of template, and 40 pmol of each primer. The PCR profile was as follows, with an initial denaturation of 94°C for 3 min; 35 cycles of amplification at 94°C for 30 s, 59°C for 30 s, and 72°C for 1.5 min; and a final extension at 72°C for 5 min. The amplified PCR product and the pMAL-c5X vector were then digested using the corresponding restriction enzymes. The resultant products were electrophoresed on a 1% agarose gel and the appropriate gel bands were purified using the Accuprep™ gel purification kit (Bioneer, Korea) following the manufacturer's instructions. The purified digested PCR products and

vector were incubated overnight at 16°C with Mighty Mix (TaKaRa, Japan) to allow for ligation of the PCR product into the pMAL-c5X vector. The ligated product was then transformed into *Escherichia coli* DH5α and the coding sequence was confirmed by sequencing.

2.8 Overexpression and purification of recombinant AbGST proteins

To express the recombinant AbGST proteins (rAbGSTθ and rAbGSTκ), the pMal-c5X/AbGST constructs were transformed into *E. coli* BL21 (DE3) (New England BioLabs, USA) and incubated at 37°C in LB broth medium containing 100 μg/mL ampicillin, until the OD_{600} reach 0.6. Isopropyl-β-galactoside (IPTG) was then added to the culture at a final concentration of 0.5 mM and incubated for 8 h at 20°C to induce the expression of the recombinant protein. After incubation, the cells were harvested by centrifugation at 1200×g for 30 min at 4°C. The resultant pellet was resuspended in column buffer (20 mM Tris-HCl, pH 7.4, 200 mM NaCl) and stored overnight at −20°C. Lysozyme (1 mg/mL) was added to the thawed cell suspension and the suspension was sonicated on ice. The resultant cell lysate was centrifuged at 9000×g for 30 min at 4°C. The rAbGST proteins were purified from the supernatant using maltose affinity chromatography, as described previously (Alexandrov et al., 2001). The same protocol was repeated to overexpress and purify the maltose binding protein (MBP). The size of the recombinant proteins were determined by 12% SDS-PAGE along with molecular standards (Enzynomics[TM], Korea) and the protein concentrations were assessed using a Bradford assay (Bradford, 1976).

2.9 GST enzyme assay

The specific activities of rAbGSTs were measured, as described previously (Michel and McGovern, 1974). The reactions were performed in a final volume of 200 μL containing 0.1 M phosphate buffer pH 6.5, 100 mM reduced GSH, 100 mM substrate,

and the appropriate amount of enzyme. The activity was measured separately using CDNB, DCNB, 4-NPB, 4-NBC, and ECA as substrates. The absorbance of the reaction was measured at the corresponding wavelengths indicated in Table 2, immediately and 5 minutes after addition of the substrate. The temperature was kept constant at 25°C throughout the experiment. All assays were performed in triplicate.

2.10 Michaelis-Menten Kinetics

To determine the Michaelis-Menten kinetics, different concentrations of the CDNB substrate (0.25−4 mM) were used to measure the activity of the recombinant proteins, as described in 2.8.1, while maintaining the GSH concentration constant. The Michaelis-Menten constant (K_m) and the maximum reaction velocity (V_{max}) values were analyzed using a Lineweaver-Burk plot (Maciolek et al., 1963). The activity of the recombinant proteins was measured in the same manner using different concentrations of GSH (0.25−4 mM), while maintaining the CDNB concentration constant.

2.11 The effect of temperature, pH and inhibitors on rAbGSTs activity

To determine the effect of pH on activity of the recombinant rAbGST proteins using CDNB as the specific substrate, a pH buffer series, ranging from pH 3–11 was used while maintaining all other reaction conditions the same, as described in section 2.8.1. The effect of temperature on the activity of recombinant rAbGST proteins was measured using water baths ranging in temperature from 10–60°C, with CDNB as the substrate. The effect of the GST inhibitor Cibacron blue (CB), on the recombinant rAbGST protein was assessed over a range of CB concentrations (0.001–100 μM) as described previously (Jayasinghe et al., 2016).

2.12 Disk diffusion assay

To compare the survival efficiency of the untransformed *E. coli* (DE3), *E. coli*

transformed with pMAL-c5X vector, and *E. coli*. transformed with the AbGST /pMAL-c5X construct, a disk diffusion assay was performed, as described previously (Lee et al., 2007). LB bacterial cultures were induced with 0.5 mM IPTG and incubated at 25°C for 4 hours. The bacterial cultures were then evenly spread on LB agar plates and four Whatman filter-paper disks (3 mm diameter) were placed on each agar plates in equal distance. The disks were treated with 5 µL of H_2O_2, 1 M $CdCl_2$, 1 M $CuSO_4$ or 1 M $ZnCl_2$, respectively as determined by a preliminary assay. Treated plates were incubated overnight at 37°C and the diameter of the cleared zones was measured.

2.13 Statistical Analysis

All experiments were performed in triplicate. The data are reported as mean ± standard deviation (SD). For the evaluation of the significance differences between groups, an unpaired Student's t-test was used, and for the disk diffusion assay, the statistical analysis was performed using, a one-way analysis of variance (ANOVA) with Duncan's Post Hoc multiple comparisons to evaluate the significance differences within groups. *P*-values less than 0.05 ($P < 0.05$) were considered as being statistically significant.

3. Results

3.1 Molecular characterization of AbGSTs

The amino acid sequences of AbGSTθ (GenBank Accession No: MK226199) and AbGSTκ (GenBank Accession No: KY022631) were deduced from the abalone cDNA database. Based on the ExPASy-ProtParam analysis, the predicted AbGSTθ and AbGSTκ proteins consisted of 230 and 227 amino acids, with a predicted molecular weight of 26.6 kDa and 25.6 kDa, and a theoretical isoelectric point (pI) of 8.9 and 7.78, respectively. The instability indexes were 40.73 and 45.79 for AbGSTθ and AbGSTκ, respectively. Several bioinformatics tools were used to identify protein domains, families, functional sites, and associated patterns and profiles present in AbGSTθ and AbGSTκ.

AbGST-θ contained two soluble GST domains: a thioredoxin like N-terminal domain (Residues 1-75) and a C- terminal domain (110-203). Eight GSH binding sites (G-sites) at the positions of: S^{11}, Q^{12}, H^{40}, K^{41}, K^{52}, L^{53}, E^{66}, S^{67} and one sulfate binding site (Q^{12}) were identified at the N- terminal of AbGST-θ. Moreover, ten substrate binding sites (H-sites) were observed in the AbGST-θ C-terminal at: H^{104}, R^{108}, G^{109}, A^{112}, M^{113}, F^{115}, R^{116}, I^{120}, E^{174} and Q^{177}. Furthermore, the motif scan analysis revealed that AbGST-θ consists with three casein kinase II phosphorylation sites (146-149); 165-168; 206-209) and two protein kinase C phosphorylation sites (192-194; 211-213).According to the analysis AbGSTκ protein contains GSH binding sites (G-sites) at Pro^{16}, Tyr^{17}, Ser^{18}, Asn^{54}, Lys^{63}, Phe^{182}, Gly^{183}, Lys^{184}, Phe^{199}, Ser^{201}, Asp^{202}, and Arg^{203}; no hydrophobic ligand binding sites (H-sites) were observed. AbGSTκ also possessed the same general fold as DsbA, consisting of a thioredoxin domain (5–212 aa), which is interrupted by an alpha-helical domain. SignalP 4.1 software analysis did not reveal any signal peptide in both AbGST-θ and AbGSTκ

proteins.

3.2 Homology analysis and phylogenetic relationship

The pairwise sequence alignment analysis was carried out to compare the identity and

similarity percentages of AbGSTs, with other known GST homologues.

Table 2. Pairwise identity (I%), similarity (S%), and gaps (G%) of disk abalone GST-θ protein toward selected orthologs at amino acid levels

Name	Accession no	Identity (%)	Similarity (%)	Gaps (%)	Amino acids
Mizuhopecten yessoensis	XP_021358629.1	59.1	75.3	2.1	235
Lingula anatina	XP_013408169.1	53.2	69.3	1.7	231
Alitta succinea	ABQ82132.1	49.4	69.3	2.6	231
Osmerus mordax	ACO09513.1	45.7	64.5	4.3	234
Danio rerio	NP_956815.2	44.4	61.5	4.3	234
Ruditapes philippinarum	AFB83399.1	39.9	59.3	14.1	248
Cephus cinctus	XP_015598273.2	39.6	54.9	15.7	255
Mus musculus	CAA66666.1	35.6	53.8	12.6	253
Macaca mulatta	NP_001244563.1	34.9	54.9	14.1	255
Homo sapiens	AAC13317.1	34.1	53.3	14.9	255

According to the observed data, corresponding to AbGST-θ, the highest sequence

identity and similarity was observed from *Mizuhopecten yessoensis* (Japanese

Weathervane Scallop) as 59.1% and 75.3%, respectively. The predicted multiple

sequence alignment of AbGST-θ with other molluscan and non-molluscan organisms

demonstrated that the N-terminal region is highly conserved through the evolution

compared to the C-terminal region (Fig. 1). Highly conserved GSH binding sites

were observed in the N-terminal at S^{11}, Q^{12}, E^{66}, S^{67} while substitutions were

제주대학교 중앙도서관
JEJU NATIONAL UNIVERSITY LIBRARY

observed in H^{40}, F^{41}, K^{52}, L^{53} positions. Out of the C-terminal H-sites, R^{108}, E^{174}, Q^{177} were highly conserved among all the species through the evolution although H^{104}, G^{109}, A^{112}, M^{113}, F^{115}, R^{116}, I^{120} sites exhibited replacements.
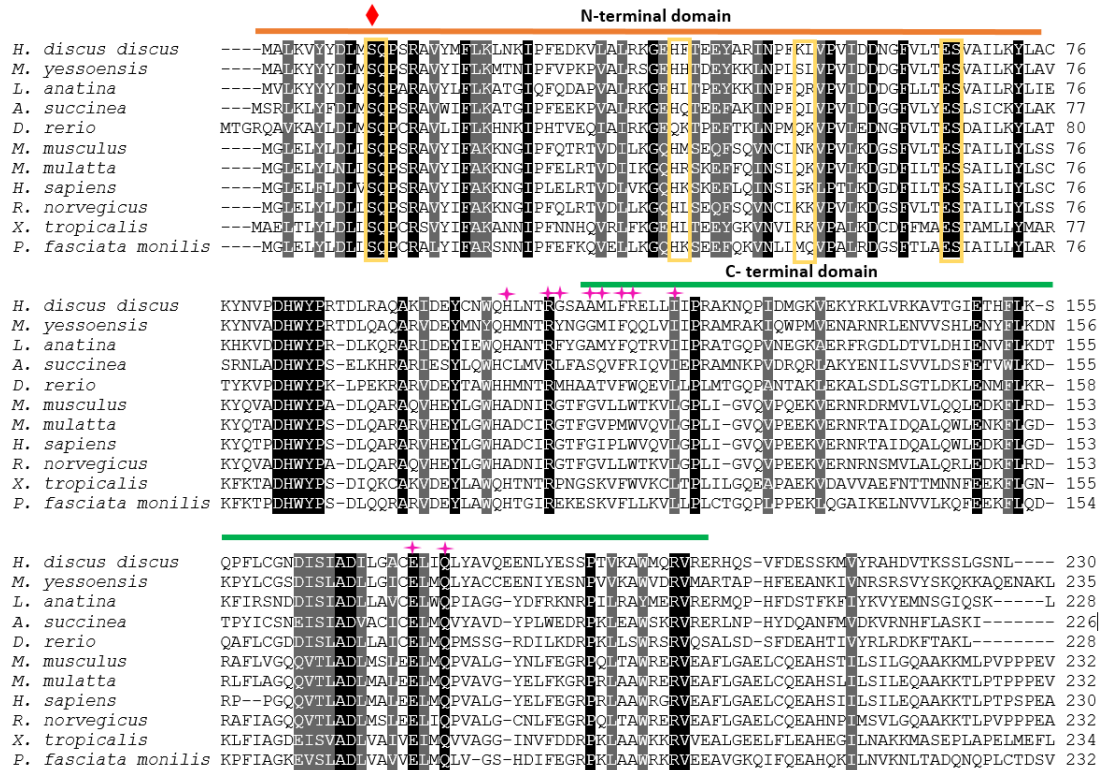
Fig. 1. Multiple sequence alignment of the amino acid sequences of AbGST-θ and its orthologs from different organisms. Fully conserved amino acids are shown in black, and strongly conserved and weakly conserved amino acids are shown in dark grey and light grey, respectively. The N-terminal domain and the C-terminal domain are marked with orange and green color lines, respectively. The conserved Ser^{11} and sulfate binding site (Q^{12}) are marked with red and green color symbols, respectively. The putative G-sites are shown with yellow color boxes and the pink color symbols indicate the H-sites.

However, all the aligned GSTκs contained highly conserved G−sites. Based on the pairwise sequence identity analysis of AbGSTκ, the highest identity was found with the pufferfish (*Takifugu obscurus*) (60.0%) ortholog with which it shared a 73.0% sequence similarity. Sequence alignment analysis of AbGSTκ with respective GSTκ from other species including fish, mollusk, amphibian, nematodes, and mammals,

showed that both the N and C−termini were found to be relatively diverse and did not contain any conserved amino acid sequences (Fig. 2).
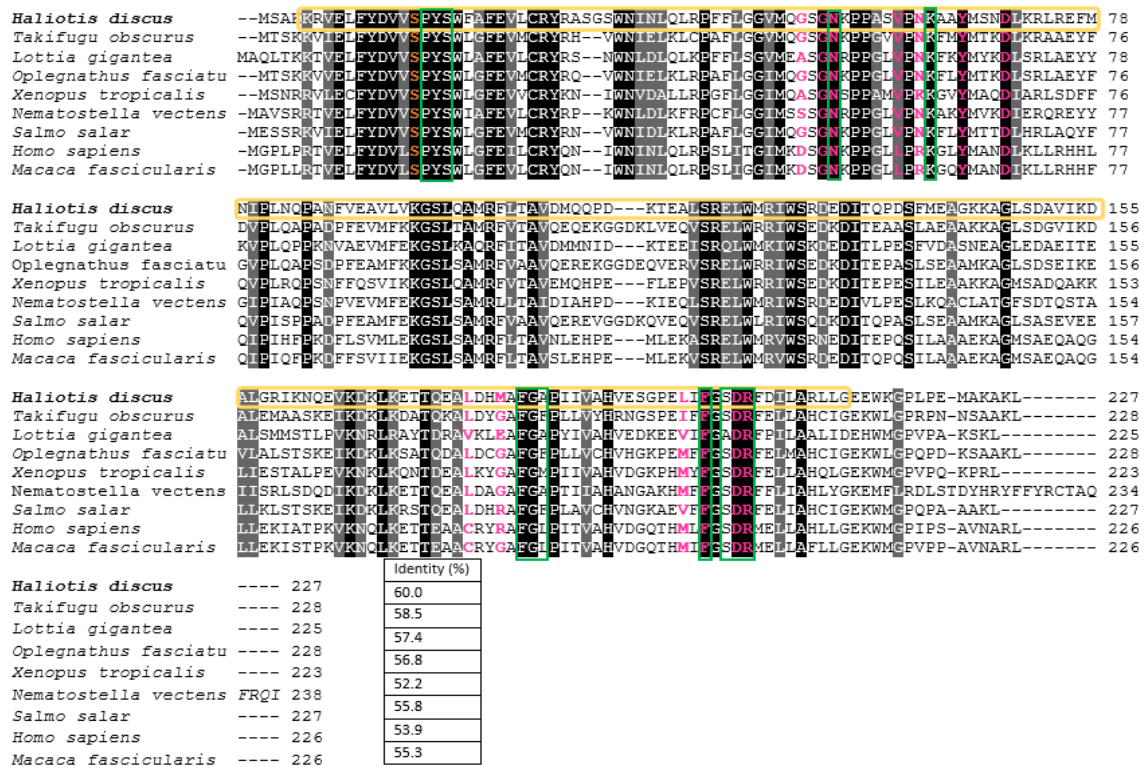
Fig. 2. Multiple sequence alignment of the amino acid sequences of AbGSTκ and its orthologs from different organisms. Fully conserved amino acids are shown in black, and strongly conserved and weakly conserved amino acids are shown in dark grey and light grey, respectively. The conserved DSBA-like thioredoxin domain (5-212) is marked in yellow. The putative GSH binding sites, and the residues involved in the dimer interface, are shown with green lines and pink letters, respectively. The catalytic serine residue is shown in orange. The % identity of each orthologue with AbGSTκ is shown at the end of each respective sequence in the alignment.

A phylogenetic tree was constructed for AbGST-θ together with other various GST classes, using the neighbor joining method (Fig. 3). According to the figure, GST-θ had form a separate clade including evolutionary different organisms together. However, AbGST-θ clearly clustered together with molluscan GST-θ: *Mizuhopecten yessoensis* and *Crassostrea gigas*. Separate sub clades were observed for other GST classes and previously identified disk abalone (*Haliotis discus discus)* GSTs had appropriately placed in the respective classes.
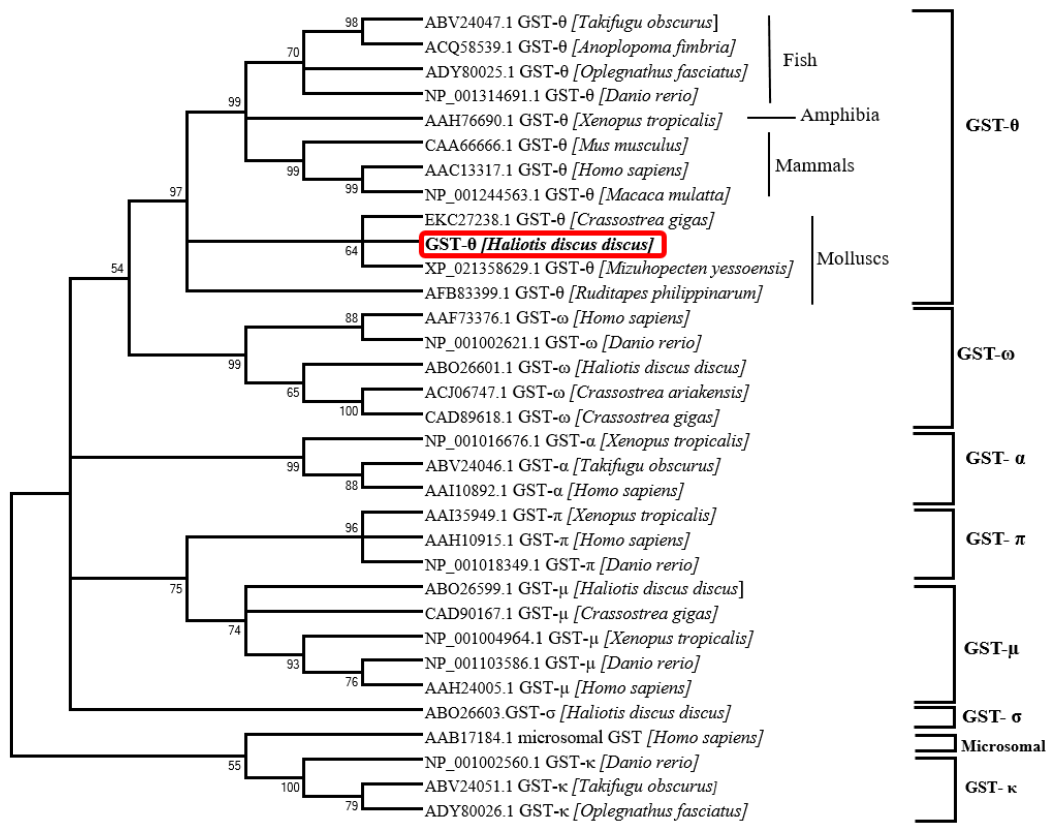
Fig. 3. A phylogenetic tree constructed using the neighbor-joining method based on different classes of GSTs. The bootstrap values are shown at the node of each branch. The NCBI accession numbers are given with the organism name.

The constructed phylogenetic tree for AbGSTκ shows the relationship between AbGSTκ and the different sub-families of the GST superfamily (Fig. 4). The tree branched into two main clusters separating the cytosolic GSTs and the mitochondrial GSTs. AbGSTκ was found to be clustered with the mitochondrial GSTs. Moreover, AbGSTκ was found to be closely clustered with other fish GSTκs.
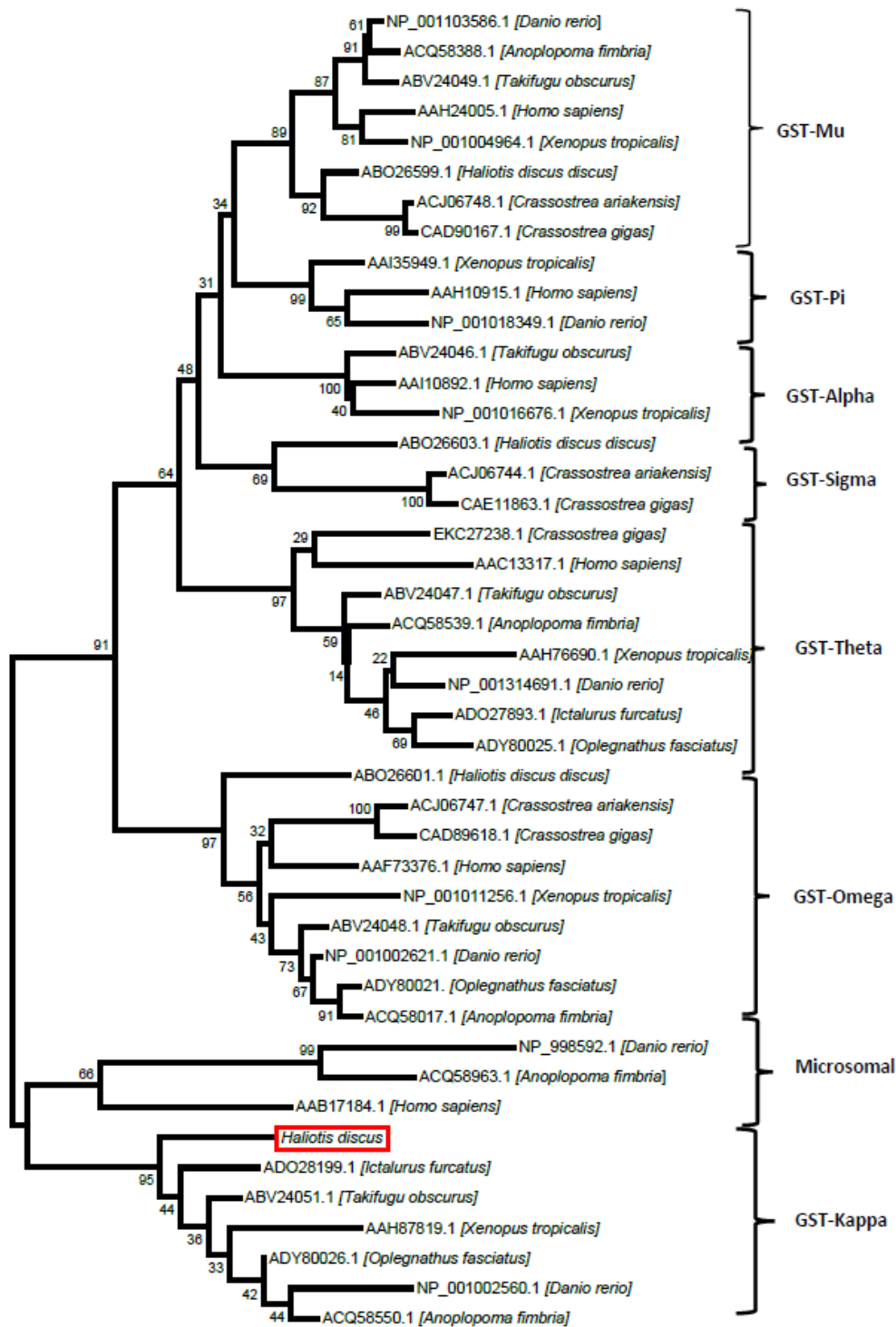
Fig. 4. A phylogenetic tree constructed using the neighbor-joining method based on different classes of GSTs. The bootstrap values are shown at the node of each branch. The NCBI accession numbers are given with the organism name.

3.3 Tertiary structural model of AbGSTs

In order to analyze the structural features of AbGST-θ, a three-dimensional model was constructed using Swiss-Modeling and then it was analyzed by the PyMOL computer software (Fig. 5A).

A)
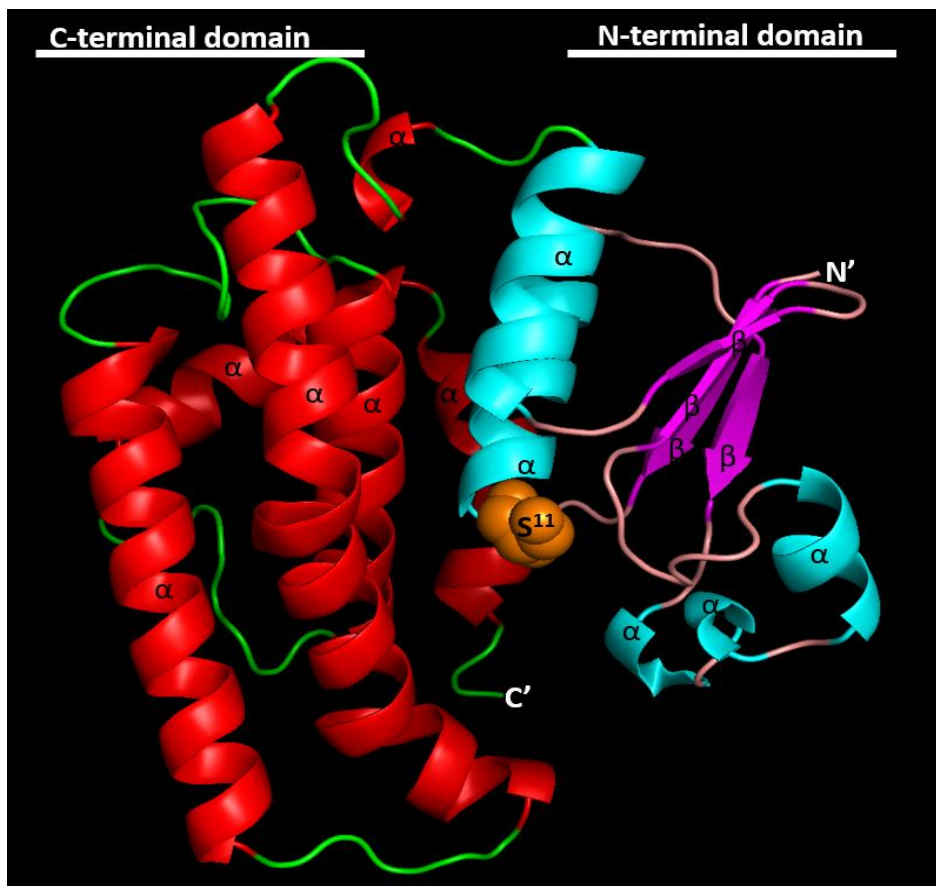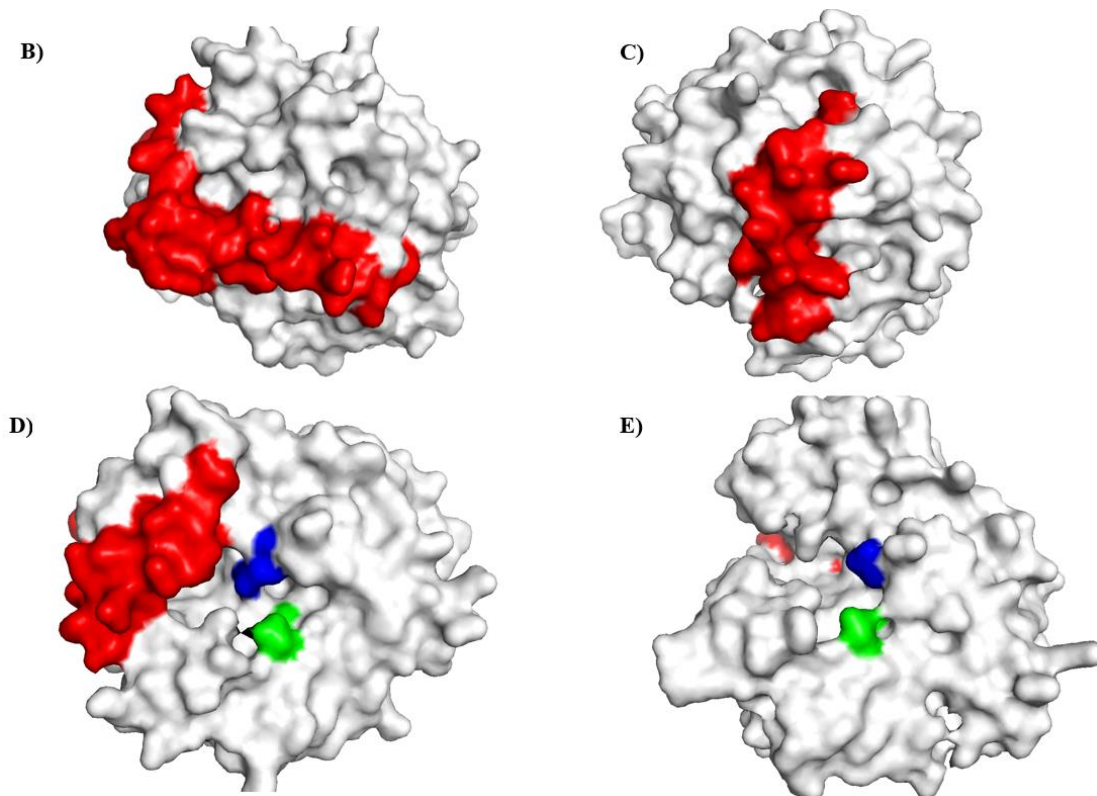
Fig. 5.Surface representations of human GST-θ (B, D) and AbGST-θ (C, E) highlighting the C-terminal tails in red color. The blue color surface representing the H-site and green color surface representing the G-site region in each figure. The 3D structure models were predicted using the Swiss-model server and visualized using PyMOL software.

N- terminal and C-terminal domains could identified separately which were connecting each other by a short tract. The N-terminal domain consisted with βαβ unit connected to ββα unit by a surface exposed region which contain two small α-helices. The structural topology of the C-terminal domain consisted with only six α-helices. The orange color sphere represented the Ser[11] residue which is considered as a characteristic feature in GST- θ class. The surface representations of human GST- θ (Fig. 5 B, D) and AbGST-θ (Fig. 5 C, E) demonstrated the highlighted C-terminal tail in red color. According to the figure, human GST- θ showed a long C-terminal extension compared to AbGST-θ. The blue color surface represented the H-site and green color surface represented the G-site region in both figures.

3D structure modeling of AbGSTκ was performed using the SWISS-MODEL server

and visualized using the PyMOL surface viewer program (Fig. 6A).

A)
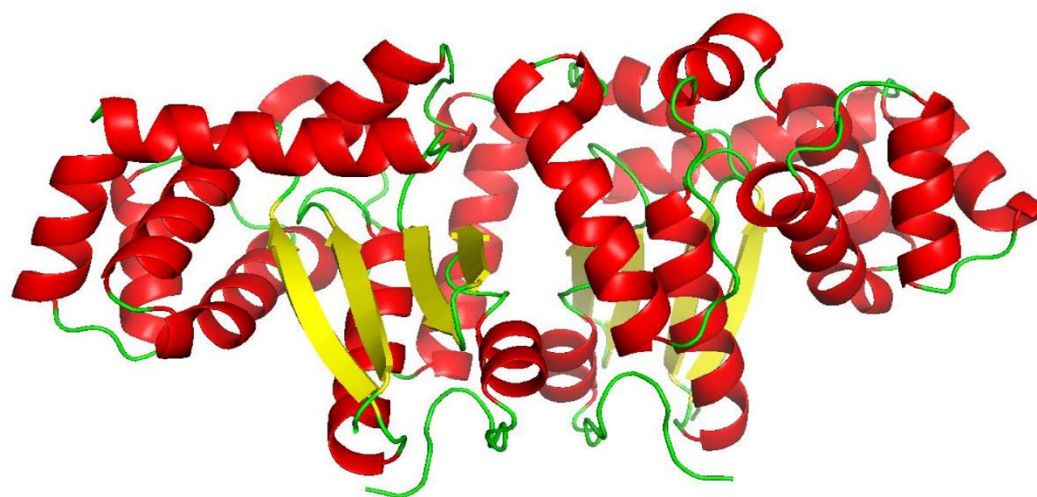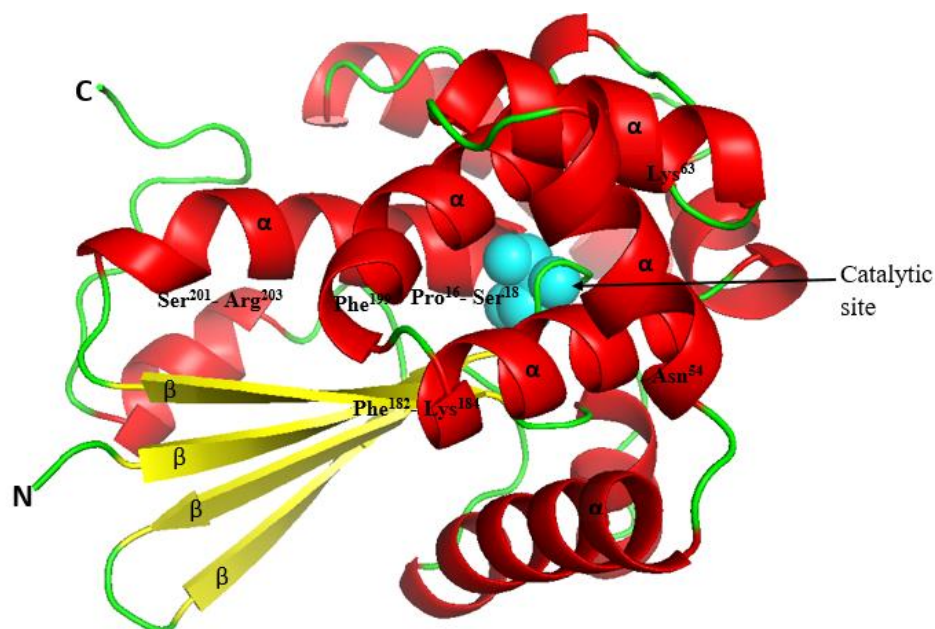
B)

Fig. 6. A) Predicted three-dimensional structure of AbGSTκ. The α-helices and β-sheets are marked, and the positions of the predicted G-sites are labeled. The catalytic residue is shown as a blue colored sphere. **B)** The butterfly-like shape adopted by the AbGSTκ dimer. The 3D structure models were predicted using the Swiss-model server and visualized using PyMOL software.

The crystal structure of glutathione transferase belonging to the human kappa class

was used as a template. This template shares 53.78% sequence identity and 0.99

coverage with the AbGSTκ sequence. The 3D structure analysis showed the presence of α-helices and four conserved antiparallel β-sheets. The functional DSBA domain of AbGSTκ is distributed throughout the helices, coils, and sheets while forming the butterfly-like shape of the dimer (Fig. 6B).

3.4 Tissue-specific expression of AbGSTs

To understand the potential endogenous functions of *AbGST-θ* and *AbGSTκ*, their relative expressions were examined in different tissues. To achieve this, cDNA samples were prepared from the disk abalone organs and analyzed using qPCR. According to the analysis of the expression profiles from the disk abalone revealed that the highest expression level of *AbGST-θ* was observed from the digestive tract (~26 fold), followed by hepatopancreases (~20 fold). All the examined tissues had expressed *AbGST-θ* in different levels indicating their potential physiological roles within the body (Fig. 7A). AbGSTκ was highly expressed in the digestive tract (~20 fold), mantle (~20-fold), and muscles (~18-fold), whereas the lowest expression was observed in the hepatopancreas (Fig. 7B).

A)
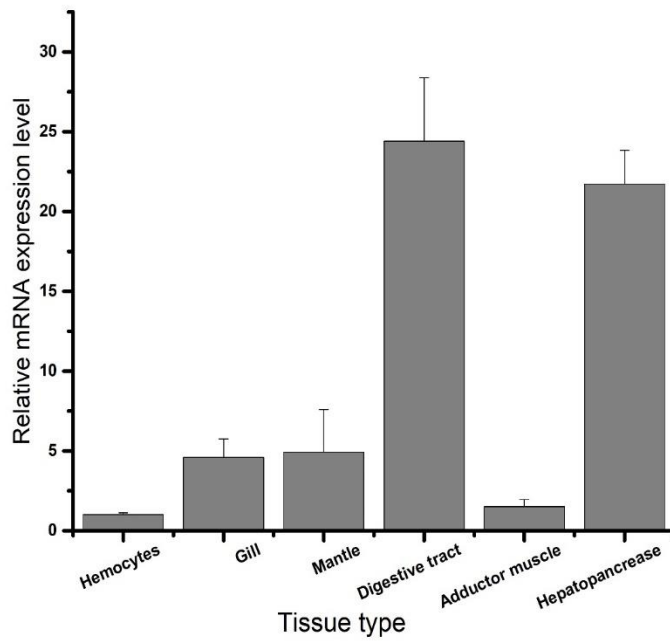
B)
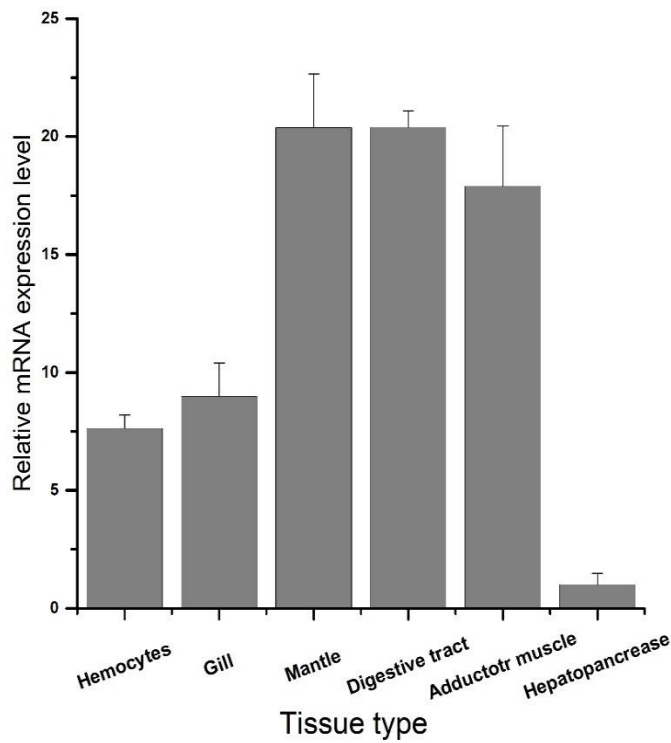
Fig. 7. Tissue specific transcriptional profile of **A)** *AbGST-θ* and **B)** *AbGSTκ* in disk abalone (*Haliotis discus discus*). Data are presented as mean ± standard deviation (n=3).

25

3.5 AbGSTs expressions against pathogenic stress

In order to understand the roles of *AbGST-θ* and *AbGSTκ* in immune responses, we examined the transcriptional levels of both *AbGSTs* in gill tissue and hemocytes after immune challenges with bacteria, a viral mimic, and LPS (Fig. 8). *V. parahaemolyticus,* Poly (I:C), and LPS were used to challenge the abalones to assess the immune responses.

The *AbGST-θ* was significantly upregulated after 48 h (~ 4-fold) p.i. of LPS in abalone gills (Fig. 8A). Meanwhile the poly I:C injection was able to significantly upregulate *AbGST-θ* in abalone gill tissue at 48h (~5-fold) of p.i. (Fig. 8B). Furthermore, *V. parahaemolyticus* injection resulted with significant upregulations in abalone gill tissue at 24h (~2-fold) and 72h (~3-fold) of p.i (Fig. 8C). The mRNA expression of *AbGST-θ* was significantly upregulated at 72 h and 120 h p.i. of LPS and *V. parahaemolyticus* in hemocytes (Fig. 8D and F). Moreover, poly I:C stimulation significantly upregulated the expressions of *AbGST-θ* only at 72h of p.i (Fig. 8E).

A)
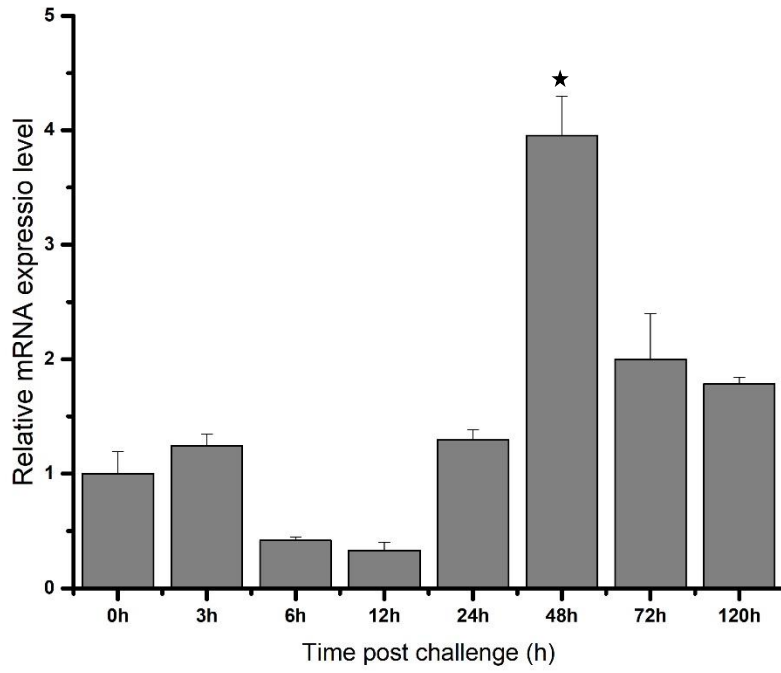
B)
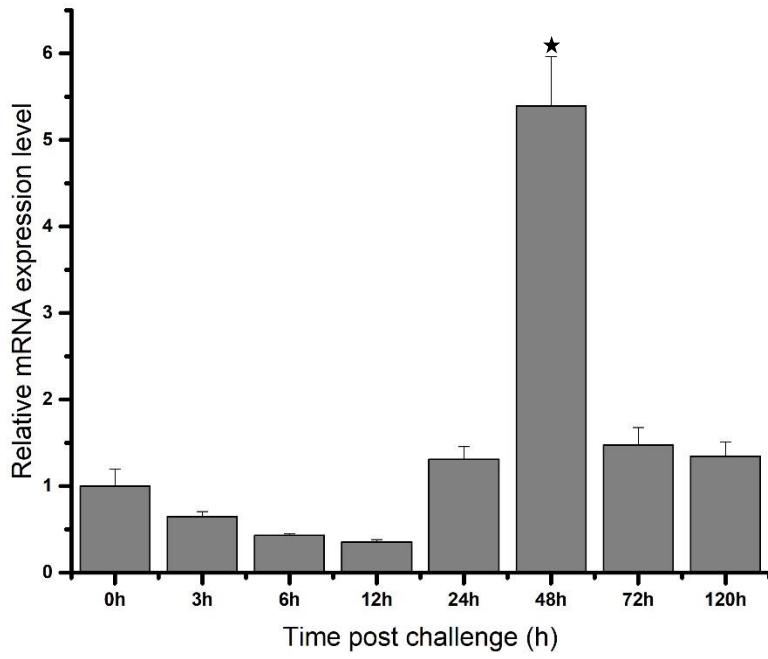
C)
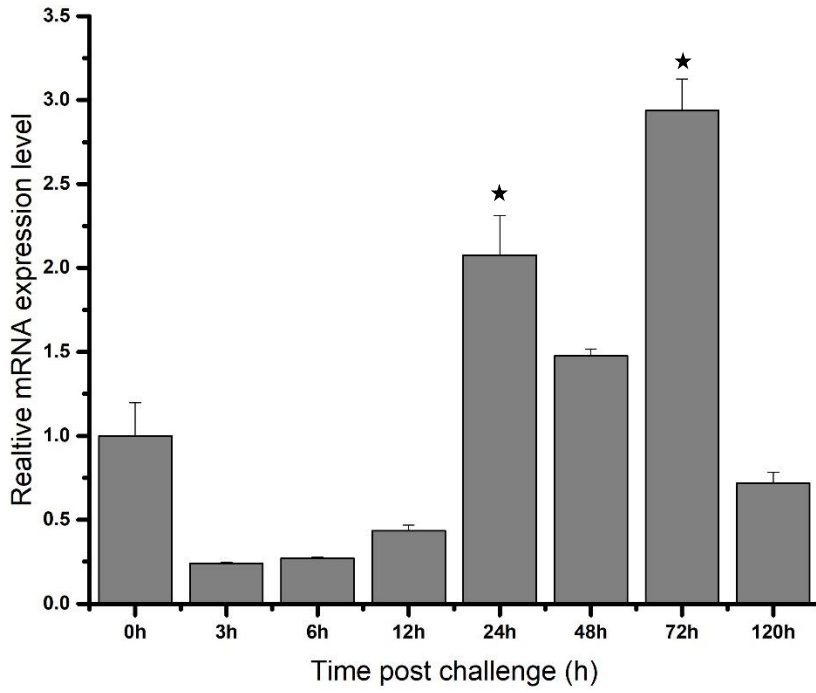
D)
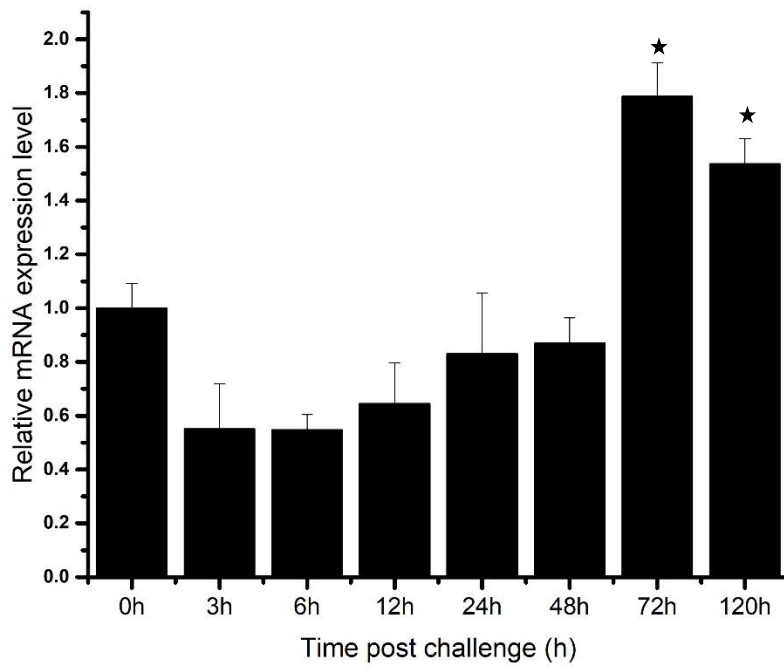
E)
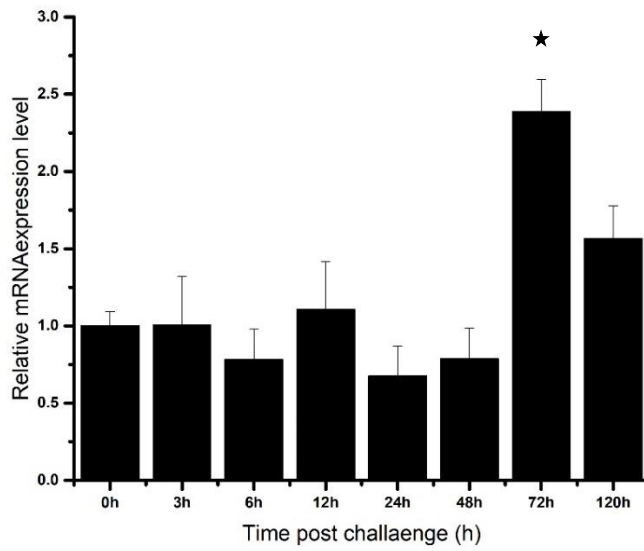
F)
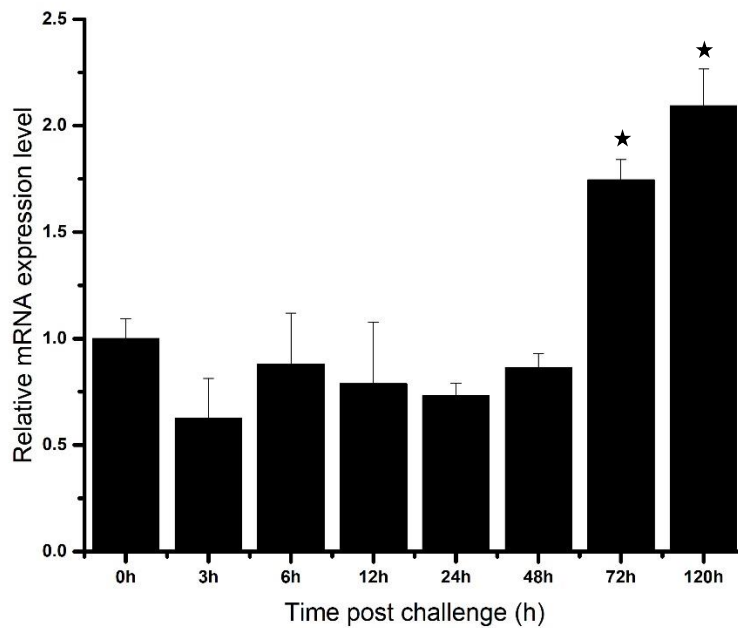
Fig. 8. Relative mRNA expression, analyzed by qPCR of *AbGST-θ* over time in gill tissue (A, B, C), and hemocytes (D, E, F) in response to challenges with LPS (A, D), poly I:C (B, E), and *Vibrio parahaemolyticus* (C, F). Data are presented as mean ± standard deviation (n=3). Data with marked with a ∗ represent a statistical difference in expression compared with the 0 h post-injection baseline.

Following LPS treatment, the basal transcriptional level of *AbGSTκ* in the gills rapidly decreased at 3 h of p.i, and then increased gradually up to 48 h of p.i. This upregulation at 48 h of p.i. was significant ($P < 0.05$) compared with that in the un-injected control animals (Fig. 9A). Following *V. parahaemolyticus* injection, the mRNA level of *AbGSTκ* in gill tissue decreased as well as increased at different time points, not showing any significant up or downregulation overall (Fig. 9B). Treatment with poly I:C resulted in a fluctuating pattern of *AbGSTκ* mRNA levels in gills, with both upregulation and downregulation being observed (Fig. 9C). Following the same immune challenges, the relative mRNA level of *AbGSTκ* in hemocytes showed different expression patterns from those seen in the gills. In hemocytes, following LPS treatment, the *AbGSTκ* mRNA levels were significantly upregulated at 48 and 72

제주대학교 중앙도서관
JEJU NATIONAL UNIVERSITY LIBRARY

h.p.i. but were significantly downregulated at 6, 24, and 120 h.p.i (Fig. 9D). *V. parahaemolyticus* treatment significantly downregulated *AbGSTκ* mRNA levels at 12 and 72 h.p.i (Fig. 9E). The viral mimic, poly I:C, caused a significant upregulation of *AbGSTκ* mRNA levels at 3 h.p.i., and a significant downregulation at 24 and 48 h.p.i. (Fig. 9F).

A)
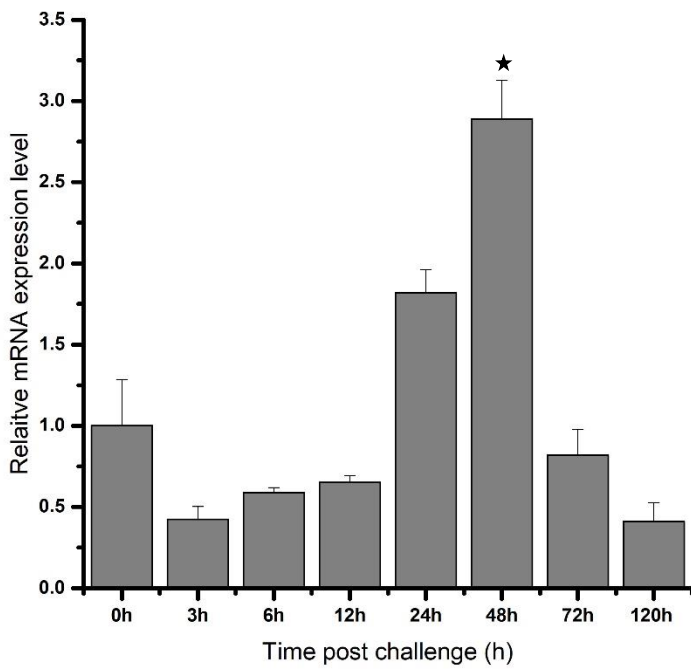
B)
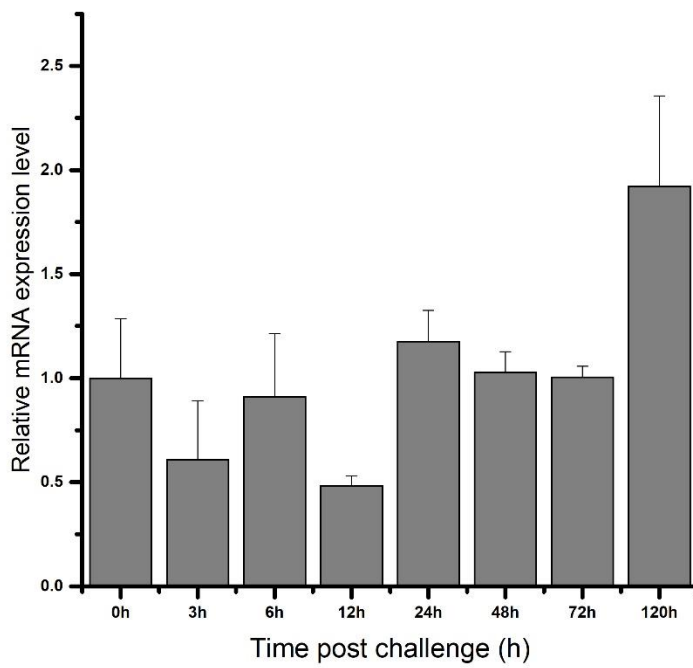
C)
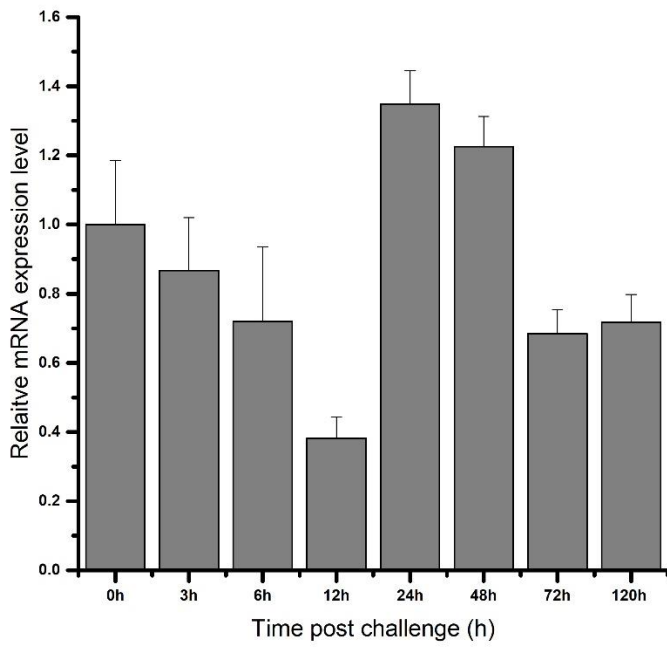
D)
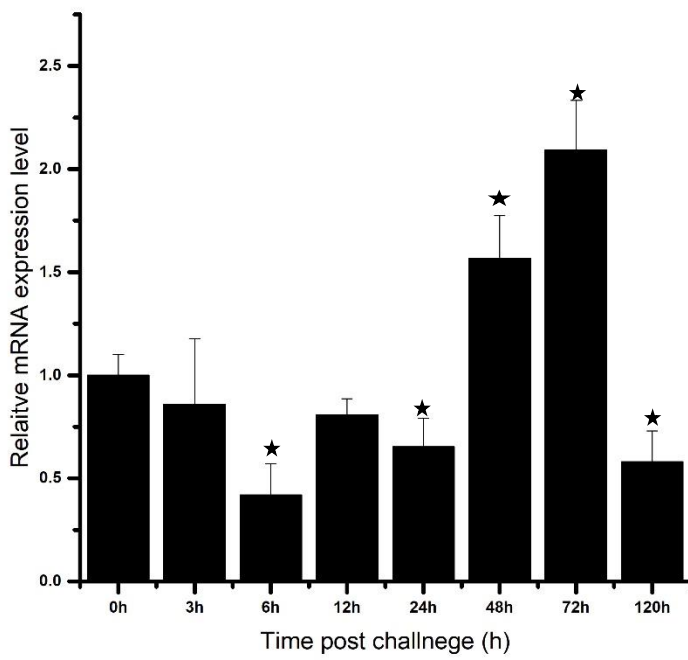
E)
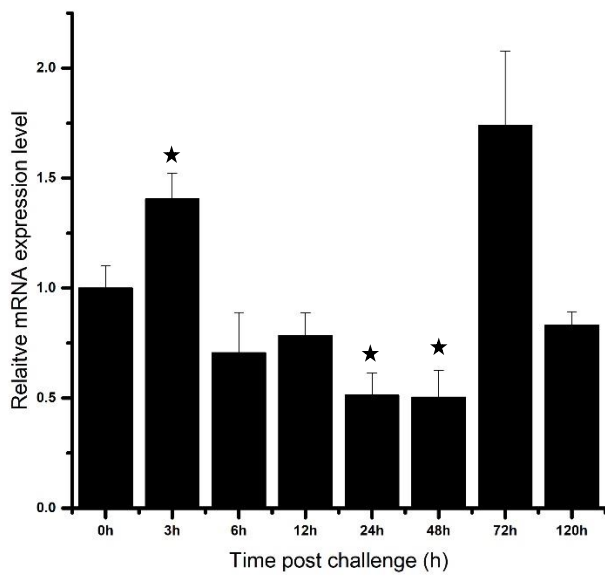
F)
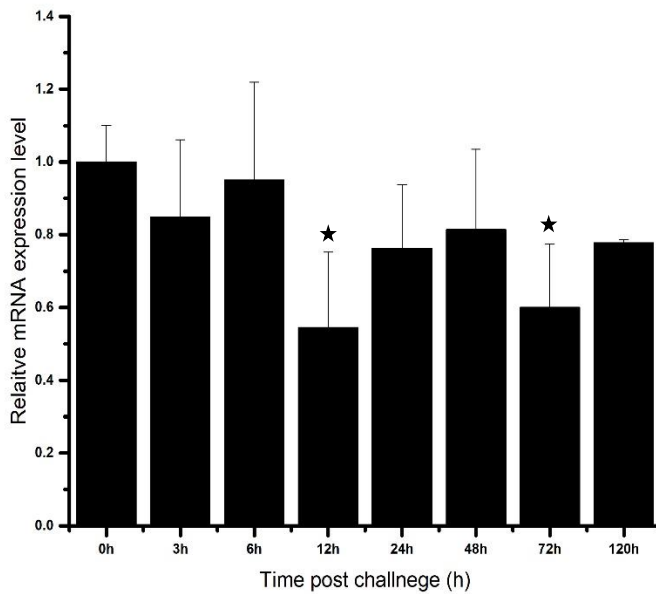
Fig. 9. Relative mRNA expression, analyzed by qPCR of *AbGST-κ* over time in gill tissue (A, B, C), and hemocytes (D, E, F) in response to challenges with LPS (A, D), poly I:C (B, E), and *Vibrio parahaemolyticus* (C, F). Data are presented as mean ± standard deviation (n=3). Data with marked with a ∗ represent a statistical difference in expression compared with the 0 h post-injection baseline.

3.6 Construction of recombinant AbGST proteins and purification

Recombinant AbGST proteins (rAbGST-θ and rAbGSTκ) were over-expressed using the pMal-c5X/ AbGSTs construct in *E. coli* BL21 after induction with IPTG. After purifying the recombinant protein using affinity chromatography based on the presence of the maltose binding protein (MBP) fusion tag, their approximate molecular masses were determined by electrophoresis on a 12% SDS-PAGE gel using molecular mass markers (Fig. 10). The resultant AbGST-θ/MBP fusion protein exhibited a band of ~70 kDa being compatible with the predicted molecular mass of AbGST-θ-26.6 kDa; MBP 42.5 kDa (Fig. 10A). Moreover, the AbGSTκ/MBP fusion protein had a size of ~68 kDa, including the 42.5 kDa MBP tag, confirming AbGSTκ's predicted molecular mass of 25.6 kDa (Fig. 10B). Both proteins were considered as pure based on the presence of only those appropriate single bands.

A)
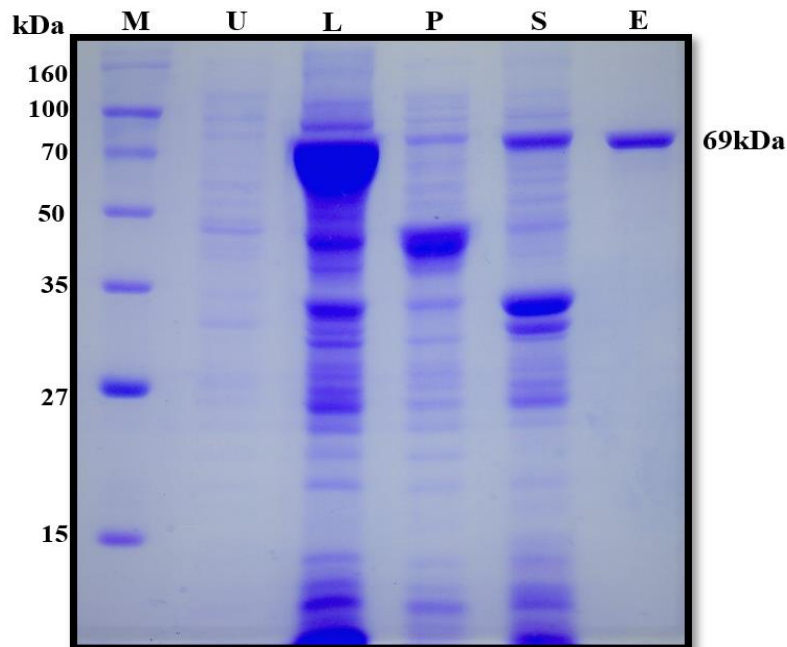
B)
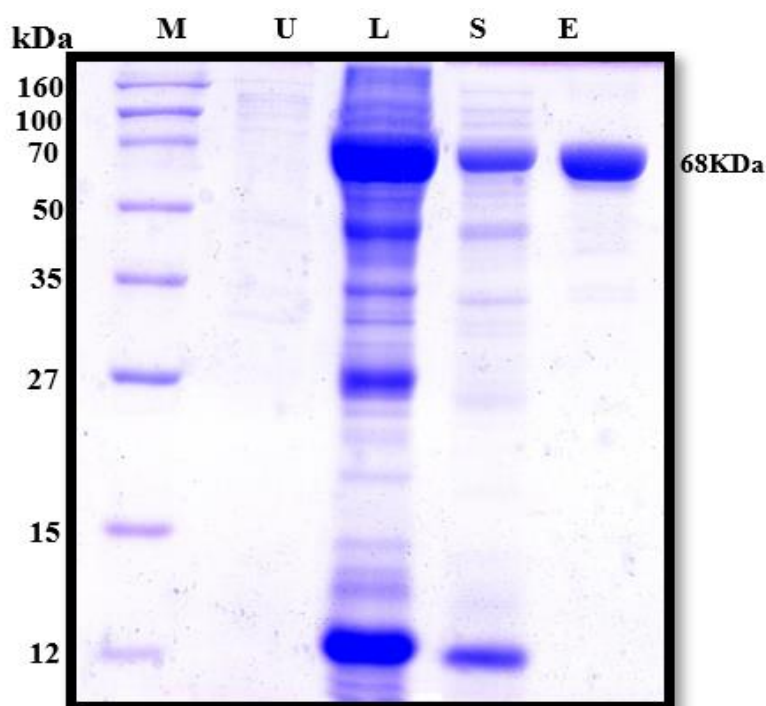
Fig. 10. SDS-PAGE analysis of purified **A)** rAbGST-θ and **B)** AbGSTκ. M: protein marker, U: un-induced extract, L: lysate from IPTG induced cells, P: pellet from IPTG induced cells, S: supernatant from IPTG induced cells, E: purified recombinant protein after elution.

3.7 Specific activity and kinetic assay

The activities of rAbGST-θ, rAbGSTκ and MBP against different substrates, including CDNB, DCNB, 4-NPB, 4-NBC, and ECA were measured, as described previously (Board et al., 2000) (Table 5). Detectable activity was observed only using CDNB as the substrate. No significant activity was detected for MBP against any of the substrates and therefore it was treated as a control and further functional studies were conducted only with rAbGST-θ and rAbGSTκ.

Table 3. Substrate specific parameters at 25°C, when the substrate and GSH concentrations were 1.0 mM each, and the specific activities of AbGST-θ and AbGSTκ towards the different substrates.

Substrate	pH	λ_{max} (nm)	Molecular extinction Coefficient (ϵ) ($mM^{-1}\ cm^{-1}$)	AbGST-θ Specific activity ($\mu mol\ min^{-1}\ mg^{-1}$)	AbGSTκ Specific activity ($\mu mol\ min^{-1}\ mg^{-1}$)
CDNB	6.5	340	9.6	5.38 ± 0.09	6.51 ± 0.09
DCNB	7.5	345	8.5	n.d	n.d
4-NPB	6.5	310	1.2	n.d	n.d
4-NBC	6.5	310	1.9	2.52 ± 0.08	n.d
ECA	6.5	270	5.0	0.52 ± 0.07	n.d

n.d – not detected

The rAbGST-θ showed highest catalytic activity towards the CDNB substrate (5.38 ± 0.09 $\mu mol\ min^{-1}\ mg^{-1}$) with detectable activities towards 4-NBC (2.52 ± 0.08 $\mu mol\ min^{-1}\ mg^{-1}$) and ECA ($0.52 \pm 0.07$ $\mu mol\ min^{-1}\ mg^{-1}$) substrates. No detectable activities were observed for DCNB and 4-NPB substrates. The specific activity of rAbGSTκ against the CDNB substrate was 6.51 ± 0.09 µmol/min/mg. No detectable activities for rAbGSTκ were observed with other substrates.

The enzyme activity for rAbGST-θ and rAbGSTκ were measured with different concentrations of CDNB and GSH. For rAbGST-θ, with a fixed concentration of CDNB, the K_m and V_{max} were calculated as 5.21 ± 0.22 mM and 10.68 ± 0.10 $\mu mol\ min^{-1}\ mg^{-1}$, respectively. Meanwhile with a fixed concentration of GSH, the K_m and V_{max} values were calculated to be as 2.65 ± 0.18 mM and 8.23 ± 0.09 $\mu mol\ min^{-1}\ mg^{-1}$, respectively (Table 6.). For rAbGSTκ, at a fixed CDNB concentration, the K_m and V_{max} values for GSH were 2.95 ± 0.28 mM and 12.77 ± 0.29 µmol/min/mg, respectively. At a fixed GSH concentration, the K_m and V_{max} values for CDNB were 3.81 ± 0.30 mM and 14.35 ± 0.30 µmol/min/mg, respectively.

Table 4. Optimum temperature, pH, Michaelis-Menten kinetic parameters, and inhibitor IC_{50} values for AbGST-θ and AbGSTκ using CDNB as the substrate (n=3).

Protein	Optimum Temp. (^{o}C)	Optimum pH	Inhibitory IC_{50} (μM)	Kinetics CDNB$_{(GSH(1mM))}$		Kinetics GSH$_{(CDNB(1mM))}$	
				$K_{m(mM)}$	V_{max} (μmol mg^{-1} min^{-1})	$K_{m(mM)}$	V_{max} (μmol mg^{-1} min^{-1})
AbGSTθ	37	7.5	0.08±0.01	5.21 ± 0.22	10.68 ± 0.10	2.65 ± 0.18	8.23 ± 0.09
AbGSTκ	35	8	0.05±0.01	3.81 ± 0.30	14.35 ± 0.30	2.95 ± 0.28	12.77 ± 0.29

3.8 Effect of temperature, pH, and an inhibitor on GSTs activity

Using CDNB as the specific substrate, the optimum pH and temperature for maximum catalytic activity of rAbGST-θ and rAbGSTκ were determined. For rAbGST-θ the optimum pH was detected as pH:7.5 while giving highest activities within a narrow range from pH 7 to 9 (Fig. 7A). The optimum temperature of rAbGST-θ for CDNB conjugation activity was ~ 37 °C (Fig. 7B). Moreover, the higher temperatures resulted the loss of enzymatic activities. Furthermore, 100% inhibition of rAbGST-θ-CDNB conjugation activity was observed with 100 μM concentration of CB (Fig. 7C). The IC_{50} value for CB was calculated as 0.08 ± 0.01 μM.
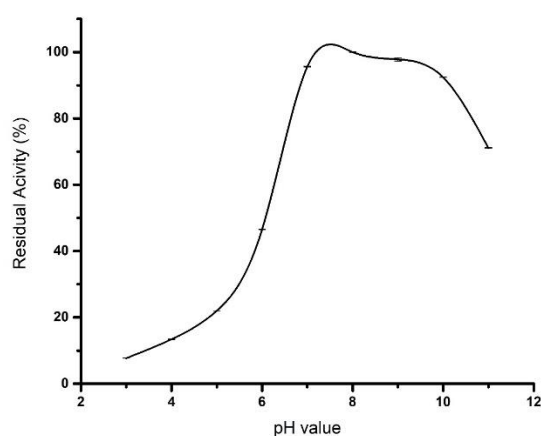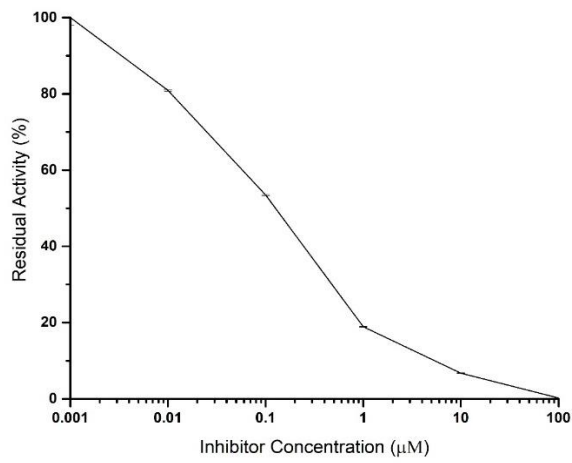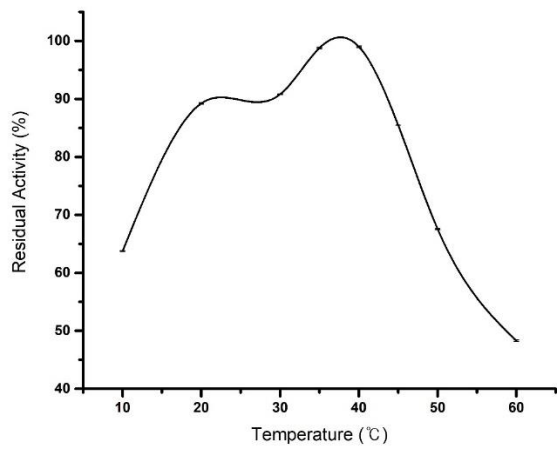
Fig. 11. A) The effect of pH, B) temperature and C) inhibitor (Cibacron Blue) concentration on the GSH conjugating activity of AbGST-θ.
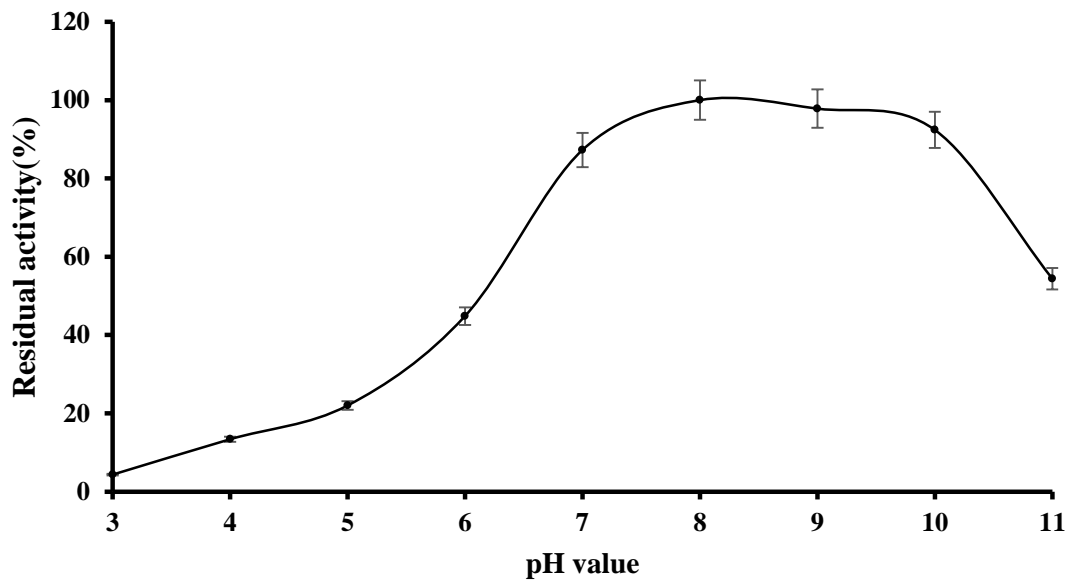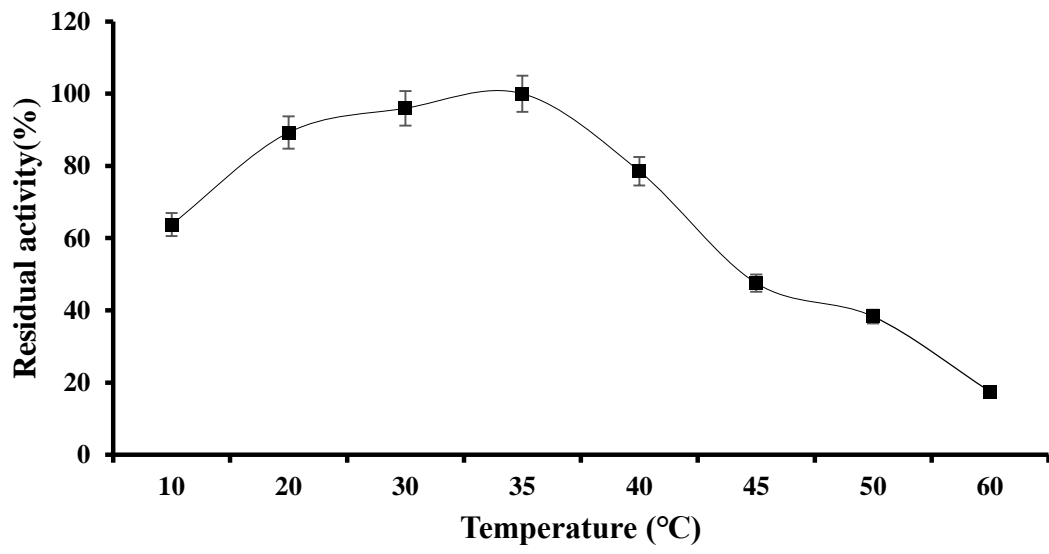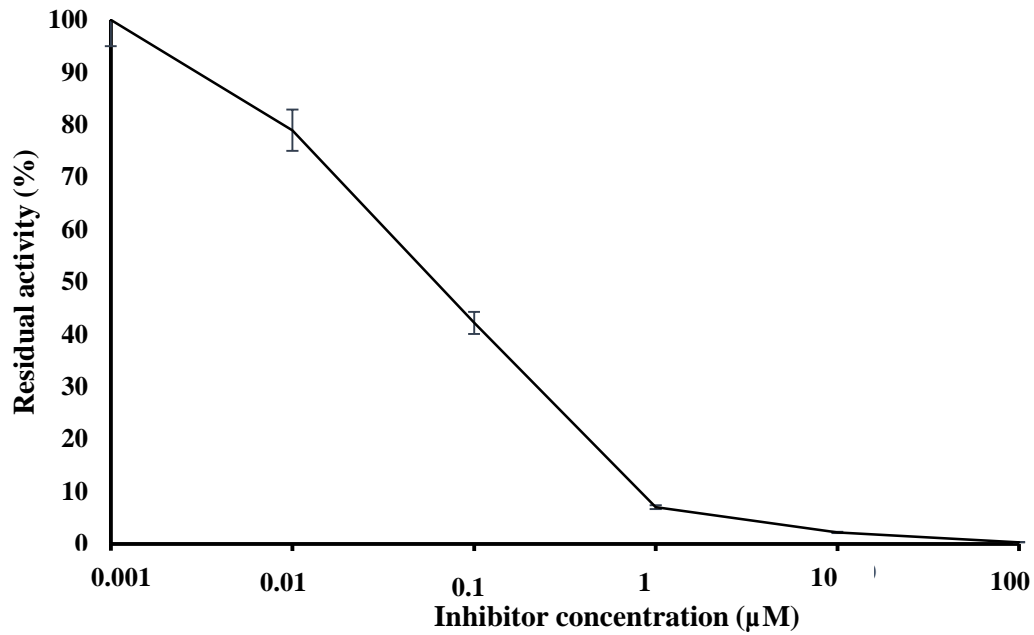
Fig. 12. Effect of **A)** Temperature, **B)** pH, and **C)** Inhibitor (Cibacron Blue) concentration on the GSH conjugating activity of AbGSTκ.

The optimum temperature for the CDNB conjugation activity of rAbGSTκ was 35°C (Fig. 7A). rAbGSTκ was also shown to have GSH: CDNB conjugating activity over a broad pH range from 4 to >11, with an optimum activity at pH 8 (Fig. 7B). The highest activities were observed over the pH range of 7–10. Moreover, CB (100 μM) inhibited rAbGSTκ by 100% using CDNB as the substrate (Fig. 7C). The IC_{50} value for CB was 0.05 μM.

3.9 Disk diffusion assay

In AbGST-θ, Clearance zones with various diameters were observed around all the H_2O_2 treated disks. Among them the largest clearance zone was observed at the untransformed *E. coli* plate while other two were smaller than that. Apart from that, all the heavy metal treated disks also exhibited clearance zones with different diameters. Maximum diameters for $CdCl_2$, $ZnCl_2$ and $CuSO_4$ treatments were observed in the untransformed *E. coli* plates, whereas the AbGST-θ transformed plates showed significant smaller clearance zones around the disks.
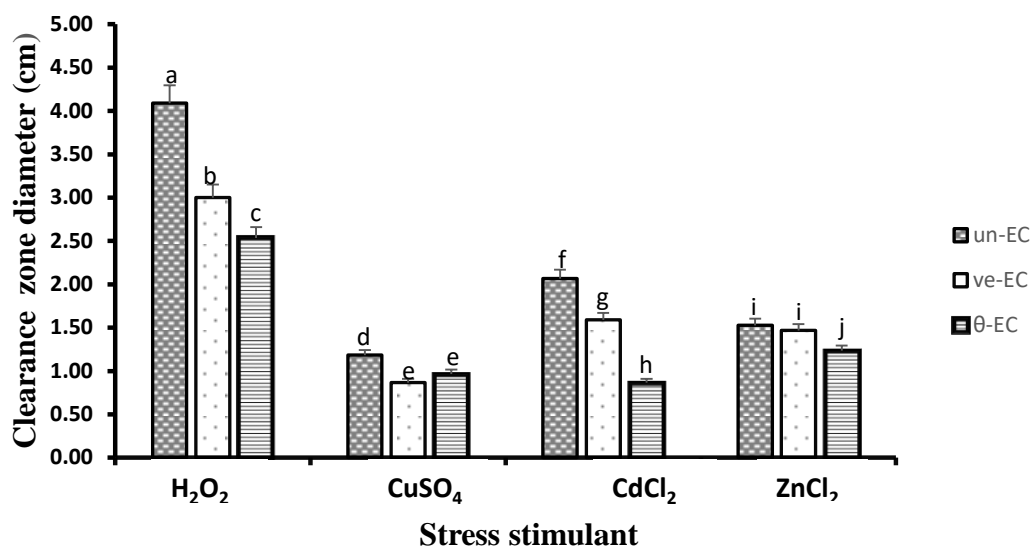
Fig. 13. Disk diffusion assay of AbGST-θ against E. coli BL21. The diameter of the clearance zone (cm) was measured in plates with untransformed E. coli (un-EC), E. coli transformed with the pMALc2X vector (ve-EC), and E. coli transformed with the AbGST-θ /pMAL-c2X vector (θ-EC). Disks were impregnated with H_2O_2, $CdCl_2$, $CuSO_4$, and $ZnCl_2$. Data are presented as mean ± standard deviation (n=3). Significant differences within each group were analyzed using a one-way analysis of variance (ANOVA) with Duncan's Post Hoc multiple comparisons test. Data indicated with different letters are significantly different (p < 0.05) within the group.

In the disk diffusion assay for AbGSTκ using H_2O_2, clearance zones were observed to varying degrees (Fig. 8) around all the disks. The largest clearance zone was observed in the untransformed *E. coli* plate, whereas the clearance zones of the other two plates were significantly smaller. At the same time, we demonstrated the effect of three

heavy metals (Cd, Zn, Cu) on AbGSTκ (Fig. 8) using the disk diffusion assay. All the disks treated with heavy metals in the LB agar plates showed clearance zones of varying degrees. For $CdCl_2$-treated disks, the maximum diameter of the clearance zone was observed for the untransformed *E. coli* plate, whereas the other plates had significantly smaller clearance zones (Fig. 8). For the $CuSO_4$-treated disks, the AbGSTκ-transformed plate did not show any significant change in the clearance zone diameter compared with that of the untransformed and vector transformed plates. Finally, for the $ZnCl_2$-treated disks, the highest clearance zone diameter was observed on the untransformed *E. coli* plate, whereas the AbGSTκ-transformed *E. coli* plate had a significantly smaller clearance zone diameter (Fig. 8).
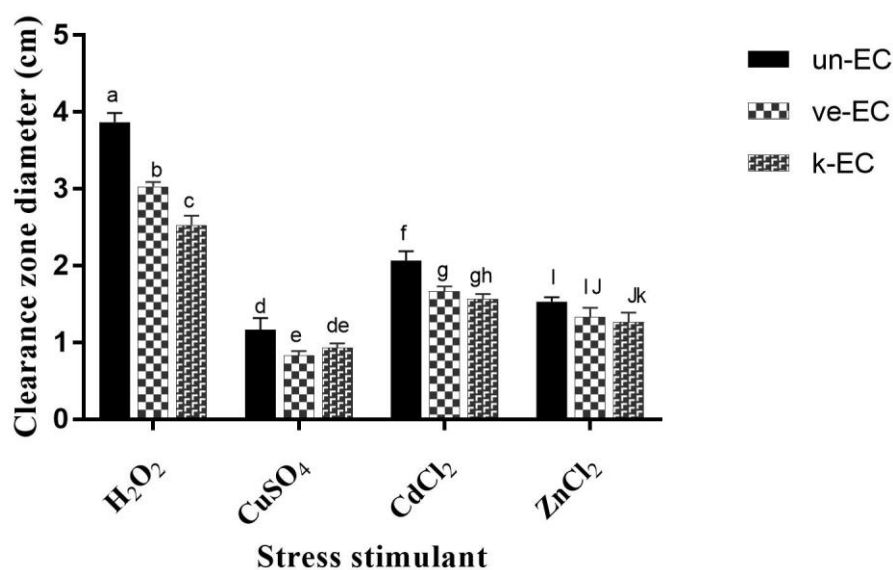
Fig. 14. Disk diffusion assay of AbGSTκ against E. coli BL21. The diameter of the clearance zone (cm) was measured in plates with untransformed E. coli (un-EC), E. coli transformed with the pMALc5x vector (ve-EC), and E. coli transformed with the AbGSTκ/pMALc5x vector (k-EC). Disks were impregnated with H_2O_2, $CdCl_2$, $CuSO_4$, and $ZnCl_2$. Data are presented as mean ± standard deviation (n=3). Significant differences within each group were analyzed using a one-way analysis of variance (ANOVA) with Duncan's Post Hoc multiple comparisons test. Data indicated with different letters are significantly different (p < 0.05) within the group.

4. Discussion

GSTs are identified as a diverse and important class of isoenzymes involved in the phase II detoxification system (Glisic et al., 2015). GST-θ is considered as the most ancient group which consists with two different types; GST-θ1 and GST-θ2 sharing 55% sequence identity in their protein structure. Among the numerous studies on GSTs, kappa class has been recognized as the least studied class (Hayes et al., 2005). Limited reports are available on their gene expression and functional studies, especially in mollusks. Therefore, in this study we are focusing on these two genes from GST superfamily: GST-θ and GST-κ identified from disk abalone (*Haliotis discus discus*).

In our study, we identified several characteristics of AbGST-θ and AbGSTκ by means of in silico analysis. Most of the cytosolic GSTs are available in nature as dimers with a molecular mass of a subunit varies from 23 kDa to 27 kDa (Blanchette et al., 2007). The predicted molecular weight of AbGST-θ (26.6 kDa) was agreed with other previously identified theta class GSTs (Saranya Revathy et al., 2012)(Bathige et al., 2014) and this also indicates the cytosolic nature of AbGST-θ. Furthermore, the absence of signal peptides within AbGST-θ also proposed it to be a cytosolic protein (Talmud et al., 1996). The instability index, which predicts the regional instability is calculated based on the weighted sum of dipeptides that occur more frequently in unstable proteins than in stable proteins, was 45.79 for AbGSTκ. This high value, being greater than 40, classifies this protein as being unstable (Guruprasad et al., 1990). The lack of a signal peptide suggests that the both proteins do not have any secretion properties. AbGSTκ also possessed the same general fold as DsbA, consisting of a thioredoxin domain (5–212 aa), which is interrupted by an alpha-helical domain, a characteristic feature of the GSTκ family. All members of the GST

super-family have the ability to bind glutathione tripeptides and therefore it has been suggested that G−sites have a highly conserved amino acid sequence (Ren et al., 2009) in GSTs. Agreed with that, NCBI-CDD analysis was exhibited the presence of N- terminal and C-terminal domains in AbGST-θ. According to the multiple sequence alignment, the N-terminal region can be determined as highly conserved while expressing more diversification in the C-terminal region. The G-sites in the N-terminal domain are involving in the maintenance of high affinity for GSH, while H-sites in the C-terminal domain are responsible for increasing the capability of enzyme in detoxifying high amount of substrates (Armstrong, 1997). The C- terminal variability indicates the diversification in the substrate specificity of the enzyme within the class towards xenobiotics (Blanchette et al., 2007). Altogether these binding sites are contributing in the catalytic activities of GSTs by forming multifunctional dimeric forms. The presence of H-site residues: G^{109}, A^{112}, M^{113}, F^{115}, I^{120} were identified as hydrophobic residues contributing in the hydrophobic nature of the protein surface. This hydrophobic nature is required for the binding of hydrophobic electrophiles. Moreover, theta class possess a conserved Ser residue at their N-terminal, instead of Tyr residue in other GSTs (α, π, μ) which is an unique feature of GST- θ (Board et al., 1995). This Ser^{11} residue is involving in the enzyme activation (Board et al., 1995). However it was stated that any mutation in this Ser^{11} residue has experienced in enzyme inactivation and therefore it is highly conserved among the theta class members (Board et al., 1995). Thereby the presence of Ser^{11} in AbGST-θ confirms its classification as a member of theta class GST and allow to possess proper enzyme activities in it. Comparing with the surface representations of human GST-θ with AbGST-θ, it is possible to identify a long extension of C-terminal tail in human GST-θ (Rossjohn et al., 1998). This explains the differences of GSH

binding affinity of mammalian and non-mammalian GST-θ (Rossjohn et al., 1998) as this extended C-terminal tail together with adjacent H-site can block the GSH binding site in mammals. However non-mammalian GST-θ possess very deep but accessible G-sites in their structure (Rossjohn et al., 1998) as already resulted from our study. Therefore, it is possible to expect high affinity of GSH binding activity from AbGST-θ comparing with human GST-θ according to structural analysis.

AbGSTκ protein also contains GSH binding sites (G-sites) in its amino acid sequence. Furthermore, the alignment analysis suggests that the AbGSTκ shares a putative conserved DSBA domain, which is an oxidoreductase domain involved in disulfide bond formation in the periplasm of gram-negative bacteria (Morel et al., 2004). Based on this fact, AbGSTκ can be recognized as part of the DSBA family, which is a subfamily of the thioredoxin family (Morel et al., 2004). Moreover, the catalytic residue (Ser) is highly conserved within the kappa class, which suggests that this residue plays a major role in the catalytic activation of GSH.

The primary structural analysis of AbGST-θ showed higher sequence similarities with other invertebrate and vertebrate orthologues (>53%). This allowed to suggest that GST-θ had relatively conserved through the evolution among all the analyzed organisms. Nonetheless the maximum identity and similarity of AbGST-θ could be observed from the molluscan orthologues indicating their evolutionary relatedness with the phylum Mollusca. Although the marine GSTs are not well classified up to date, in this study, it is possible to define a relationship for AbGST-θ with other previously identified GST-θ enzymes using the constructed phylogenetic tree.

Based on the sequence identity analysis of AbGSTκ, the highest identity was found with the pufferfish (*Takifugu obscurus*) (60.0%) ortholog with which it shared a 73.0% sequence similarity. Compared with the owl limpet *(Lottia gigantea),* AbGSTκ

had a 58.5% sequence identity demonstrating its similarity to other mollusks. The constructed phylogenetic tree branched into two main clusters separating the cytosolic GSTs and the mitochondrial GSTs. Clustering together with mitochondrial GSTs, AbGSTκ showed genetic distance from cytosolic GSTs. Collectively, these data clearly demonstrate that AbGSTκ is a member of the GSTκ class, and it has an evolutionarily distant relationship with other cytosolic GSTs. This finding is also supported by those of Ladner et.al (Ladner et al., 2004) and Robinson et.al (Robinson et al., 2004) who proposed that GSTκ exhibits structural, catalytic, and functional differences from other members of the cytosolic GST family, suggesting that it originated along a separate evolutionary pathway.

The 3D structure of AbGSTκ was modelled using the crystal structure of human kappa class glutathione transferase as a template, which shares satisfactory sequence identity and coverage with the AbGSTκ sequence. The 3D structure analysis showed the presence of α-helices and four conserved antiparallel β-sheets, which were also identified in *M. rosenbergii* GSTκ (Chaurasia et al., 2016). As illustrated in Fig. 3B the functional DSBA domain of AbGSTκ is distributed throughout the helices, coils, and sheets forming the butterfly-like shape of the dimer. These features are in agreement with the 3D model analysis of *M. rosenbergii* GSTκ performed previously (Chaurasia et al., 2016). Collectively, AbGSTκ possesses all the features of kappa class GSTs, as exemplified by its similarity at the tertiary structural level.

The level of GSTs expressions in different tissues showed significant variations due to number of factors as identified in early studies. For instance, sex of the organism, developmental stage, different tissue specific factors and the type of the xenobiotics in contact are some of the factors which can modulate the regulation and expression of GSTs (Saranya Revathy et al., 2012). Moreover, these variations may (Wan et al.,

2008a)(Wan et al., 2008a) have occurred due to the multiple functions of the GSTs (Wan et al., 2008a). Human *GST-θ* expressed highly in kidney, liver, small intestine and in brain (Chandra, 2017). In hermaphroditic fish *Rivulus marmoratus GST-θ* has given its higher expression in liver, intestine, gonad, and in skin (Lee et al., 2006). Apart from that, *GST-θ* from *Macrobrachium rossenbergii* was expressed highly in hepatopancreases and hemocytes (Arockiaraj et al., 2014). Moreover*, in Apostichopus japonicus,* highest expression levels of *GST-θ* were observed in intestine and in respiratory tree (Shao et al., 2017). As reported in a previous study on Manila clam (*Ruditapes philippinarum*), *GST-θ* highly expressed in hemocytes, gill and in mantle (Saranya Revathy et al., 2012). Furthermore, previous studies focused on disk abalone GST isoforms have demonstrated that their expressions in wide range of tissues in different extent. Disk abalone *GST-μ* (Wan et al., 2008b) has resulted with its highest expressions in gill and gonad while *GST-σ* showed its higher expressions in gonad, foot, gill and digestive tract (Wan et al., 2008a). Moreover, disk abalone *GST -ω* was highly expressed in gonad and digestive tract and *GST-κ* highest expressions were observed in digestive tract, mantle and in muscle (Sandamalika et al., 2018). Since the highest expressions of disk abalone *GST-θ* was observed in digestive tract and in hepatopancreases in this study, it also suggests the tissue specific and isoform specific manner of GSTs along with previous evidences. Usually various exogeneous and endogenous harmful compounds get directly contact with the digestive tract of the aquatic animals. Furthermore, in mollusks, digestive tract is one of the main organ involving in the accumulation and detoxification of toxins apart from the immune defense and the metabolic and homeostatic regulation (Marigómez et al., 2002). Therefore, the digestive tract should be equipped with free radical scavengers to mediate the high level of ROS produced during the oxidative respiration (Ataya et al.,

2014). Glutathione (GSH) is identified with its antioxidant potentials in cells which is regulated and controlled by GSTs in different cellular compartments (Ataya et al., 2014). At the same time GSTs are capable enough to detoxify various other electrophilic xenobiotics, such as environmental pollutions (Chen et al., 2017). Therefore, it is possible to have high amount of *AbGST-θ* in the digestive tract of the disk abalone as we have observed in this study, to maintain an effective detoxification system for the host. Moreover, hepatopancreases gets closely contact with the food digestion process of the organisms and in invertebrates it works as a functional analogue to liver in vertebrates (Contreras-Vergara et al., 2004). Therefore, hepatopancreases is required to contain high level of detoxification enzymes and thus we may have obtained higher expression of *AbGST-θ* in disk abalone hepatopancreases.

To understand the potential endogenous functions of AbGSTκ, its relative expression was examined in different tissues, which were prepared from the disk abalone organs and were analyzed using qPCR. In this study, the highest expression was observed in the digestive tract (Fig. 4). Based on previous studies on human GSTs, GSTκ mRNA was ubiquitously expressed in all the examined tissues at different levels (Morel et al., 2004). The highest expression of human GSTκ mRNA was observed in the kidney, liver, and adrenal gland (Morel et al., 2004). Based on the prawn (*M. rosenbergii*) tissue distribution, the highest GSTκ expression was found in the hepatopancreas, whereas the intestine had relatively low levels of expression (Chaurasia et al., 2016). In the domesticated one-humped camel (*Camelus dromedaries)*, the highest expression level was found in the liver, followed by the testis, spleen, kidney, and lung (Ataya et al., 2014). Several bivalve GST isoforms are expressed with differing abundances in different tissues. Disk abalone and rock shell have the highest

expression of GSTμ in the gill tissue (Rhee et al., 2008; Wan et al., 2008b) whereas the Manila clam has the highest GSTμ expression in the hepatopancreas (Zhang et al., 2012). In contrast, the Manila clam has the highest levels of expression of GSTδ and GSTθ in the gills and hemocytes, respectively (Kasthuri et al., 2013)(Umasuthan et al., 2012). As shown in previous studies on the black rockfish, the digestive glands of aquatic animals are usually associated with harmful exogenous and endogenous compounds (Jayasinghe et al., 2016). Therefore, it seems reasonable that it possesses an appropriate protection mechanism to allow for the survival of the organism. Previous evidence from a study in marine limpets has suggested that the digestive gland is involved in the accumulation and detoxification of toxins, and that the metabolizing enzymes act against ROS and xenobiotics, and are produced as a response to environmental and dietary factors (Cunha et al., 2008). Free radical scavengers are required in the digestive glands as high levels of ROS are produced due to oxidative respiration (Ataya et al., 2014). GSH is an important cellular antioxidant, and its regulation in different cellular compartments is critically controlled by GSTs (Ataya et al., 2014). Moreover, GSTs have the ability to detoxify multiple compounds, such as electrophilic xenobiotics, including environmental pollutants (Chen et al., 2017). Therefore, the data from our present study suggest that AbGSTκ is highly expressed in the digestive tract in order to ensure an effective protective detoxification mechanism in disk abalones.

Abalones live in dynamic environment filled with several pathogens and immunologically harmful conditions. To understand the role of *AbGSTs* in immune responses, we examined the transcriptional levels of *AbGST-θ* and *AbGSTκ* in gill tissue and in hemocytes after an immune challenge with bacteria, a viral mimic, and LPS. *V. parahaemolyticus* is a marine gram-negative bacterium that is considered to

be highly pathogenic to abalones, causing a withering syndrome (Zorrilla et al., 2003). Moreover, *V. parahaemolyticus* strongly affects the abalone post-larval stage resulting in a large degree of abalone mortality in the population (Lee et al., 2003). This high pathogenicity of *V. parahaemolyticus* was the reason we selected it as the bacterial pathogen in the immune challenge experiment in this study. Poly (I:C) is a double-stranded viral mimic, and we used this to assess the *AbGSTκ* response towards viral infections (Reisinger et al., 2015). LPS is a well-known pro-inflammatory immune stimulant and was used in this study to examine the mRNA expression patterns of *AbGSTκ* over immune stimulations (Nya and Austin, 2010). Abalones live in a marine aquatic environment and their gills are directly in contact with sea water, and consequently the gills act as one of the first target tissues for the entry and adhesion of bacteria. In addition, the mucus covering the gills may attract, or serve as a nutrient for several microbes (Rosenberg and Falkovitz, 2004). As a result of the circulation of hemolymph through the gills, pathogens can spread throughout the host and can infect other parts of the body. Several studies have revealed that gill tissues show significant changes in their expression of immune- and antioxidant-related genes in response to changes in environmental conditions (De Zoysa et al., 2009). Therefore, we selected gill tissues as a target site to analyze transcriptional changes in immune-related molecules. Evidence suggests that, hematopoietic tissue, hematopoiesis, and hemocyte circulation, are important basic immune system components in mollusks (Wang et al., 2017). As hemocytes can circulate freely, they can contribute to many different biological processes in bivalves including immunological homeostasis (Cochennec-Laureau et al., 2003). Hemocytes can come in contact with xenobiotics and are involved in the activation of phagocytosis, apoptosis, encapsulation, and several other cellular responses (Wang et al., 2017). Studies in mollusks have revealed

51

that following a challenge with the live bacteria *V. splendidus*, there is a significant increase in the total hemocyte count, number of regenerated hemocytes, and expression levels of hematopoiesis-related genes, suggesting an immune-related response (Wei et al., 2017). Based on these facts, we also selected hemocytes as another target tissue to analyze changes in *AbGSTs* mRNA levels in abalones following an immune challenge.

The results of our study suggest that the *AbGSTκ* gene is induced in response to challenge with bacteria, viruses, and LPS injection, and that there is a considerable variability in the patterns of expression that can be observed depending on the tissue type and the time. GSTs are detoxification enzymes that can act on several xenobiotics and many aquatic organisms show increased GST expressions after exposure to pollutants (Lee et al., 2007; Wan et al., 2008). Moreover, changes in GST expression have been observed following exposure to biological stresses, including different types of infectious pathogens (Umasuthan et al., 2012). Previous studies on abalone GSTs have indicated that both hemocytes and digestive glands have a higher expression of GSTs following bacterial invasion, than the gill and the mantle (Wang et al., 2016). This suggests that internal tissues are more sensitive to bacterial infections than external tissues (Umasuthan et al., 2012). In our study, we found that, although the gill tissue exhibited higher mRNA levels of *AbGSTs* under normal conditions, a much greater and significant relative induction was observed in hemocytes after the immune challenge. Similar data have been reported for the Manila clam GSTσ (Umasuthan et al., 2012), and thus it appears that hemocytes act as a secondary target tissue in the pathogen invasion process.

Our data also suggest that *AbGSTs* are associated with the mechanism underlying the protective effects against microorganisms' post invasion. Based on previous studies of

GSTs in *M. rosenbergii* (Arockiaraj et al., 2014), infection of prawns with pathogenic bacteria and viruses can affect the ability of GSTs to modulate the respiratory burst that is involved in stimulating ROS production, which is responsible for destroying pathogens and protecting the host cell (Hunaiti and Soud, 2000). The generation of ROS is considered to be one of the early responses in aerobic organisms following the recognition of a pathogen (Liu et al., 2000). A downregulation of *AbGSTκ* mRNA was observed in hemocytes following an immune challenge. This response is different from what has been observed for other invertebrate GSTs, which showed a significant upregulation after a challenge with immune stimulants (De Zoysa et al., 2008)(Li et al., 2012). However a downregulation of GSTδ has been observed in the razor clam (*Solen grandis*) following a challenge with a gram-negative bacteria (Yang et al., 2012), in agreement with our data. These downregulations suggest that the activation of various GSTs might occur through different mechanisms. *GSTκ* is localized to the mitochondria and peroxisomes, which are both involved in lipid metabolism and oxygen consumption (Sasagawa et al., 2016). Therefore, downregulation of GSTκ may increase oxidative stress and lipid peroxidation, and contribute to mitochondrial dysfunction (Sasagawa et al., 2016). This increase in oxidative stress activates the serum response factor (SRF), resulting in an increase in serum-inducible genes, which can affect many physiological processes such as proliferation, wound healing, migration, and tissue remodeling (Sasagawa et al., 2016). Therefore, we suggest that, in hemocytes, as a highly sensitive internal tissue, *AbGSTκ* has a different expression pattern after a challenge with immune stimulants. GSTs act as major antioxidant defense system to combat pathogens and being a member of this superfamily, it is logical that GSTθ and GSTκ also play a role in the anti-infection process. Collectively, with the data obtained on *AbGSTs* mRNA levels following bacterial,

viral mimetic, or LPS treatments, the present study has provided evidence for the involvement of *AbGSTs* in protecting the host by functioning in the innate immune response.

To determine the optimal conditions and the specific activities of AbGSTs, different substrates, including CDNB, DCNB, 4-NPB, 4-NBC and ECA were used with rAbGSTs and MBP (Table 2). Detectable activity was obtained only using CDNB as the substrate. No significant activity was detected for MBP against each substrate and therefore it was treated as a control and further functional studies were conducted only with rAbGSTs. The rAbGST-θ showed its highest activity towards the CDNB; an universal GST substrate, comparable with GST-θ homologues from Manila clam (Saranya Revathy et al., 2012) and silkworm (Yamamoto et al., 2005) but in contrast with human (Hayes and Pulford, 1995) and rat (Harris et al., 1991). The contrasted results with human GST-θ is agreed with the structural variations observed between mammalian and non-mammalian GST-θ as described in 3D structural analysis. However, no detectable activity of rAbGST-θ was observed towards the DCNB substrate comparable with mammalian (Tan and Board, 1996) and molluscan (Saranya Revathy et al., 2012) GST-θ homologues. Although the level of activity varies among different species, activation of rAbGST-θ towards predominantly halogenated aromatics suggests that rAbGST-θ possess the same substrate profile along with the GST-θ class enzymes from Manila clam and silk worm.

Based on previous studies using CDNB as a substrate, the specific activity of human GSTκ1 was 7.4 μmol/min/mg (Robinson et al., 2004), mouse GSTκ was 154.8 μmol/min/mg, and rat GSTκ was 54.4 μmol/min/mg (Jowsey et al., 2003). These data reflect the fact that the human, mouse, and rat, kappa class enzymes, along with disk abalone, have a similar substrate profile, being active towards predominantly

halogenated aromatics; however, the level of activity does vary across species.

To analyze the catalytic properties of rAbGST-θ, Michelis-Menten kinetic parameters were determined. The V_{max} and K_m values for any molluscan GST-θ have not been determined up to date. However, by the values obtained from the Lineweaver-Burk plot, rAbGST-θ showed relatively similar enzyme kinetic parameters along with Australian sheep blowfly (Board et al., 1995), silkworm (Yamamoto et al., 2005) and fish (Lee et al., 2006) with CDNB substrate.

Apart from that, rAbGST-θ showed their optimum CDNB conjugation activity at a higher temperature (~37 °C) proposing GST-θ high temperature adaptability, in line with the study of Manila clam GST-θ (Saranya Revathy et al., 2012). Moreover, the CDNB: GSH conjugation activity of rAbGST-θ extended for a range of pH. Early study based on Manila clam (Saranya Revathy et al., 2012) reported that a narrow pH range (5.5-6.5) contrast with our study. Collectively, having maximum activities of rAbGST-θ in a diverse range of temperature and pH, allow us to expect AbGST-θ mediated host defensive activity of abalones in a dynamic environment. For the determination of the inhibition of CDNB-GSH conjugating activity of rAbGST-θ, CB was used as pre-defined GST inhibitor by previous studies. The activity inhibition indicates the presence of a dinucleotide fold in the protein which facilitates the binding of CB to the protein although this was challenged by the lack of inhibition by NAD^+ or $NADP^+$ (Kalim Tahir et al., 1985).

To the best of our knowledge, the substrate affinity and specific enzyme activity of the mollusk GST kappa using CDNB as a substrate have not been studied to date. Based on a previous study of human GST kappa (hGSTκ1) (Robinson et al., 2004), the K_m and V_{max} for variable GSH concentration were 3.3 mM and 21.4 μmol/min/mg, respectively, which agree with our data. From the same previous study (Robinson et

al., 2004), a V_{max} value for hGSTκ1 of 40.3 μmol/min/mg was reported when CDNB was used as the variable substrate. However, the data from our study were fitted with the Michaelis-Menten equation and clearly show that rAbGSTκ has a low affinity for both CDNB and GSH, indicating that catalyzing a conjugation reaction may not be the natural role for the kappa-class GSTs, as has been stated previously (Robinson et al., 2004).

In our study, we determined the optimum temperature for the CDNB conjugation activity of rAbGSTκ (35°C). This temperature was higher than the optimum temperature of *Pseudomonas sp.* DJ77 GST (30°C) (Kim et al., 2000), and agreed well with that of *E. coli* JM83 GST (35°C) (Arca et al., 1990), and was lower than that for *Culex pipiens* GST (44°C) (Samra et al., 2012) and *Monopterus albus* GST (45°C) (Huang et al., 2008). By achieving its highest CDNB conjugation activity at a comparatively high temperature (35°C), AbGSTκ was found to adapt to a higher temperature. rAbGSTκ was also shown to have GSH: CDNB conjugating activity over a broad pH range (Fig. 7B). hGSTκ1 exhibited its conjugating activity over a pH range of 6−10.5 with an optimum activity at ~ pH 9, having the highest activity between pH 8 and 9.5, which is line with our data (Robinson et al., 2004). However, to date, there have been no reports on the optimal temperature or pH for GSTκ mollusk counterparts. The data of this study indicate that the maximal activity of rAbGSTκ is observed over a diverse range of temperature and pH values. This may explain the fact that AbGSTκ individually, and other GSTs together, have helped the abalones to adapt successfully to life in an environment with a wide range of temperatures and pHs. More studies using different mollusks will be required to address this matter further.

CB has often been used as an inhibitor of rAbGSTs, since it has been identified to be

an effective inhibitor of GSTs in previous studies (Jayasinghe et al., 2016). Therefore, we used CB in our study to determine the complete inhibition and IC_{50} value of CB for rAbGSTκ. Although CB is an effective GST inhibitor, it is thought that CB binding indicates the presence of a dinucleotide fold in AbGSTκ. This is contradicted by the lack of inhibition of GST transferases by NAD^+ or $NADP^+$ (Mannervik et al., 1985).

H_2O_2 is a well-known source of oxidative stresses, and is involved in pathological damage in several diseases (De Zoysa et al., 2008). GST's capacity to protect the oxidative cell from stress induced by H_2O_2 has been clearly documented in a previous study (Fiander and Schneider, 1999). From the results obtained in the disk diffusion assay, it is clear that AbGSTκ expressed in *E. coli* is more efficient at overcoming the oxidative stress caused by H_2O_2.

Heavy metals are common aquatic pollutants that are released into the aquatic environment through both natural and anthropogenic sources. Cd is a heavy metal that is toxic to a variety of aquatic species, affecting their growth, behavior, and physiological functions (Bertin and Averbeck, 2006). Cd can interfere with cell cycle progression, proliferation, differentiation, DNA replication and repair, and apoptotic pathways (Bertin and Averbeck, 2006). It can also induce oxidative stress by increasing the levels of superoxide anions and hydrogen peroxide. Cu is a trace mineral essential for all living organisms which functions as a cofactor in numerous enzymes and is required for their structural and catalytic properties (Reports, 2014). Excess Cu induces ROS formation through the production of hydroxyl radicals, and ultimately is toxic to cells (Reports, 2014). Zinc (Zn) is also an essential trace element involved in protein synthesis, enzyme catalytic function, and carbohydrate metabolism (Hambidge and Krebs, 2001). An excessive amount of Zn can play either

an inhibitory or enhancing role in H_2O_2-induced transcriptional changes in GSTs (Hodgson, 2010).

Our results from the disk diffusion assay suggest that AbGSTs has a significant protective activity against the stress caused by exposure of cells to H_2O_2, Cd, and Zn, consistent with the data from previous studies (Hambidge and Krebs, 2001; Reports, 2014). Moreover, the oxidative stress caused by H_2O_2, was significantly reversed by the presence of AbGSTs, indicating its strong ability to protect the cell from oxidative stress. AbGSTs expression was not able to protect *E. coli* from cell stress caused by excess Cu since there were no significant differences in the clearance zone diameters compared with that of the untransformed *E. coli* plate. The clearance zone around the $CdCl_2$ disks were not clearly defined, as has been reported previously (Jayasinghe et al., 2016), suggesting that toxicity retards bacterial growth rather than causing the death of the bacteria. Collectively, AbGSTs has a significant protective activity against Cd and Zn toxicities but does not have a significant protective effect against Cu toxicity. These data provide evidences that the antioxidant role of GSTθ and GSTκ in disk abalones is involved in overcoming heavy metal stress in their living environment to allow them to survive. However, once abalones are exposed to heavy metal pollution, the extent of survival may vary depending on the concentration of the heavy metal, time of exposure, and other environmental conditions.

5. Conclusion

In conclusion, we have identified a full-length cDNA encoding disk abalone GSTθ and GSTκ and cloned them into their corresponding expression vectors and characterized the purified recombinant AbGST-θ and AbGSTκ proteins. Functional domains and conserved regions were identified by sequence analysis and query of publicly available databases. Different xenobiotic substrates were used to analyze the

GSH-conjugating enzymatic activities of GSTs and as a result, from kinetic studies, we found the both enzymes had a low affinity for both CDNB and GSH as substrates. The pH and temperature optima for enzymatic activity were determined and suggest that abalones can adapt to a wide range of environmental changes. A tissue distribution analysis of *AbGSTκ* mRNA showed the highest level of expression in the digestive tract and the mantle. The digestive tract and the hepatopancreas showed the highest tissue specific distribution for *AbGST-θ*. By analyzing the relative mRNA expression of *AbGSTs* after different immune stimulants, their responsive to pathogens was determined. Finally, a disk diffusion assay was used to assess the ability of AbGSTs to protect the cells from oxidative and heavy metal stresses. Apart from the classical view of detoxifying xenobiotics by GSTs, our data suggest that the theta and kappa class GST isoenzymes are also involved in the modulating the cellular stress response in abalones.

CHAPTER 2:

Two phospholipid scramblase 1–related proteins (PLSCR1like-a & -b) from Liza *haematocheila*: Molecular and transcriptional features and expression analysis after immune stimulation

1. Introduction

In all living organisms, cellular membranes consist of a double layer of lipids known as phospholipids where proteins are embedded (Pomorski and Menon, 2006). In the plasma membrane, out of a variety of phospholipids, phosphatidylcholine (PC) and sphingomyelin (SM) are located in the extracellular leaflet, while phosphatidylethanolamine (PE) and phosphatidylserine (PS) are present only in the cytoplasmic leaflet (Contreras et al., 2010). Under normal conditions, cells maintain this membrane asymmetry, and it gets disrupted under some critical conditions, such as activation of cells, coagulation, and apoptosis, which may be affected by the phospholipid translocation (Sahu et al., 2007).

Amino phospholipid translocases are the enzymes that can move PS to the cell surface from the inner leaflet by means of passive diffusion (Bevers et al., 2016; Srinivasan and Basu, 1996). Nonetheless, when considering the time required for the overall process of apoptotic cell death culminating cell lysis, it takes a similar amount of time or less than that of the halftime for trans-bilayer diffusion (Srinivasan and Basu, 1996). Therefore, it is clear that another membrane protein is involved in the above process for the rapid movement of PS to the cell surface and effective removal of apoptotic cells before the initiation of cell lysis and inflammation (Srinivasan and Basu, 1996). This protein has been identified as phospholipid scramblase (PLSCR), a nonspecific lipid flippase, which allows for rapid flipping through lipid bilayers and effectively disturbs the asymmetry of phospholipid bilayers (Williamson and Schlegel, 2002). Aside from apoptotic cells, this mechanism can also be observed in platelets, which eventually activate the process of blood coagulation (Zwaal et al., 1998).

It has been reported that the recognition of cell membrane surface PS and limiting the

PS localization to the outer leaflet of the plasma membrane have been phylogenetically conserved in vertebrates and mammals for millions of years (Williamson et al., 2001). However the identity and the mechanisms of their regulation for control over PS distribution are not clarified well (Williamson and Schlegel, 2002). On the other hand, scramblases get activated in response to an increment of Ca^{2+} concentration, and after activation they get redistributed throughout the plasma membrane rapidly via an unknown mechanism. As a result of this change, the targeted cellular membrane PL bilayer loses its asymmetry (Williamson and Schlegel, 2002).

PLSCRs consist of several functionally important domains. They are named as proline-rich N-terminal domain, cysteine-rich region, the Ca^{2+}-binding motif, a nuclear localization signal (NLS), the DNA-binding motif, and a transmembrane region (Chen et al., 2005; Sahu et al., 2007). All these identified domains have specific functions. The N-terminal region contains multiple proline-rich domains, which interact with SH3 and WW domain–containing proteins (Rayala et al., 2014). The Ca^{2+}-binding motif is required for Ca^{2+}-binding and activation (Sahu et al., 2009), whereas the cysteine-rich motif is involved in membrane anchoring (Wiedmer et al., 2003). The DNA-binding motif is responsible for the protein–DNA interactions in transcriptional regulation (Sahu et al., 2007). A nonclassical NLS is essential for the nuclear localization of PLSCRs (Chen et al., 2005), and the transmembrane region is required for insertion into the membrane (Sahu et al., 2007).

PLSCRs are a group of homologous proteins, and four isoforms have been identified in humans named as hPLSCR1–hPLSCR4 (Zhou et al., 2000). The functions of hPLSCR1 have been identified as expression of different levels of PS on the cell surface, regulation of blood coagulation properties, and effective contribution to

apoptosis (Sahu et al., 2009). Besides, recent studies revealed that hPLSCR1 interacts with cell signaling pathways and works as a transcription factor in activation of other genes (Sahu et al., 2007; Zhou et al., 1997). Although hPLSCR1, -3, and -4 are detectable in various types of tissues, there are a few exceptions (Sahu et al., 2007). hPLSCR1 and -3 are undetectable in the brain, whereas hPLSCR4 is absent in peripheral-blood lymphocytes (Sahu et al., 2007). Moreover, hPLSCR2 is restricted to testes (Sahu et al., 2007). hPLSCRs have been documented as multifunctional proteins because they are involved in the main cellular processes like cell proliferation (Huang et al., 2006), antiviral responses (Dong et al., 2004; Lizak and Yarovinsky, 2012; Sivagnanam et al., 2017), apoptosis (Segawa and Nagata, 2015; Sivagnanam et al., 2017; Williamson et al., 2001), transcriptional regulation (Sivagnanam et al., 2017), tumor suppression, and protein interactions. Most of the documented experiments with PLSCRs are carried out to identify the roles of human PLSCRs. Recently, aside from human studies, some reports on PLSCRs of planarian *Dugesia japonica* (Han et al., 2017), mice, and *Drosophila melanogaster* became available (Acharya et al., 2006). Moreover, a study focused on PLSCRs of *D. japonica* have explained the involvement of PLSCRs in immune responses upon pathogen invasion (Han et al., 2017). To date, no records are available for any study on PLSCRs in fish. Therefore, this report is the first attempt at characterization of PLSCR1 from fish, with a focus on its molecular mechanism of action and immunological functions.

Red lip mullets (*Liza haematocheila*) are naturally populated among the tropical and temperate regions of the world and are considered an important species in aquaculture (Han et al., 2015). Recently, mass mortality of red lip mullets was observed during cultivation, owing to disease outbreaks caused by pathogenic species (Han et al., 2015). Therefore, identification of novel immunity-related genes as well as their

responses to pathogens is essential for disease prevention and development of the aquaculture industry. In this study, two *PLSCR1*-related genes: *PLSCR1like-a* and *PLSCR1like-b* were identified in the red lip mullet and molecularly characterized (Sahu et al., 2007). Furthermore, their involvement in post-immune responses to live bacteria and potent immune stimulants were determined.

2. Materials and methods

2.1. Experimental fish rearing and tissue collection

Red lip mullets were purchased from the Sangdeok fishery in Hadong, Korea. The average body weight of selected fish was set to be as 100 g. They were acclimated to the laboratory conditions, by rearing in 40 L flat-bottomed tanks with aerated and sand-filtered sea water for 7 days prior to the experiment. Salinity and temperature were maintained at 34 ± 0.6 ‰ and 20 ± 1 °C, respectively.

For tissue-specific expression analysis, five mullets were selected with the 100 g average body weight and were anesthetized conventionally (MS-222; 40 mg/L). For blood collection, heparin sodium salt (USB, USA)-coated sterile syringes were used to withdraw whole blood from the caudal vein of a mullet (~1 mL/fish), and the peripheral blood cells were separated immediately by the means of centrifugation at $3000 \times g$ for 10 min at 4 °C. After collection of blood, 11 types of tissues were collected including the head kidney, spleen, liver, muscle, gills, intestine, kidneys, brain, skin, heart, and stomach by dissection. All the collected tissues were immediately snap-frozen in liquid nitrogen and stored at -80 °C.

Another set of mullets was divided into four groups with 100 g average body weight and was subjected to an immune challenge experiment. Lipopolysaccharide (LPS; 1.25 μg/g, from *Escherichia coli* 055:B5; Sigma, St. Louis, MO, USA), polyinosinic:polycytidylic acid [poly(I:C) 1.5 μg/g], and *Lactococcus garvieae* (1×10^3 colony-forming units [CFU]/μL), were prepared in phosphate-buffered saline (PBS), and 100 μL was injected intraperitoneally into the fish. The control group of fish was injected with 100 μL of PBS. After the challenge, tissues from the spleen & head kidney were collected from five individuals at 0, 6, 24, 48, or 72 h post injection (p.i.) by the same method as described above. All the collected samples were snap-

frozen and stored at −80 °C until used for RNA extraction.

2.2. RNA extraction and cDNA synthesis

For tissue distribution and immune-challenge experiments, the collected tissue samples were pooled (n = 5), and total RNA was extracted by means of RNAiso plus (TaKaRa, Japan) followed by clean-up on RNeasy Spin Columns (Qiagen). The quality of RNA was determined by running 1.5% agarose gel electrophoresis and the concentration at 260 nm was measured using μDrop Plate (Thermo Scientific). The first-strand cDNA was synthesized with the Prime Script™ II 1st strand cDNA Synthesis Kit (Takara, Japan). The total volume of 20 μL reaction mixture was prepared which contained 2.5 μg of total RNA. Synthesized cDNA was diluted 40-fold with nuclease-free water and stored at −80 ℃ until further use.

2.3. Identification and sequence analysis of MuPLSCR1like proteins

A cDNA database of the red lip mullet was established via the PacBio sequencing technology (Rhoads and Au, 2015). The Basic Local Alignment Search Tool (BLAST) (Altschul et al., 1990), at the National Center for Biotechnology Information (NCBI) web-based query system (http://www.ncbi.nlm.nih.gov/BLAST), was used to identify putative *MuPLSCR1like-a & -b*. The complete open reading frames (ORFs) and their corresponding amino acid sequences were determined by means of an online server, ORF finder (https://www.ncbi.nlm.nih.gov/orffinder/). The SignalP software was used (http://www. cbs.dtu.dk/services/SignalP) to determine the availability and the localization of signal peptides (Petersen et al., 2011), while predicting the protein domains and functional sites by analysis in ExPASy prosite (http://prosite.expasy.org) (Sigrist et al., 2013). The Molecular Evolutionary Genetics Analysis (MEGA) version 6.0 software served for comparative analysis of evolutionary relations by constructing the phylogenetic tree via the Neighbor-joining method with 1000 bootstrap replicates

(Tamura et al., 2011). Pairwise sequence alignment was performed with the EMBOSS Needle (https://www.ebi.ac.uk/Tools/services/web/toolresult.ebi) web-based tool (McWilliam et al., 2013). Multiple sequence alignment was generated by Clustal omega (http://www.ebi.ac.uk/Tools/msa/clustalo) (Sievers et al., 2014) and Color align conservation (http://www.bioinformatics.org/sms2/color_align_cons.html) (Manipulation, 2000) web-based tool using the amino acid sequences obtained from the BLAST analysis. 2D structure was modeled on the PRED-TMBB (http://bioinformatics.biol.uoa.gr/PRED-TMBB/) web server (Bagos et al., 2004). To reveal 3D structure of MuPLSCR1like-a & -b, Swiss model (https://swissmodel.expasy.org) protein structure homology-modeling server (Schwede et al., 2003) was used, and the results were visualized in PyMOL v.1.5 software (DeLano, 2002).

2.4. Transcriptional analysis by Quantitative real time PCR (qPCR)

Transcriptional analysis in groups of unchallenged and immune challenged mullets was performed by qPCR on a Thermal Cycler Dice™ TP950 (Takara, Japan) following manufacturer's instructions. SYBR Green served as the fluorescent agent. For amplification of genes, gene-specific primers were designed according to the MIQE guidelines (Page, 2010) (Table 1).

Table 5. Sequences of primers used in this study

Primer name	Application	Sequence of primer (5'-3')
MuPLSCR1like-a _qF	qPCR amplification	GTGAGGTCTCTGGATGAGTCGATGG
MuPLSCR1like-a _qR		TCCCACCATCACAGCCTTCAT
MuPLSCR1like-b _qF		GCGTAACTCCATGGGCCAGAAC
MuPLSCR1like-b _qR		AGTGGTCTGGTGACGCTGATG
MuEF1α F	qPCR Internal reference	CCCTGGTCAGATCAGTGCTGGTTAT
MuEF1α R		AGCGTCGCCAGACTTTAGGGATTT

제주대학교 중앙도서관
JEJU NATIONAL UNIVERSITY LIBRARY

The total reaction mixture was 10 µL and consisted of 3 µL of a diluted cDNA template, 5 µL of 2× TaKaRa ExTaq™ SYBR premix, 0.4 µL of each forward and reverse primer (10 pmol/µL), and 1.2 µL of dH$_2$O (PCR grade). The qRT-PCR cycling program included a single cycle of 95 °C for 10 s; followed by 45 cycles of 95 °C for 5 s, 58 °C for 10 s, and 72 °C for 20 s; and a final single cycle of 95 °C for 15 s, 60 °C for 30 s, and 95 °C for 15 s. All the analyses were performed in triplicate to increase accuracy. For the standardization, mullet elongation factor 1 alpha (EF1α) (accession No.: MH017208) served as the internal control gene in the analysis with corresponding primers. By the Livak ($2^{-\Delta\Delta CT}$) method (Livak and Schmittgen, 2001) the relative mRNA expression levels were analyzed quantitatively. All the data from challenged groups were normalized to the relevant PBS control at each time point. All the obtained data were presented as fold changes (means ± standard deviation [SD]) using the 0 h expression of un-injected control as the basal level reference. To evaluate the statistical significance of the data, they were subjected to statistical analysis in the SPSS 16.0 software (USA). One-way analysis of variance (ANOVA) followed by Duncan's *post hoc* comparison test was carried out for the analysis of tissue-specific mRNA expression levels. The unpaired Student's *t* test was conducted in the immune challenge experiment for analyzing the significance of differences between control and experimental groups. Statistically significant data were obtained by considering the *P* values, less than 0.05 ($P < 0.05$).

3. Results

3.1. Identification and characterization of MuPLSCR1like-a and b

Two cDNA contigs belonging to the PLSCR family were identified in the red lip mullet transcriptome database using BLAST analysis and were designated as *MuPLSCR1like-a and MuPLSCR1like-b.*

The *MuPLSCR1like-a* (GenBank accession No: MH511809) encodes a polypeptide of 245 aa with a predicted 27.82 kDa molecular weight. The theoretical isoelectric point (pI) and the instability index of MuPLSCR1like-a were found to be 4.79 and 53.59, respectively. *MuPLSCR1like-b* (GenBank accession No: MH511810) encodes a polypeptide of 228 aa with predicted 25.74 kDa molecular weight. *MuPLSCR1like-b* has a theoretical pI value of 4.75. The instability index for *MuPLSCR1like-b* was calculated too: 49.51.

To identify the different characteristics of MuPLSCR1like-a and -b, analyses of several domains and motifs were performed. The protein sequence analysis performed by SignalP 4.1 server revealed that both MuPLSCR1like-a and MuPLSCR1like-b do not contain any signal peptides. Remarkably, in MuPLSCR1like-a, a DNA-binding motif was identified at positions 18–51 (aa), and a cysteine-rich region was identified at aa positions 113–121. MuPLSCR1like-a contained the NLS domain at aa positions 188–198 and a Ca^{2+}-binding motif was detected in the region 203–216 aa. Furthermore, a transmembrane region was detected at the C terminus at aa positions 220–238 in MuPLSCR1like-a. By contrast, in MuPLSCR1like-a, no proline-rich N-terminal domain could be detected by the protein sequence analysis. Similarly, MuPLSCR1like-b contains a DNA-binding motif at aa positions 5–37, an NLS domain at 175–186, and a Ca^{2+}-binding motif in the region 190–203 aa. The transmembrane region was detected at aa positions 207–225 in MuPLSCR1like-b.

69

Nonetheless, no proline-rich N-terminal domain or cysteine-rich region were detected in MuPLSCR1like-b. Moreover, both MuPLSCR1like proteins have a final short exoplasmic tail at their C terminus. In MuPLSCR1like-a, the exoplasmic tail extends up to 7 aa (^{239}IKPQRDS^{245}), and in MuPLSCR1like1-b, it is only 3 aa long (^{226}ITN^{228}; Fig. 15).
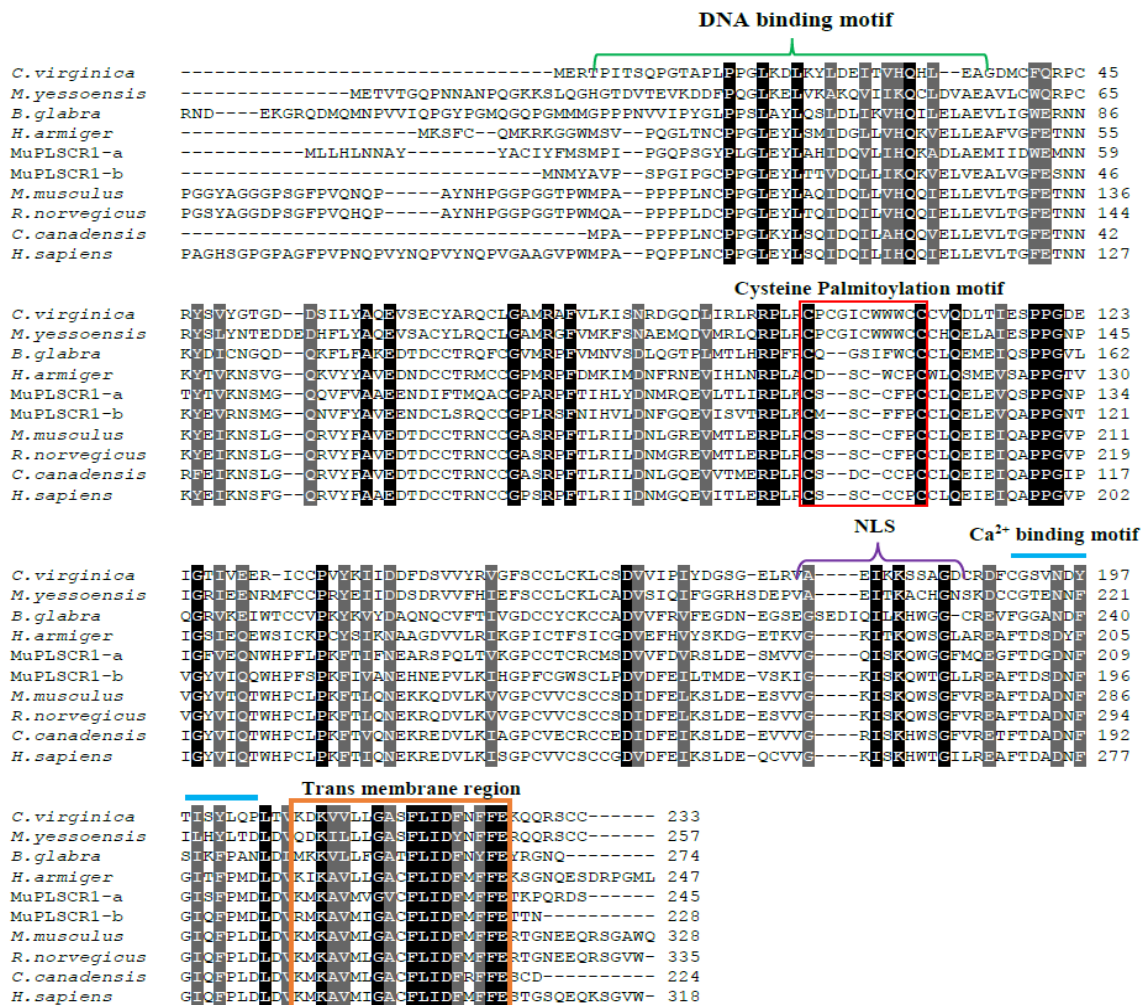

Fig. 15. Multiple-sequence alignment of the amino acid sequences of MuPLSCR1like-a & -b and its orthologs from different species. Fully conserved amino acids are shown in black, and strongly conserved and weakly conserved amino acids are highlighted in dark grey and light grey, respectively.

3.2. Homology analysis of MuPLSCR1like-a and -b

Protein BLAST analysis suggested that MuPLSCR1like-a and -b were similar to other (previously described) PLSCR1 and PLSCR1like homologues. The identity and similarity percentages were determined using the pairwise sequence alignment (Table 2). The results indicated that the highest identity (I%) and similarity (S%) for both MuPLSCR1like-a (I-53.5%, S-66.9%) and MuPLSCR1like-b (I-96.9%, S-98.2%) were shared with PLSCR1like of a fish, *Fundulus heteroclitus.* Moreover, the data revealed that both MuPLSCR1like-a and -b share greater than 48% identity with other fish homologues (Table 6).

Table 6. Pairwise identity (I%), similarity (S%), and gaps (G%) of red lip mullet PLSCR1like proteins toward selected orthologs at amino acid levels.

Gene	Species	Accession no.	MuPLSCR1like-a			MuPLSCR1like-b			Taxonomy
			I (%)	S (%)	G (%)	I (%)	S (%)	G (%)	
MuPLSCR1like-a	*Liza hematochelia*		100%	100%	0.0	54.7%	67.3%	6.9%	Fish
MuPLSCR1like-b	*Liza hematochelia*		54.7%	67.3%	6.9%	100%	100%	0.0	Fish
PLSCR2	*Larimichthys crocea*	KKF30002.1	54.7%	67.3%	6.9%	96.5%	98.7%	0.0%	Fish
PLSCR1 Like	*Fundulus heteroclitus*	XP_012708587.1	53.5%	66.9%	6.9%	96.9%	98.2%	0.0%	Fish
PLSCR1 Like	*Danio rerio*	XP_693207.5	51.6%	63.4%	12.9%	52.7%	66.4%	17.7%	Fish
PLSCR1 Like	*Oncorhynchus mykiss*	XP_021420053.1	48.2%	61.8%	9.2%	53.8%	70.4%	7.5%	Fish
PLSCR1 Like	*Cyanistes caeruleus*	XP_023788895.1	46.2%	56.8%	24.3%	47.5%	60.9%	19.7%	Aves
PLSCR1 Like	*Lonchura striata domestica*	XP_021392490.1	44.9%	55.1%	24.6%	48.8%	60.4%	19.4%	Aves
PLSCR1 Like	*Rattus norvegicus*	XP_017451607.1	47.2%	63.6%	8.8%	51.5%	71.1%	7.1%	Mammal
PLSCR1	*Homo sapiens*	NP_066928.1	44.0%	54.7%	23.0%	45.6%	56.3%	28.3%	Mammal
PLSCR1 Like	*Macaca nemestrina*	XP_011720023.1	42.1%	61.9%	6.5%	47.4%	67.9%	3.0%	Mammal
PLSCR1 Like	*Bos indicus*	XP_019816762.1	37.3%	56.8%	14.0%	39.8%	57.2%	15.5%	Mammal
PLSCR1 Like	*Xenopus laevis*	XP_018121282.1	39.2%	50.9%	31.3%	45.1%	57.6%	25.1%	Amphibia
PLSCR1 Like	*Mizuhopecten yessoensis*	XP_021374068.1	39.2%	50.7%	22.3%	44.1%	58.4%	18.9%	Mollusk
PLSCR1 Like	*Crassostrea virginica*	XP_022345293.1	21.5%	35.2%	24.4%	24.0%	38.3%	26.0%	Mollusk
PLSCR1 Like	*Limulus polyphemus*	XP_022256660.1	37.7%	48.9%	27.5%	47.1%	59.6%	23.9%	Arthropoda

The amino acid sequences of MuPLSCR1like-a and -b were compared with other orthologs from different taxonomic groups, and it was revealed that MuPLSCR1like-a and -b contain a conserved DNA-binding motif, a Ca^{2+}-binding motif, an NLS, and a C-terminal transmembrane region in their structure (Fig. 15). Only MuPLSCR1like-a has a conserved cysteine-rich region as identified by the sequence analysis. Nonetheless, both MuPLSCR1like-a and -b do not contain N-terminal proline-rich domains in their structures (Fig. 15).

3.3. The 2D and 3D structural analysis of MuPLSCR1like-a & -b

The 3D structures of both MuPLSCR1like proteins showed a 12-stranded symmetrical β-barrel, which encloses a central C-terminal α-helix (Fig. 16)
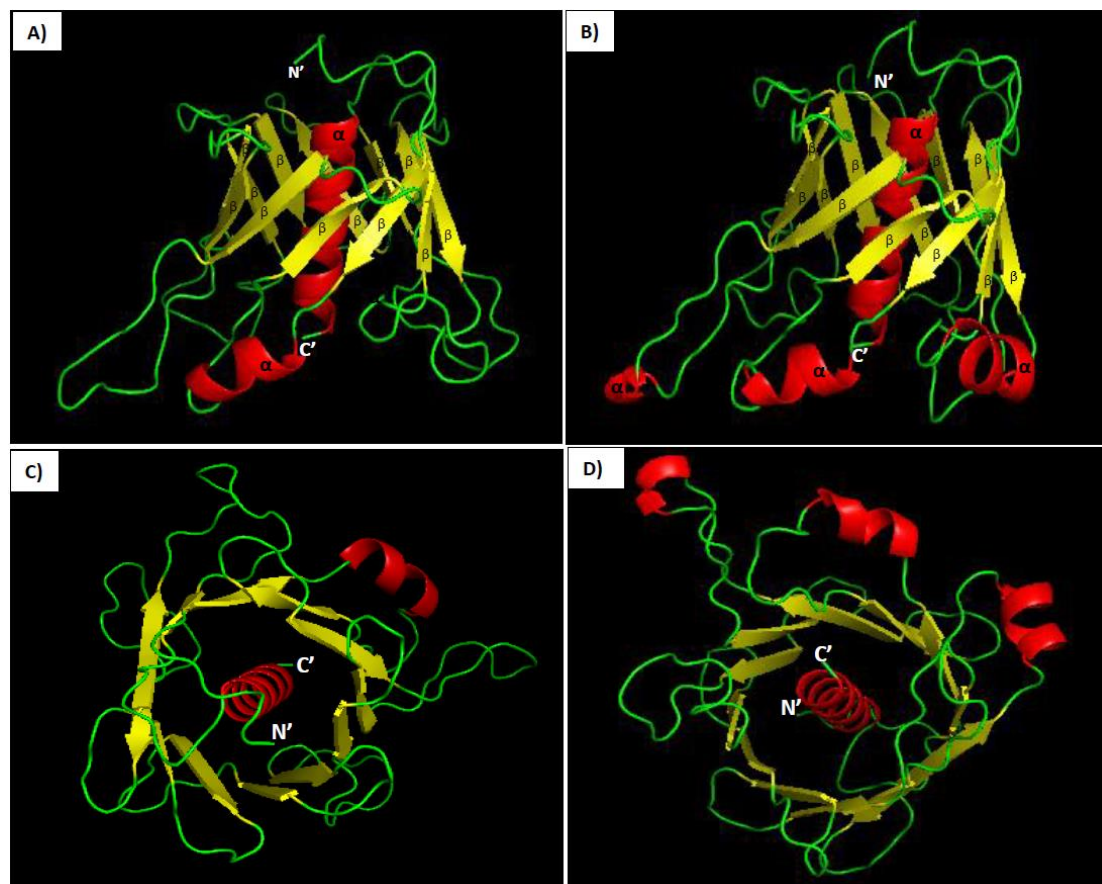
Fig. 16. A & B) Predicted 3D structures of MuPLSCR1like-a & -b, respectively. The α-helices and β-sheets are marked with the corresponding letters. **C & D)** The 12-stranded symmetrical β- barrel which encloses a central C-terminal α-helix in MuPLSCR1like-a & -b, respectively. The models of 3D structure were predicted using the Swiss-model server and were visualized in the PyMOL software.

The C-terminal helix is shown in side-to-outside orientation from the hollow cylinder.

Based on the Posterior decoding algorithm in PRED-TMBB, topology of the protein structures was clearly determined with respect to the phospholipid bilayer (Fig. 17).
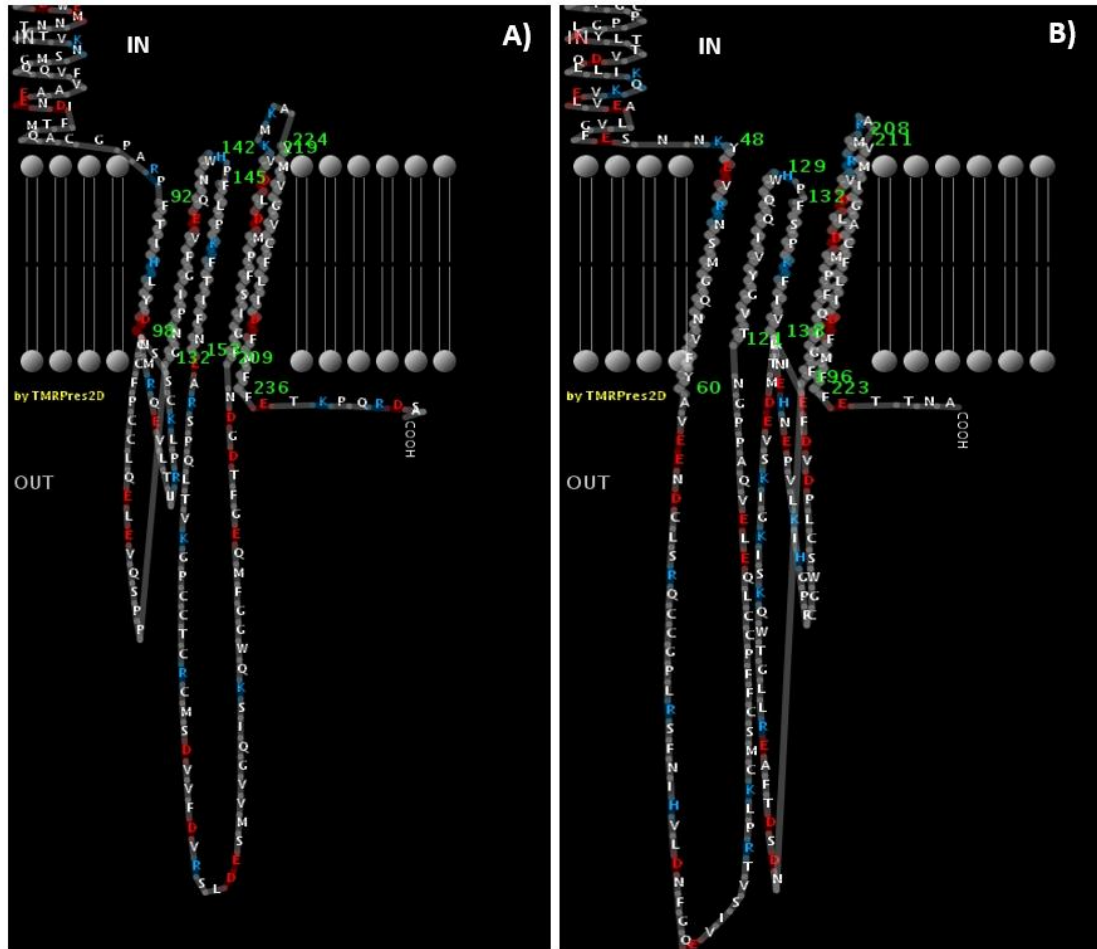
Fig. 17. A & B) Graphical representation of the predicted topology of MuPLSCR1like-a & -b with respect to the lipid bilayer. Output of the prediction obtained in the PRED-TMBB software by the posterior decoding method.

3.4. Construction of the phylogenetic tree

The phylogenetic tree was constructed by the neighbor-joining method to evaluate the evolutionary relations among MuPLSCR1like proteins (Fig. 18.).
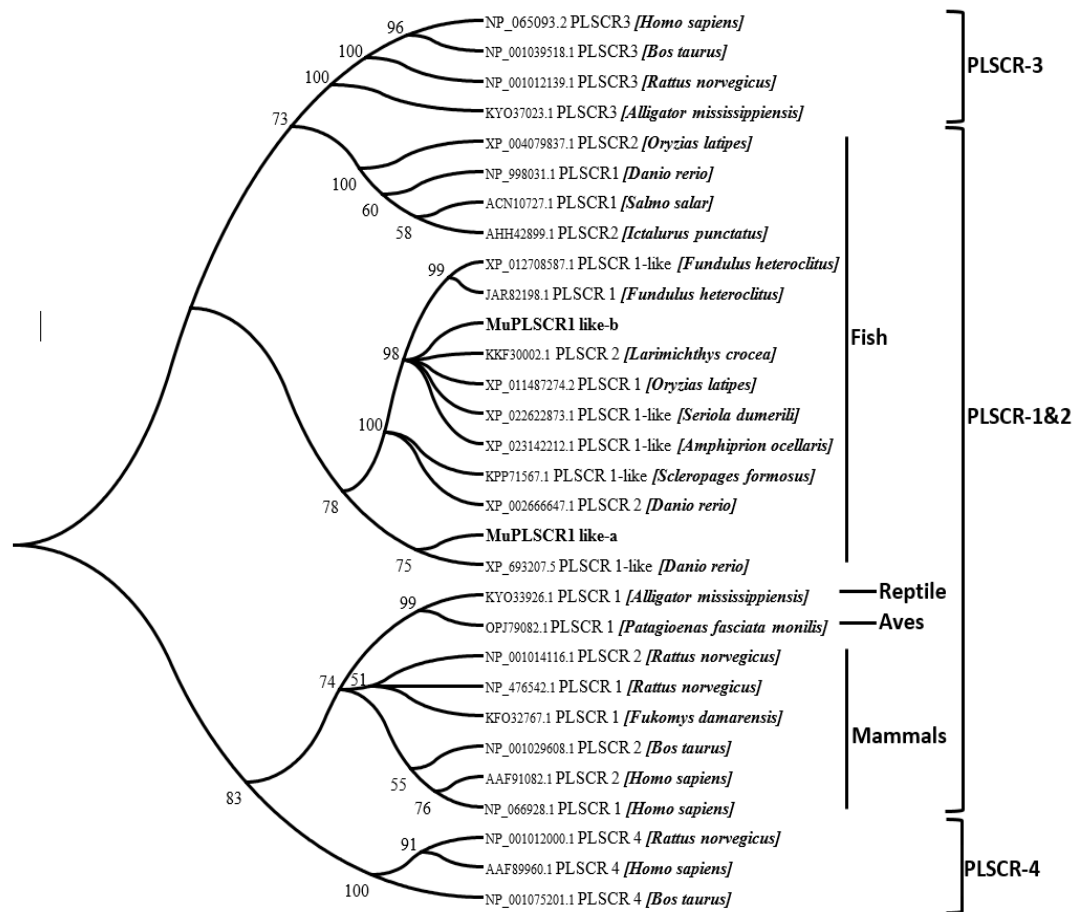
Fig. 18. A phylogenetic tree constructed by the neighbor-joining method based on different classes of PLSCRs. The bootstrap values are shown at the node of each branch. The NCBI accession numbers are given with each organism name.

According to these data, MuPLSCR1like-a and MuPLSCR1like-b are clustered in the same clade but from different branches together with other fishes' PLSCR1, PLSCR2, and PLSCR1like homologues. MuPLSCR1like-a showed close relatedness to PLSCR1like from *Danio rerio.* Additionally, MuPLSCR1like-b manifested a close relationship with PLSCR2 from *Larimichthys crocea* including PLSCR1 and PLSCR1like from other fish species.

3.5. Tissue distribution analysis of MuPLSCR1like-a and -b

Both *MuPLSCR1like-a* and *-b* were found to be expressed in all the examined tissues, including the head kidney, spleen, liver, gills, intestine, kidneys, brain, muscle, skin, heart, stomach, and blood, at different mRNA levels (Fig. 19.). *MuPLSCR1like-a* showed its highest expression in the intestine with ~56-fold value, following skin and muscle with ~43- and ~37-fold values, respectively ($p < 0.05$). In contrast, *MuPLSCR1like-b* manifested its strongest expression in the brain with a ~182-fold value, followed by muscle with a ~73-fold value ($p < 0.05$).

A)
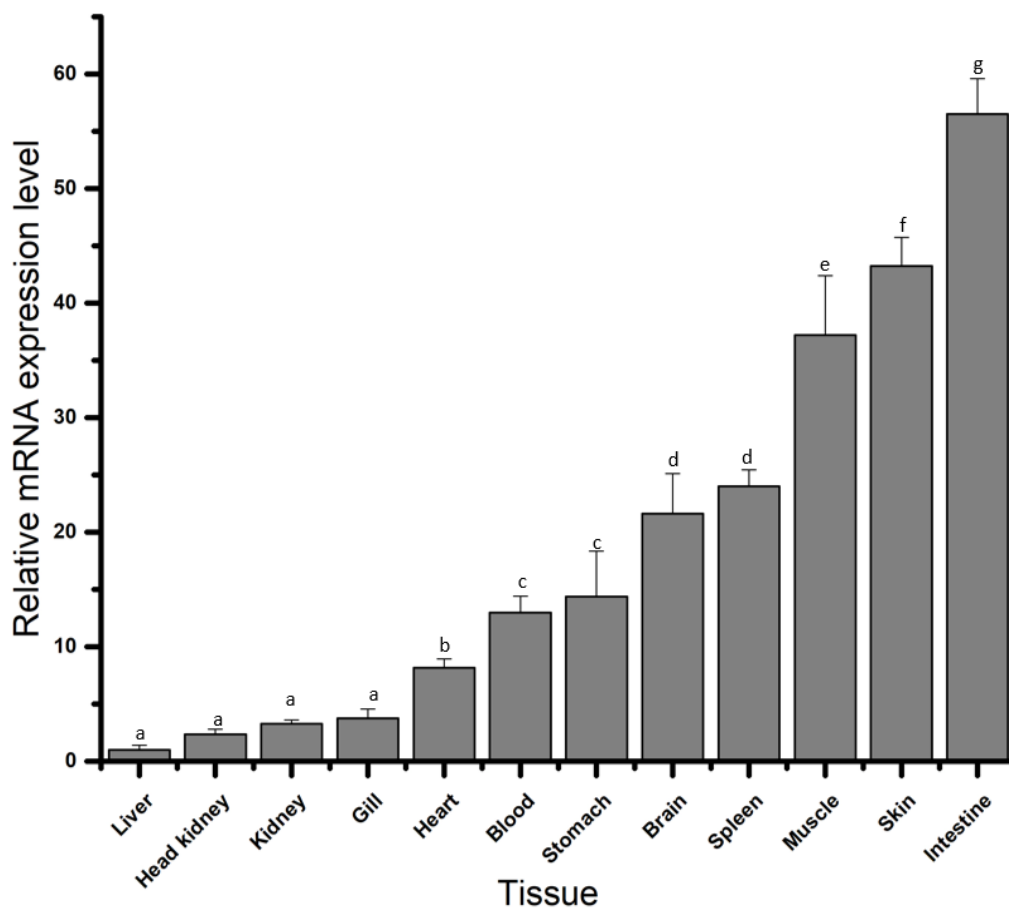
B)
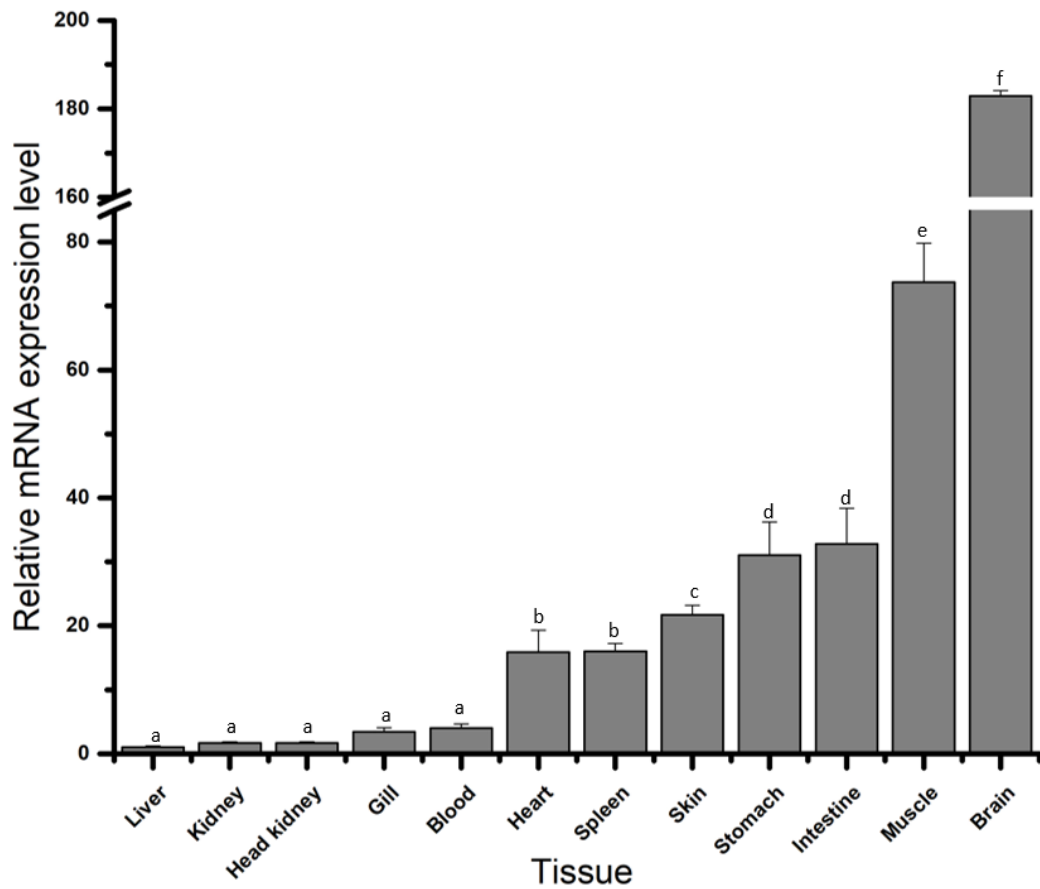
Fig. 19. **A) & B)** Tissue-specific transcriptional profiles of MuPLSCR1like-a & -b in red lip mullets. The calculations were performed by the Livak method. Data are presented as mean ± standard deviation (n = 3). Significance of inter-tissue differences was evaluated by one-way analysis of variance (ANOVA) followed by Duncan's multiple-range test in the SPSS 16.0 software. Identical letters indicate the absence of a significant difference (p < 0.05) between the tissues.

3.6. Expression analysis of MuPLSCR1like proteins after immune stimulation

To determine the potential involvement of *MuPLSCR1like-a* and *-b* in immune responses, transcriptional regulation in the spleen (Fig. 20 A–F) and the head kidney (Fig. 21 A–F) was analyzed at different time points, after injection of the fish with various immune stimulants including LPS, poly(I:C), or *Lactococus garvieae.*
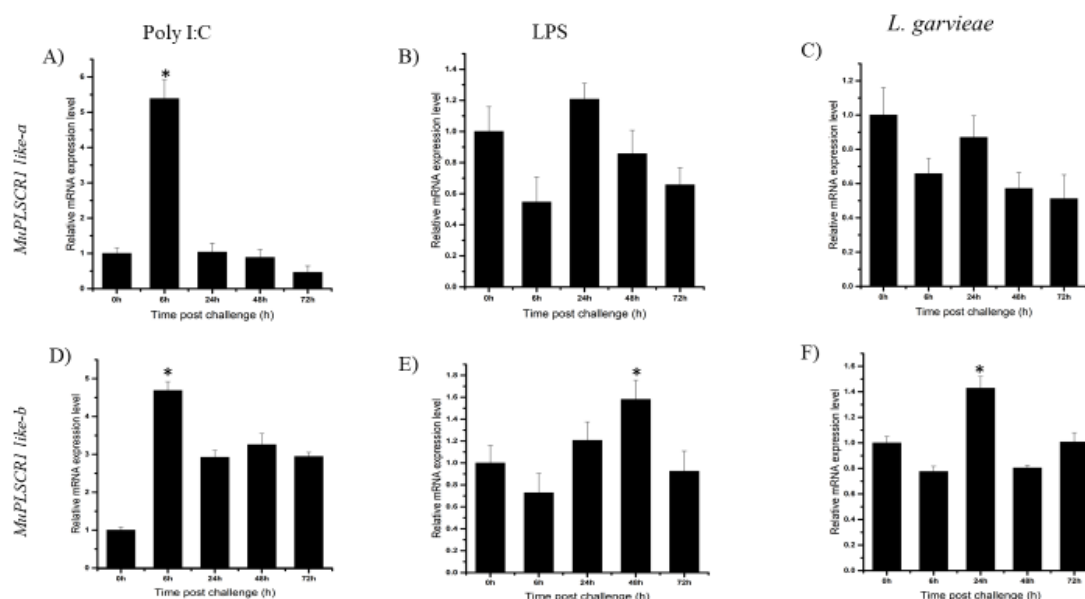
Fig. 20. Relative mRNA expression of MuPLSCR1like-a and MuPLSCR1like-b analyzed by qPCR over time in the spleen of red lip mullets (A–F) in response to challenges with poly(I:C) (A, D), LPS (B, E), and *L. garvieae* (C, F). Data are presented as mean ± standard deviation (n = 3). Data marked with a * represent a statistical difference in expression as compared with the 0 h p.i. baseline.

In the spleen, after stimulation with poly(I:C), the expression of *MuPLSCR1like-a* and *MuPLSCR1like-b* was significantly upregulated at 6 h p.i. (Fig. 20 A&D). The LPS treatment did not cause any significant upregulation or downregulation pattern for *MuPLSCR1like-a* as compared to the unchallenged group. Nevertheless, mRNA expression of *MuPLSCR1like-b* was significantly upregulated after 48 h p.i. (Fig. 20E).

As for *MuPLSCR1like-a*, the treatment with *L. garvieae* did not significantly alter gene expression either. By contrast, regarding *MuPLSCR1like-b*, the *L. garvieae*

treatment significantly upregulated the mRNA expression levels at 24 h p.i. (Fig. 20F).
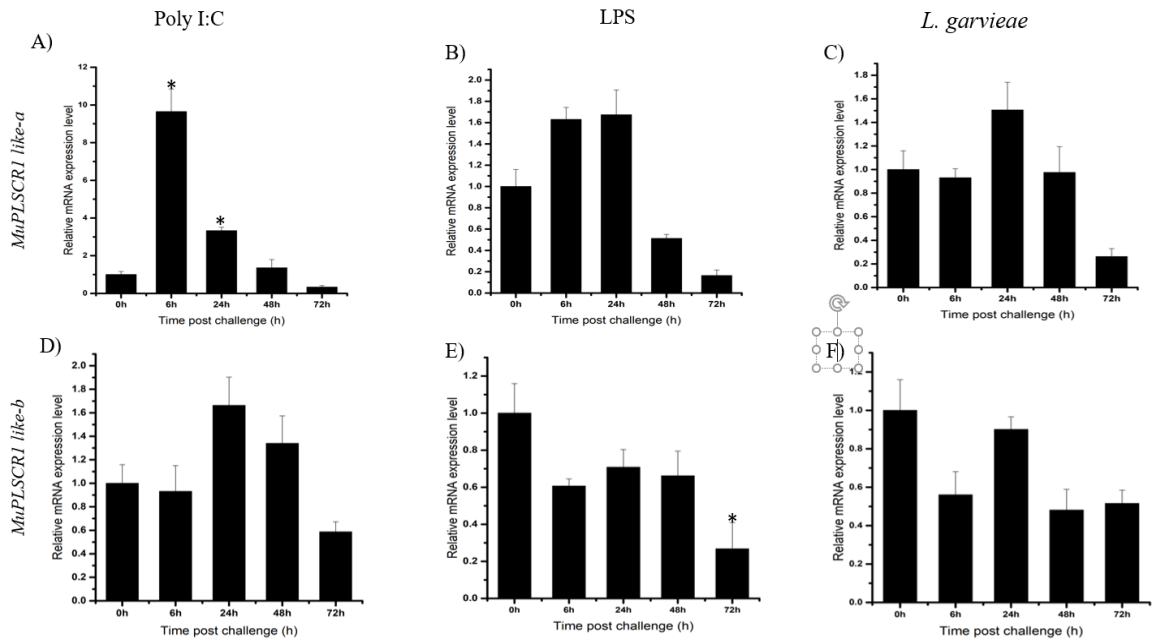
Fig. 21. Relative mRNA expression of MuPLSCR1like-a and MuPLSCR1like-b, analyzed by qPCR over time in the head kidney of red lip mullets (A–F) in response to challenges with poly(I:C) (A, D), LPS (B, E), or *L. garvieae* (C, F). Data are presented as mean ± standard deviation (n = 3). Data with marked with a * represent a statistical difference in expression as compared with the 0 h p.i. baseline.

In the head kidney, after poly(I:C) administration, only *MuPLSCR1like-a* was significantly upregulated at 6 and 24 h p.i. (Fig. 21A), while *MuPLSCR1like-b* did not show any significant alterations (Fig. 21D). Nonetheless, LPS induction significantly downregulated *MuPLSCR1like-b* after 72 h p.i. (Fig. 21E) without any significant alterations in *MuPLSCR1like-a* expression (Fig. 21B). Moreover, *L. garvieae* treatment did not cause any significant changes in *MuPLSCR1like-a* and *MuPLSCR1like-b* expression (Fig. 21C & F).

4. Discussion

Phospholipid scramblases are the proteins that facilitate rapid movements of phospholipid molecules along bidirectional pathways, ensuring the phospholipid asymmetry in the plasma membrane (Rayala et al., 2014). The previously identified PLSCR domains have their own distinct functions, which can be clarified separately (Sahu et al., 2007). From the results obtained in our study on MuPLSCR1like-a and -b, it was possible to identify most of the conserved domains and motifs in their sequences as well as slight differences from other PLSCR1 homologues. Therefore, because they share a common structural topology with PLSCR1 orthologs, MuPLSCR1like-a and -b were categorized as members of the scramblase family. According to one study by Sims et al. (Sims and Wiedmer, 2001), human PLSCRs contain multiple PXXP and PPXY domains, which are responsible for the ability of PLSCRs to interact with SH3- and WW domain–containing proteins, except for human PLSCR2. As revealed by our results, the N termini of both MuPLSCR1like-a and -b are not enriched in proline (Pro) residues, thus pointing to their weaker interactions with SH3- and WW domain–containing proteins.

The tertiary structure analysis of MuPLSCR1like-a and -b clearly showed the 12-stranded β-barrel which encompasses the central C-terminal α-helix, which is a common feature of scramblases (Bateman et al., 2009). This C-terminal helix has been previously identified as a transmembrane helix that is believed to be hydrophobic (Bateman et al., 2009). As suggested previously, this hydrophobicity may have developed due to the packing nature of the helix in the core protein domain, and therefore it is not a true transmembrane helix (Bateman et al., 2009). The 2D graphical representation clearly revealed the membrane-spanning segments of MuPLSCR1like-a and -b. These were formed by antiparallel β-strands, constituting a

barrel shape channel that spans the membrane.

Another major feature of scramblases is a DNA-binding domain, which enables the protein to interact with DNA (Sahu et al., 2007). As illustrated in Fig. 1, the region 18–51 aa in MuPLSCR1like-a and region 5–37 aa in MuPLSCR1like-b are the DNA-binding motifs, which show low conservation with homologues. Although little evidence is available about the DNA-binding properties of scramblases, studies on human PLSCR1 indicate that it interacts with the inositol 1,4,5-tri-phosphate (IP3) receptor type 1 (*IP3R1*) promoter (Frisby, 2006) and is reported to be highly conserved in mice, the fruit fly, zebrafish, and frogs (Sahu et al., 2007). In human PLSCR1, the DNA-binding motif spans aa residues at positions 86–118 (Wiedmer et al., 2000). Its deletion causes misfolding of the β-barrel because of removal of the first β-strand in the domain; there is evidence that this removal eliminates the capacity for DNA binding (Bateman et al., 2009). Therefore, persistence of DNA-binding motifs in MuPLSCR1like-a and -b probably maintains the correct folding patterns of the β-barrel in their structures, thereby ensuring the DNA-binding ability.

The cysteine palmitoylation motif is another functionally important region that regulates the trafficking of PLSCR to the nucleus or to the plasma membrane (Wiedmer et al., 2003). In our study, the cysteine palmitoylation motif was identified only in MuPLSCR1like-a while lacking in MuPLSCR1like-b. On the other hand, this motif is conserved in most of the sequences that have been identified previously, except for yeast (Sahu et al., 2007) and planarian (*Dugesia japonica*) sequences (Han et al., 2017).

Proteins that are destined to function inside the nucleus contain a classical NLS with three Arg/Lys residues that can form a basic patch over an imported cargo (Huang et al., 2006). The classical NLS has been recognized in the SV40 virus (PKKKRLV),

which has a positively charged amino acid sequence in its NLS (Chen et al., 2005). This sequence is replaced by hydrophobic residues in nonclassical NLS, discovered in human PLSCR1 as the aa sequence [257]GKISKHWTGI[266] (Chen et al., 2005). In agreement with that finding, we observed [189]GQISKQWGGF[198] in MuPLSCR1like-a and [176]GKISKQWTGL[184] in MuPLSCR1like-b, suggesting that MuPLSCR1like-a and -b possess a nonclassical NLS. The critical lysine residue located at the 5th position of a nonclassical NLS is highly conserved throughout all the examined organisms, and same was obtained in an early study by Sahu et al. in 2007 (Sahu et al., 2007).

A Ca^{2+}-binding EF-handlike domain structure has been identified in human PLSCR1, with two short α-helical segments close to the C terminus, which are separated by 12-residue acidic loops (Notredame et al., 2000). Nevertheless, the proposed structural model for hPLSCR1 indicates that this motif overlaps with one of the core β-strands of the β-barrel formation around the C-terminal α helix (Sahu et al., 2009). The same structural features were observed in the predicted 3D structural models of MuPLSCR1like-a and MuPLSCR1like-b in our study. Both MuPLSCR1like-a and MuPLSCR1like-b showed highly conserved amino acid residues at positions 1 (D), 3 (D), 5 (F), 7 (I), 9 (F), and 12 (D), which are supposed to contribute to the octahedral loop formation for binding to Ca^{2+} ions, and this arrangement is fully consistent with the predicted EF-handlike motif in hPLSCR1 (Sahu et al., 2007). According to a hypothesis advanced in early studies, replacement of those selected residues within the motif may abrogate the Ca^{2+}-binding ability of PLSCR1 and the expression of phospholipid scramblase activity too, which depends on the concentration of Ca^{2+} (Bateman et al., 2009). Therefore, we can suggest that by having conserved amino acid residues at critical positions of the motif, MuPLSCR1like-a and MuPLSCR1like-b may have the same Ca^{2+}-binding affinity as hPLSCR1 does.

Furthermore, the transmembrane domain at the C terminus is essential for scrambling activities (Sánchez-Magraner et al., 2014; Zhou et al., 1997). Additionally, although the Ca^{2+}-binding domain exists in the sequence, deletion of the C-terminal α-helix of the transmembrane region causes misfolding of the Ca^{2+}-binding site and thereby reduces the Ca^{2+}-binding ability (Sánchez-Magraner et al., 2014). As depicted in Fig. 1, this transmembrane region is highly conserved among the PLSCR1 homologues including MuPLSCR1like-a and -b. Furthermore, the short tail extending from the C-terminal end to the plasma membrane suggests that MuPLSCR1like-a and MuPLSCR1like-b belong to type II membrane proteins (Sims and Wiedmer, 2001).

The constructed phylogenetic tree uncovered the evolutionary relation of MuPLSCR1like-a and MuPLSCR1like-b with other PLSCRs. All the fish PLSCR1like proteins were clustered in one clade with several other fish PLSCR1 and -2 proteins, thus pointing to their common ancestral origin. Fish from different taxonomic orders and their molecular similarity allowed for formation of subclades within the clade. According to the constructed phylogenetic tree, MuPLSCR1like-a and MuPLSCR1like-b diverged from each other. Because they belong to the same fish species, this divergence may be due to their molecular differences, which we have discussed from the beginning. Nevertheless, in the constructed phylogenetic tree, MuPLSCR1like-a showed a close relation with PLSCR1, just as with the *Danio rerio* protein by separately branching together in the same clade. This phenomenon was also confirmed by 51.6% of shared sequence identity and 63.4% of shared similarity in the pairwise sequence comparison. Moreover, MuPLSCR1like-b closely clustered together with *Larimichthys crocea* PLSCR2 with 96.5% sequence identity and 98.7% similarity in their sequences. In addition, *Oryzias latipes* PLSCR1 and PLSCR1like proteins from *Seriola dumerili* and *Amphiprion ocellaris* were clustered in the same

subclade.

Although PLSCR isoforms are expressed in different locations in the cell, PLSCR1 is present in the plasma membrane (Contreras et al., 2010). According to the previous studies, hPLSCR1 is expressed in various tissues including the heart, kidneys, pancreas, prostate, and colon whereas hPLSCR2 is expressed in only testis (Zhou et al., 1997). According to those studies, hPLSCR1 is not detectable in the brain (Wiedmer et al., 2000; Zhou et al., 1997). In our study, *MuPLSCR1like-a* and *MuPLSCR1like-b* were detected in all the examined tissues. Nevertheless, *MuPLSCR1like-a* showed its highest expression in the intestine, while MuPLSCR1like-b was highly expressed in the brain. Although our MuPLSCR1like-a data are consistent with the previous studies on humans, our MuPLSCR1like-b data contradict them: detection in the brain and muscle. This finding suggests that the mRNA expression levels of PLSCRs have species-specific and isoform-specific distribution patterns. The fish intestine is in contact with the external environment through the mouth and gut opening stages and at the onset of feeding, while being exposed to various unfamiliar pathogens. Therefore, the fish intestine works as a multifunctional organ both performing nutrient uptake and having pathogen recognition mechanisms (Martin et al., 2016). According to early studies, mast cells can be activated by PLSCRs, and this event stimulates the secretion of proinflammatory cytokines (Acharya et al., 2006). During a viral infection, the intestine activates the adipocytokine pathway, which can be induced by proinflammatory cytokines (Martin et al., 2016). Therefore, we suppose that the highest amount of MuPLSCR1like-a was present in the intestine for the purpose of protecting the host cells from viral infections. The brain is considered as the main component of the central nervous system (CNS), and microglia are the first

responders to CNS injury or diseases (Tufail et al., 2017). This microglial activation can induce inflammatory responses with the end result of restricting tissue injury or pathogen spread (Tufail et al., 2017). Due to a viral infection, the CNS activates its innate immune response, which includes microglial phagocytosis (Tufail et al., 2017). PLSCR1 has been identified as an effective target for the control of microglial phagocytosis, and the greatest expression of MuPLSCR1like-b in the brain as observed in the present study also provides strong evidence for this scenario.

The immune system is present in all the organisms and varies in its complexity including variation in the innate and adaptive components (Rauta et al., 2012). Fish possess both innate and adaptive immune systems by evolution. At the same time, the fish innate immune system is considered stronger than the adaptive immune system of fish (Rauta et al., 2012). Immune responses mediated by PLSCRs have been documented in the early studies on mammals (Dong et al., 2004)(Lizak and Yarovinsky, 2012) and planarians (Han et al., 2017). These data prompted us to focus on the immune responses involving *MuPLSCR1like-a* and *MuPLSCR1like-b* in red lip mullets. Out of several immune organs in the fish immune system, the spleen has been identified as a major secondary lymphatic and scavenging organ that has a critical role in hematopoiesis, antigen degradation, and the process of antibody production (Rauta et al., 2012). Moreover, it performs a major function in trapping of antigens, even though fish do not possess lymph nodes (Press et al., 1994). Furthermore, spleen size of fish is considered a primary indicator of the immune responses to parasitic infections (Lovy et al., 2007). The head kidney of fish is considered the principal immune organ responsible for phagocytosis, antigen processing, and formation of IgM and immune memory through melanomacrophagic centers (Tort et al., 2003). Moreover, the head kidney is an important endocrine organ which possesses major

regulatory functions for immune endocrine interactions (Tort et al., 2003). Therefore, the spleen and head kidney were used in this study as the sites for transcriptional analysis to evaluate the immune responses mediated by *MuPLSCR1like-a* and *MuPLSCR1like-b* induced by different immune stimulants.

In the immune challenge experiment, we injected the fish with different immune stimulants including bacteria (*L. garvieae*), a virus mimic (poly[I:C]) and LPS. *L. garvieae* is a gram-positive bacterium that is known as a causative agent of green liver syndrome of red lip mullets; it has caused outbreaks of the disease and mass mortality of mullets in several countries, including Korea (Han et al., 2015). Therefore, in the present study, we chose *L. garvieae* as a virulent bacterium for the red lip mullet considering the high pathogenicity. Furthermore, poly(I:C) is a viral mimic and it has been widely used as an immune stimulant in immune-challenge experiments because of its high antigenicity (Han et al., 2017; Reisinger et al., 2015). These data led us to challenge the mullets with poly(I:C) to examine the responses to viral infections. LPS is a main component of gram-negative bacterial cell wall and was employed in this study to determine the responses of *MuPLSCR1like-a* and *MuPLSCR1like-b* to gram-negative bacterial infections, as stated in previous studies (Han et al., 2017).

In our study, *MuPLSCR1like-a* and *MuPLSCR1like-b* from the spleen and *MuPLSCR1like-a* from the head kidney showed significant upregulation after poly(I:C) treatment, i.e., at 6 h after the injection. Induction with poly(I:C) allows the host cell to express its antiviral functions against pathogens. Viral infections can stimulate IFN-α or -β or IFN-stimulated genes, which can act as major components of an antiviral host defense mechanism (N et al., 1994). PLSCR1 has been identified as an interferon-stimulated gene (ISG) in previous antiviral studies (Dong et al., 2004), and many reports are available showing the interferon inducing ability of PLSCRs

(Han et al., 2017; Lizak and Yarovinsky, 2012; Zhou et al., 2000). Together with our results, these data led us to suggest that *MuPLSCR1like-a* and *MuPLSCR1like-b* also have the interferon inducing ability being related with PLSCR family, thereby activate the host defense mechanism while infected with viral pathogens. Moreover, in the spleen, MuPLSCR*1like-b* showed high expression levels in response to LPS and *L. garvieae* treatments. *MuPLSCR1like-a* and *MuPLSCR1like-b* in the head kidney did not show this kind of significant upregulation. One study on *Staphylococcal* α-toxin, a pore-forming toxin from a gram-positive pathogen, has described PLSCR1s' mediation of host cell defense against the critical damage caused by these toxins (Lizak and Yarovinsky, 2012). Additionally, stimulation with PGN, another component of gram-positive bacteria, significantly upregulates PLSCRs in planarians; thus, PLSCRs help to counteract gram-positive bacterial infections (Han et al., 2017). Furthermore, PLSCR1 upregulation in response to LPS has been observed since early studies on mice (Lu et al., 2007) and planarians (Han et al., 2017). Nevertheless, the effect of LPS on the PLSCRs is considered isoform-specific and tissue-specific (Lu et al., 2007). This arrangement supports the different findings about *MuPLSCR1like-a* and *MuPLSCR1like-b* in our study. Collectively, we suggest that the results obtained in the immune challenge experiment of this study may be explained by the immune response activation via MuPLSCR1like-a and MuPLSCR1like-b as immunity-related proteins.

5. Conclusion

This study provides the first experimental insights into the molecular and transcriptional characteristics of two PLSCR1-related genes in the red lip mullet. In summary, cDNA of two putative PLSCR1-related genes, *MuPLSCR1like-a* and *MuPLSCR1like-b* from the red lip mullet were identified and characterized in the present study. Because of their structural characteristics, phylogenetic relations, and homology analysis, these two genes were confirmed as *PLSCR1*-like genes belonging to the PLSCR family. Transcriptional analysis of *MuPLSCR1like-a* and *MuPLSCR1like-b* revealed their different distribution patterns in different tissues of red lip mullets. The mRNA expression levels of *MuPLSCR1like-a* and *MuPLSCR1like-b* were determined at different time points after the fish were challenged with bacterial or viral components. The significant changes in their expression allow us to propose possible functions of *MuPLSCR1like-a* and *MuPLSCR1like-b* in the innate immune system of red lip mullets.

References

Acharya, U., Edwards, M.B., Jorquera, R.A., Silva, H., Nagashima, K., Labarca, P., Acharya, J.K., 2006. Drosophila melanogaster Scramblases modulate synaptic transmission. J. Cell Biol. 173, 69–82. https://doi.org/10.1083/jcb.200506159

Alexandrov, A., Dutta, K., Pascal, S.M., 2001. MBP fusion protein with a viral protease cleavage site: One-step cleavage/purification of insoluble proteins. Biotechniques 30, 1194–1198.

Allocati, N., 2018. Glutathione transferases : substrates , inihibitors and pro-drugs in cancer and neurodegenerative diseases. Oncogenesis. https://doi.org/10.1038/s41389-017-0025-3

Altschul, S.F., Gish, W., Miller, W., Myers, E.W., Lipman, D.J., 1990. Basic local alignment search tool. J. Mol. Biol. 215, 403–10. https://doi.org/10.1016/S0022-2836(05)80360-2

Arca, P., Garc??a, P., Hardisson, C., Su??rez, J.E., 1990. Purification and study of a bacterial glutathione S-transferase. FEBS Lett. 263, 77–79. https://doi.org/10.1016/0014-5793(90)80709-R

Armstrong, R.N., 1997. Invited Review 2–18.

Arockiaraj, J., Gnanam, A.J., Palanisamy, R., Bhatt, P., Kumaresan, V., Chaurasia, M.K., Pasupuleti, M., Ramaswamy, H., Arasu, A., Sathyamoorthi, A., 2014. A cytosolic glutathione s-transferase, GST-theta from freshwater prawn Macrobrachium rosenbergii: Molecular and biochemical properties. Gene 546, 437–442. https://doi.org/10.1016/j.gene.2014.05.063

Ataya, F.S., Al-Jafari, A.A., Daoud, M.S., Al-Hazzani, A.A., Shehata, A.I., Saeed,

H.M., Fouad, D., 2014. Genomics, phylogeny and in silico analysis of mitochondrial glutathione S-transferase-kappa from the camel Camelus dromedarius. Res. Vet. Sci. 97, 46–54. https://doi.org/10.1016/j.rvsc.2014.04.004

Bagos, P.G., Liakopoulos, T.D., Spyropoulos, I.C., Hamodrakas, S.J., 2004. PRED-TMBB: A web server for predicting the topology of β-barrel outer membrane proteins. Nucleic Acids Res. 32, 400–404. https://doi.org/10.1093/nar/gkh417

Bateman, A., Finn, R.D., Sims, P.J., Wiedmer, T., Biegert, A., Söding, J., 2009. Phospholipid scramblases and Tubby-like proteins belong to a new superfamily of membrane tethered transcription factors. Bioinformatics 25, 159–162. https://doi.org/10.1093/bioinformatics/btn595

Bathige, S.D.N.K., Umasuthan, N., Saranya, K., Lee, Y., Kim, S., Young, M., Park, M., Whang, I., Lee, J., 2014. Comparative Biochemistry and Physiology , Part C A mu class glutathione S-transferase from Manila clam Ruditapes philippinarum (RpGST μ): Cloning , mRNA expression , and conjugation assays. Comp. Biochem. Physiol. Part C 162, 85–95. https://doi.org/10.1016/j.cbpc.2014.03.007

Bertin, G., Averbeck, D., 2006. Cadmium: cellular effects, modifications of biomolecules, modulation of DNA repair and genotoxic consequences (a review). Biochimie 88, 1549–1559. https://doi.org/10.1016/j.biochi.2006.10.001

Bevers, B.E.M., Wiedmer, T., Comfurius, P., Zhao, J., Smeets, E.F., Schlegel, R.A., Schroit, A.J., Weiss, H.J., Williamson, P., Zwaal, R.F.A., Sims, P.J., 2016. Is Loss A 1983–1991.

Blanchette, B., Feng, X., Singh, B.R., 2007. Review 9, 513–542. https://doi.org/10.1007/s10126-007-9034-0

Board, P.G., Coggan, M., Chelvanayagam, G., Easteal, S., Jermiin, L.S., Schulte,

G.K., Danley, D.E., Hoth, L.R., Griffor, M.C., Kamath, A. V., Rosner, M.H., Chrunyk, B.A., Perregaux, D.E., Gabel, C.A., Geoghegan, K.F., Pandit, J., 2000. Identification, characterization, and crystal structure of the omega class glutathione transferases. J. Biol. Chem. 275, 24798–24806. https://doi.org/10.1074/jbc.M001706200

Board, P.G., Coggan, M., Wilcet, M.C.J., Parkert, M.W., 1995. Evidence for an essential serine residue in the active site of the Theta class glutathione transferases 250, 247–250.

Bonekamp, N.A., Völkl, A., Fahimi, H.D., Schrader, M., 2009. Reactive oxygen species and peroxisomes: Struggling for balance. BioFactors 35, 346–355. https://doi.org/10.1002/biof.48

Bradford, M.M., 1976. A rapid and sensitive method for the quantitation of microgram quantities of protein utilizing the principle of protein-dye binding. Anal. Biochem. 72, 248–254. https://doi.org/10.1016/0003-2697(76)90527-3

Cameron, A.D., Sinning, I., L'Hermite, G., Olin, B., Board, P.G., Mannervik, B., Jones, T.A., 1995. Structural analysis of human alpha-class glutathione transferase A1-1 in the apo-form and in complexes with ethacrynic acid and its glutathione conjugate. Structure 3, 717–727. https://doi.org/10.1016/S0969-2126(01)00206-4

Chandra, P., 2017. Glutathione S-Transferases : a Brief on Classification and Gstm1-T1 Activity. https://doi.org/10.13040/IJPSR.0975-8232.8(3).1023-27

Chaurasia, M.K., Ravichandran, G., Nizam, F., Arasu, M.V., Al-Dhabi, N.A., Arshad, A., Harikrishnan, R., Arockiaraj, J., 2016. In-silico analysis and mRNA modulation of detoxification enzymes GST delta and kappa against various biotic and abiotic oxidative stressors. Fish Shellfish Immunol. 54, 353–363.

https://doi.org/10.1016/j.fsi.2016.04.031

Chen, B., Peng, W., Xu, J., Feng, J., Dong, C., Xu, P., Chen, B., 2017. Genomic Analysis of Glutathione S-transferases 49, 1437–1448.

Chen, M.H., Ben-Efraim, I., Mitrousis, G., Walker-Kopp, N., Sims, P.J., Cingolani, G., 2005. Phospholipid scramblase 1 contains a nonclassical nuclear localization signal with unique binding site in importin α. J. Biol. Chem. 280, 10599–10606. https://doi.org/10.1074/jbc.M413194200

Cochennec-Laureau, N., Auffret, M., Renault, T., Langlade, A., 2003. Changes in circulating and tissue-infiltrating hemocyte parameters of European flat oysters, Ostrea edulis, naturally infected with Bonamia ostreae. J. Invertebr. Pathol. 83, 23–30. https://doi.org/10.1016/S0022-2011(03)00015-6

Contreras-Vergara, C.A., Harris-Valle, C., Sotelo-Mundo, R.R., Yepiz-Plascencia, G., 2004. A mu-class glutathione S-transferase from the marine shrimp Litopenaeus vannamei: Molecular cloning and active-site structural modeling. J. Biochem. Mol. Toxicol. 18, 245–252. https://doi.org/10.1002/jbt.20033

Contreras, F.X., Sánchez-Magraner, L., Alonso, A., Goñi, F.M., 2010. Transbilayer (flip-flop) lipid motion and lipid scrambling in membranes. FEBS Lett. 584, 1779–1786. https://doi.org/10.1016/j.febslet.2009.12.049

Cook, P.A., 2014. The Worldwide Abalone Industry. Sci. Res. 1181–1186. https://doi.org/10.4236/me.2014.513110

Cunha, L., Amaral, A., Medeiros, V., Martins, G.M., Wallenstein, F.F.M.M., Couto, R.P., Neto, A.I., Rodrigues, A., 2008. Bioavailable metals and cellular effects in the digestive gland of marine limpets living close to shallow water hydrothermal vents. Chemosphere 71, 1356–1362. https://doi.org/10.1016/j.chemosphere.2007.11.022

De Zoysa, M., Pushpamali, W.A., Oh, C., Whang, I., Kim, S.J., Lee, J., 2008. Transcriptional up-regulation of disk abalone selenium dependent glutathione peroxidase by H2O2 oxidative stress and Vibrio alginolyticus bacterial infection. Fish Shellfish Immunol. 25, 446–457. https://doi.org/10.1016/j.fsi.2008.02.001

De Zoysa, M., Whang, I., Lee, Y., Lee, S., Lee, J.S., Lee, J., 2009. Transcriptional analysis of antioxidant and immune defense genes in disk abalone (Haliotis discus discus) during thermal, low-salinity and hypoxic stress. Comp. Biochem. Physiol. - B Biochem. Mol. Biol. 154, 387–395. https://doi.org/10.1016/j.cbpb.2009.08.002

DeLano, W., 2002. Pymol: An open-source molecular graphics tool. CCP4 Newsl. Protein Crystallogr. 700.

Dong, B., Zhou, Q., Zhao, J., Zhou, A., Harty, R.N., Bose, S., Banerjee, A., Slee, R., Guenther, J., Williams, B.R.G., Wiedmer, T., Sims, P.J., Silverman, R.H., 2004. Phospholipid scramblase 1 potentiates the antiviral activity of interferon. J. Virol. 78, 8983–93. https://doi.org/10.1128/JVI.78.17.8983-8993.2004

Droege, M., Hill, B., 2008. The Genome Sequencer FLX^{TM} System-Longer reads, more applications, straight forward bioinformatics and more complete data sets. J. Biotechnol. 136, 3–10. https://doi.org/10.1016/j.jbiotec.2008.03.021

Elvitigala, D.A.S., Jayasooriya, R.G.P.T., whang, I., Lee, J., 2015. First report on the gastropod proapoptotic AIF3 counterpart from disk abalone (Haliotis discus discus) deciphering its transcriptional modulation by induced pathogenic stress. Fish Shellfish Immunol. 47, 697–705. https://doi.org/10.1016/j.fsi.2015.10.006

Fiander, H., Schneider, H., 1999. Compounds that Induce Isoforms of Glutathione S-transferase with Properties of a Critical Enzyme in Defense against Oxidative Stress. Biochem. Biophys. Res. Commun. 262, 591–595.

https://doi.org/10.1006/bbrc.1999.1262

Frisby, C.M., 2006. A Matter of Life and Death. J. Black Stud. 37, 103–126. https://doi.org/10.1177/0021934705277499

Frova, C., 2006. Glutathione transferases in the genomics era: New insights and perspectives. Biomol. Eng. 23, 149–169. https://doi.org/10.1016/j.bioeng.2006.05.020

Glisic, B., Mihaljevic, I., Popovic, M., Zaja, R., Loncar, J., Fent, K., Kovacevic, R., Smital, T., 2015. Characterization of glutathione-S-transferases in zebrafish (Danio rerio). Aquat. Toxicol. 158, 50–62. https://doi.org/10.1016/j.aquatox.2014.10.013

Guo, X., He, Y., Zhang, L., Lelong, C., Jouaux, A., 2015. Immune and stress responses in oysters with insights on adaptation. Fish Shellfish Immunol. 46, 107–119. https://doi.org/10.1016/j.fsi.2015.05.018

Guruprasad, K., Reddy, B.V.B., Pandit, M.W., 1990. Correlation between stability of a protein and its dipeptide composition: A novel approach for predicting in vivo stability of a protein from its primary sequence. Protein Eng. Des. Sel. 4, 155–161. https://doi.org/10.1093/protein/4.2.155

Hambidge, M., Krebs, N.F., 2001. Zinc metabolism and requirements. Food Nutr. Bull. 22, 126–132. https://doi.org/10.1177/156482650102200202

Han, H.J., Lee, N.S., Kim, M.S., Jung, S.H., 2015. An outbreak of lactococcus garvieae infection in cage-cultured red lip mullet chelon haematocheilus with green liver syndrome. Fish. Aquat. Sci. 18, 333–339. https://doi.org/10.5657/FAS.2015.0333

Han, Y., Li, A., Gao, L., Wu, W., Deng, H., Hu, W., Li, N., Sun, S., Zhang, X., Zhao, B., Liu, B., Pang, Q., 2017. Identification and characterization of a phospholipid

scramblase encoded by planarian Dugesia japonica. Gene 602, 43–49. https://doi.org/10.1016/j.gene.2016.11.029

Hao, L., Xie, P., Fu, J., Li, G., Xiong, Q., Li, H., 2008. The effect of cyanobacterial crude extract on the transcription of GST mu, GST kappa and GST rho in different organs of goldfish (Carassius auratus). Aquat. Toxicol. 90, 1–7. https://doi.org/10.1016/j.aquatox.2008.07.006

Harris, J.M., Meyer, D.J., Coles, B., Ketterer, B., 1991. A novel glutathione transferase (13-13) isolated from the matrix of rat liver mitochondria having structural similarity to class theta enzymes. Biochem. J. 278, 137–41.

Hayes, J.D., Flanagan, J.U., Jowsey, I.R., 2005. Glutathione Transferases. Annu. Rev. Pharmacol. Toxicol. 45, 51–88. https://doi.org/10.1146/annurev.pharmtox.45.120403.095857

Hayes, J.D., Pulford, D.J., 1995. The Glut athione S-Transferase Supergene Family: Regulation of GST and the Contribution of the lsoenzymes to Cancer Chemoprotection and Drug Resistance Part I. Crit. Rev. Biochem. Mol. Biol. 30, 445–520. https://doi.org/10.3109/10409239509083491

Hodgson, E., 2010. Chapter 36 - Introduction to Biotransformation (Metabolism), in: Krieger, R. (Ed.), Hayes' Handbook of Pesticide Toxicology (Third Edition). Academic Press, New York, pp. 865–875. https://doi.org/https://doi.org/10.1016/B978-0-12-374367-1.00036-7

Huang, Q., Liang, L., Wei, T., Zhang, D., Zeng, Q.Y., 2008. Purification and partial characterization of glutathione transferase from the teleost Monopterus albus. Comp. Biochem. Physiol. - C Toxicol. Pharmacol. 147, 96–100. https://doi.org/10.1016/j.cbpc.2007.08.004

Huang, Y., Zhao, Q., Zhou, C.X., Gu, Z.M., Li, D., Xu, H.Z., Sims, P.J., Zhao, K.W.,

Chen, G.Q., 2006. Antileukemic roles of human phospholipid scramblase 1 gene, evidence from inducible PLSCR1-expressing leukemic cells. Oncogene 25, 6618–6627. https://doi.org/10.1038/sj.onc.1209677

Hunaiti, A.A., Soud, M., 2000. Effect of lead concentration on the level of glutathione , glutathione S -transferase , reductase and peroxidase in human blood 45–50.

Jayasinghe, J.D.H.E., Bathige, S.D.N.K., Nam, B.H., Noh, J.K., Lee, J., 2016. Comprehensive characterization of three glutathione S-transferase family proteins from black rockfish (Sebastes schlegelii). Comp. Biochem. Physiol. Part - C Toxicol. Pharmacol. 189, 31–43. https://doi.org/10.1016/j.cbpc.2016.07.003

Ji, X., Zhang, P., Armstrong, R.N., Gilliland, G.L., 1992. The Three-Dimensional Structure of a Glutathione S-Transferase from the Mu Gene Class. Structural Analysis of the Binary Complex of Isoenzyme 3-3 and Glutathione at 2.2-Å Resolution. Biochemistry 31, 10169–10184. https://doi.org/10.1021/bi00157a004

Jowsey, I.R., Thomson, R.E., Orton, T.C., Elcombe, C.R., Hayes, J.D., 2003. Biochemical and genetic characterization of a murine class Kappa glutathione S-transferase. Biochem. J. 373, 559–569. https://doi.org/10.1042/BJ20030415

Kalim Tahir, M., Guthenberg, C., Mannervik, B., 1985. Inhibitors for distinction of three types of human glutathione transferase. FEBS Lett. 181, 249–252. https://doi.org/10.1016/0014-5793(85)80269-6

Kasthuri, S.R., Wan, Q., Umasuthan, N., Bathige, S.D.N.K., Lim, B.S., Jung, H.B., Lee, J., Whang, I., 2013. Genomic characterization, expression analysis, and antimicrobial function of a glyrichin homologue from rock bream, Oplegnathus fasciatus. Fish Shellfish Immunol. 35, 1406–1415.

https://doi.org/10.1016/j.fsi.2013.08.008

Kim, S.J., Chun, J., Bae, K.S., Kim, Y.C., 2000. Polyphasic assignment of an aromatic-degrading Pseudomonas sp., strain DJ77, in the genus Sphingomonas as Sphingomonas chungbukensis sp. nov. Int. J. Syst. Evol. Microbiol. 50, 1641–1647.

Ladner, J.E., Parsons, J.F., Rife, C.L., Gilliland, G.L., Armstrong, R.N., 2004. Parallel Evolutionary Pathways for Glutathione Transferases: Structure and Mechanism of the Mitochondrial Class Kappa Enzyme rGSTK1-1. Biochemistry 43, 352–361. https://doi.org/10.1021/bi035832z

Landi, S., 2000. Mammalian class theta GST and differential susceptibility to carcinogens: A review. Mutat. Res. - Rev. Mutat. Res. 463, 247–283. https://doi.org/10.1016/S1383-5742(00)00050-8

Lee, K.K., Liu, P.C., Huang, C.Y., 2003. Vibrio parahaemolyticus infectious for both humans and edible mollusk abalone. Microbes Infect. 5, 481–485. https://doi.org/10.1016/S1286-4579(03)00065-0

Lee, Y.M., Lee, K.W., Park, H., Park, H.G., Raisuddin, S., Ahn, I.Y., Lee, J.S., 2007. Sequence, biochemical characteristics and expression of a novel Sigma-class of glutathione S-transferase from the intertidal copepod, Tigriopus japonicus with a possible role in antioxidant defense. Chemosphere 69, 893–902. https://doi.org/10.1016/j.chemosphere.2007.05.087

Lee, Y.M., Seo, J.S., Jung, S.O., Kim, I.C., Lee, J.S., 2006. Molecular cloning and characterization of θ-class glutathione S-transferase (GST-T) from the hermaphroditic fish Rivulus marmoratus and biochemical comparisons with α-class glutathione S-transferase (GST-A). Biochem. Biophys. Res. Commun. 346, 1053–1061. https://doi.org/10.1016/j.bbrc.2006.06.014

Li, C., Su, X., Li, Y., Li, T., Sun, C., Zhou, T., Liu, H., 2012. Two classes of glutathione S-transferase genes with different response profiles to bacterial challenge in Venerupis philippinarum. Fish Shellfish Immunol. 32, 219–222. https://doi.org/10.1016/j.fsi.2011.10.032

Li, J.I.E., Xia, Z., Ding, J., 2005. Thioredoxin-like domain of human k class glutathione transferase reveals sequence homology and structure similarity to the y class enzyme 1, 2361–2369. https://doi.org/10.1110/ps.051463905.Glutathione

Liu, M., Zhou, L., Xu, A., Lam, K.S.L., Wetzel, M.D., Xiang, R., Zhang, J., Xin, X., Dong, L.Q., Liu, F., 2008. A disulfide-bond A oxidoreductase-like protein (DsbA-L) regulates adiponectin multimerization. Proc. Natl. Acad. Sci. U. S. A. 105, 18302–18307. https://doi.org/10.1073/pnas.0806341105

Liu, P.C., Chen, Y.C., Huang, C.Y., Lee, K.K., 2000. Virulence of Vibrio parahaemolyticus isolated from cultured small abalone, Haliotis diversicolor supertexta, with withering syndrome. Lett. Appl. Microbiol. 31, 433–437. https://doi.org/10.1046/j.1365-2672.2000.00843.x

Livak, K.J., Schmittgen, T.D., 2001. Analysis of Relative Gene Expression Data Using Real-Time Quantitative PCR and the $2^{-\Delta\Delta CT}$ Method. Methods 25, 402–408. https://doi.org/10.1006/meth.2001.1262

Lizak, M., Yarovinsky, T.O., 2012. Phospholipid scramblase 1 mediates type i interferon-induced protection against staphylococcal ??-toxin. Cell Host Microbe 11, 70–80. https://doi.org/10.1016/j.chom.2011.12.004

Lovy, J., Becker, J.A., Speare, D.J., Wadowska, D.W., Wright, G.M., Powell, M.D., 2007. Ultrastructural examination of the host cellular response in the gills of Atlantic salmon, Salmo salar, with amoebic gill disease. Vet. Pathol. 44, 663–671. https://doi.org/10.1354/vp.44-5-663

Lu, B., Sims, P.J., Wiedmer, T., Moser, A.H., Shigenaga, J.K., Grunfeld, C., Feingold, K.R., 2007. Expression of the phospholipid scramblase (PLSCR) gene family during the acute phase response. Biochim. Biophys. Acta - Mol. Cell Biol. Lipids 1771, 1177–1185. https://doi.org/10.1016/j.bbalip.2007.05.002

Maciolek, J. a, Basin, C.C., County, M., 1963. The determination 530–533.

Manipulation, T.S., 2000. Internet On-Ramp Internet On-Ramp 28.

Mannervik, B., Alin, P., Guthenberg, C., Jensson, H., Tahir, M.K., Warholm, M., Jörnvall, H., 1985. Identification of three classes of cytosolic glutathione transferase common to several mammalian species: correlation between structural data and enzymatic properties. Proc. Natl. Acad. Sci. U. S. A. 82, 7202–7206. https://doi.org/10.1073/pnas.82.21.7202

Marigómez, I., Soto, M., Cajaraville, M.P., Angulo, E., Giamberini, L., 2002. Cellular and subcellular distribution of metals in molluscs. Microsc. Res. Tech. 56, 358–392. https://doi.org/10.1002/jemt.10040

Martin, J.L., 1995. Thioredoxin -a fold for all reasons. Structure 3, 245–250. https://doi.org/10.1016/S0969-2126(01)00154-X

Martin, S.A.M., Dehler, C.E., Król, E., 2016. Transcriptomic responses in the fish intestine. Dev. Comp. Immunol. 64, 103–117. https://doi.org/10.1016/j.dci.2016.03.014

McWilliam, H., Li, W., Uludag, M., Squizzato, S., Park, Y.M., Buso, N., Cowley, A.P., Lopez, R., 2013. Analysis Tool Web Services from the EMBL-EBI. Nucleic Acids Res. 41, 597–600. https://doi.org/10.1093/nar/gkt376

Michel, R.H., McGovern, P.E., 1974. The first. J. Biol. Chem. 249, 7130–7139.

Morel, F., Rauch, C., Petit, E., Theret, N., Coles, B., 2004. Gene and Protein Characterization of the Human Glutathione S -Transferase Kappa and Evidence

for a Peroxisomal Localization * 279, 16246–16253. https://doi.org/10.1074/jbc.M313357200

Motoyama, N., Dauterman, W.C., 1977. Purification and properties of housefly glutathione S-transferase. Insect Biochem. 7, 361–369. https://doi.org/10.1016/0020-1790(77)90039-7

MURRAY, C.C., MACH, M.E., MARTONE, R.G., 2014. Cumulative effects in marine ecosystems : scientific perspectives on its challenges and solutions. WWF-Canada Cent. Ocean Solut. 60.

N, J., Homola, a M., Muller, U., Steinhoff, U., Reis, L.F.L., Hemmi, S., Paviovic, J., Zinkernagel, R.M., Aguet, M., 1994. Functional Role of Type I and Type 11 Interferons in Antiviral Defense. Science (80-.). 264.

Notredame, C., Higgins, D.G., Heringa, J., 2000. T-coffee: A novel method for fast and accurate multiple sequence alignment. J. Mol. Biol. 302, 205–217. https://doi.org/10.1006/jmbi.2000.4042

Nya, E.J., Austin, B., 2010. Use of bacterial lipopolysaccharide (LPS) as an immunostimulant for the control of Aeromonas hydrophila infections in rainbow trout Oncorhynchus mykiss (Walbaum). J. Appl. Microbiol. 108, 686–694. https://doi.org/10.1111/j.1365-2672.2009.04464.x

Oakley, A.J., Harnnoi, T., Udomsinprasert, R., Jirajaroenrat, K., Ketterman, A.J., Wilce, M.C.J., 2001. The crystal structures of glutathione S-transferases isozymes 1 – 3 and 1 – 4 from Anopheles dirus species B 2176–2185. https://doi.org/10.1101/ps.21201.no

Page, A.F., 2010. The MIQE Guidelines and Assessment of Nucleic Acids Prior to qPCR and RT-qPCR. Thermo Sci. 1–3. https://doi.org/T097

Perry, W.L., 2002. JavaScript DNA Translator: DNA-aligned protein translations.

Biotechniques 33, 1318–1320.

Petersen, T.N., Brunak, S., von Heijne, G., Nielsen, H., 2011. SignalP 4.0: discriminating signal peptides from transmembrane regions. Nat. Methods 8, 785–786. https://doi.org/10.1038/nmeth.1701

Polekhina, G., Board, P.G., Blackburn, A.C., Parker, M.W., 2001. Crystal structure of maleylacetoacetate isomerase/glutathione transferase zeta reveals the molecular basis for its remarkable catalytic promiscuity. Biochemistry 40, 1567–1576. https://doi.org/10.1021/bi002249z

Pomorski, T., Menon, A.K., 2006. Lipid flippases and their biological functions. Cell. Mol. Life Sci. 63, 2908–2921. https://doi.org/10.1007/s00018-006-6167-7

Press, C.M., Dannevig, B.H., Landsverk, T., 1994. Immune and enzyme histochemical phenotypes of lymphoid and nonlymphoid cells within the spleen and head kidney of atlantic salmon (salmo salar l.). Fish Shellfish Immunol. https://doi.org/10.1006/fsim.1994.1007

Rauta, P.R., Nayak, B., Das, S., 2012. Immune system and immune responses in fish and their role in comparative immunity study: A model for higher organisms. Immunol. Lett. 148, 23–33. https://doi.org/10.1016/j.imlet.2012.08.003

Rayala, S., Francis, V.G., Sivagnanam, U., Gummadi, S.N., 2014. N-terminal proline-rich domain is required for scrambling activity of human phospholipid scramblases. J. Biol. Chem. 289, 13206–13218. https://doi.org/10.1074/jbc.M113.522953

Reisinger, S., Khan, D., Kong, E., Berger, A., Pollak, A., Pollak, D.D., 2015. The Poly(I:C)-induced maternal immune activation model in preclinical neuropsychiatric drug discovery. Pharmacol. Ther. 149, 213–226. https://doi.org/10.1016/j.pharmthera.2015.01.001

Ren, H.L., Xu, D.D., Gopalakrishnan, S., Qiao, K., Huang, W. Bin, Wang, K.J., 2009. Gene cloning of a sigma class glutathione S-transferase from abalone (Haliotis diversicolor) and expression analysis upon bacterial challenge. Dev. Comp. Immunol. 33, 980–990. https://doi.org/10.1016/j.dci.2009.04.003

Reports, A.S., 2014. Differentially Expressed Genes In Cadmium-Exposed Sebastes Schlegeli Using Dd-Pcr. Appl. Sci. Reports 2. https://doi.org/10.15192/PSCP.ASR.2014.2.2.6266

Rhee, J.S., Raisuddin, S., Hwang, D.S., Horiguchi, T., Cho, H.S., Lee, J.S., 2008. A Mu-class glutathione S-transferase (GSTM) from the rock shell Thais clavigera. Comp. Biochem. Physiol. - C Toxicol. Pharmacol. 148, 195–203. https://doi.org/10.1016/j.cbpc.2008.05.011

Rhoads, A., Au, K.F., 2015. PacBio Sequencing and Its Applications. Genomics, Proteomics Bioinforma. 13, 278–289. https://doi.org/10.1016/j.gpb.2015.08.002

Robinson, A., Huttley, G.A., Booth, H.S., Board, P.G., 2004. Modelling and bioinformatics studies of the human {Kappa} class {Glutathione Transferase} predict a novel third {Glutathione Transferase} family with homology to prokaryotic 2-hydroxychromene-2-carboxylate ({HCCA}) {Isomerases}. Biochem J 379, 541–552.

Rosenberg, E., Falkovitz, L., 2004. The *Vibrio shiloi / Oculina patagonica* Model System of Coral Bleaching. Annu. Rev. Microbiol. 58, 143–159. https://doi.org/10.1146/annurev.micro.58.030603.123610

Rossjohn, J., McKinstry, W.J., Oakley, a J., Verger, D., Flanagan, J., Chelvanayagam, G., Tan, K.L., Board, P.G., Parker, M.W., 1998. Human theta class glutathione transferase: the crystal structure reveals a sulfate-binding pocket within a buried active site. Structure 6, 309–322. https://doi.org/10.1016/S0969-2126(98)00034-

3

Sahu, S.K., Aradhyam, G.K., Gummadi, S.N., 2009. Calcium binding studies of peptides of human phospholipid scramblases 1 to 4 suggest that scramblases are new class of calcium binding proteins in the cell. Biochim. Biophys. Acta - Gen. Subj. 1790, 1274–1281. https://doi.org/10.1016/j.bbagen.2009.06.008

Sahu, S.K., Gummadi, S.N., Manoj, N., Aradhyam, G.K., 2007. Phospholipid scramblases: An overview. Arch. Biochem. Biophys. 462, 103–114. https://doi.org/10.1016/j.abb.2007.04.002

Samra, A.I., Kamita, S.G., Yao, H.W., Cornel, A.J., Hammock, B.D., 2012. Cloning and characterization of two glutathione S-transferases from pyrethroid-resistant Culex pipiens. Pest Manag. Sci. 68, 764–772. https://doi.org/10.1002/ps.2324

Sánchez-Magraner, L., Posada, I.M.D., Andraka, N., Contreras, F.X., Viguera, A.R., Guérin, D.M.A., Arrondo, J.L.R., Monaco, H.L., Goñi, F.M., 2014. The C-terminal transmembrane domain of human phospholipid scramblase 1 is essential for the protein flip-flop activity and Ca2+-binding. J. Membr. Biol. 247, 155–165. https://doi.org/10.1007/s00232-013-9619-7

Sandamalika, W.M.G., Priyathilaka, T.T., Liyanage, D.S., Lee, S., Lim, H.K., Lee, J., 2018. Molecular characterization of kappa class glutathione S-transferase from the disk abalone (Haliotis discus discus) and changes in expression following immune and stress challenges. Fish Shellfish Immunol. 77, 252–263. https://doi.org/10.1016/j.fsi.2018.03.058

Saranya Revathy, K., Umasuthan, N., Lee, Y., Choi, C.Y., Whang, I., Lee, J., 2012. First molluscan theta-class Glutathione S-Transferase: Identification, cloning, characterization and transcriptional analysis post immune challenges. Comp. Biochem. Physiol. - B Biochem. Mol. Biol. 162, 10–23.

https://doi.org/10.1016/j.cbpb.2012.02.004

Sasagawa, S., Nishimura, Y., Okabe, S., Murakami, S., Ashikawa, Y., Yuge, M., Kawaguchi, K., Kawase, R., Okamoto, R., Ito, M., Tanaka, T., 2016. Downregulation of GSTK1 is a common mechanism underlying hypertrophic cardiomyopathy. Front. Pharmacol. 7, 1–13. https://doi.org/10.3389/fphar.2016.00162

Schwede, T., Kopp, J., Guex, N., Peitsch, M.C., 2003. SWISS-MODEL: An automated protein homology-modeling server. Nucleic Acids Res. 31, 3381–3385. https://doi.org/10.1093/nar/gkg520

Segawa, K., Nagata, S., 2015. An Apoptotic "Eat Me" Signal: Phosphatidylserine Exposure. Trends Cell Biol. 25, 639–650. https://doi.org/10.1016/j.tcb.2015.08.003

Shao, Y., Lv, Z., Li, C., Zhang, W., Duan, X., Qiu, Q., Jin, C., Zhao, X., 2017. Molecular cloning and functional characterization of theta class glutathione S-transferase from Apostichopus japonicus. Fish Shellfish Immunol. 63, 31–39. https://doi.org/10.1016/j.fsi.2017.02.004

Sievers, F., Wilm, A., Dineen, D., Gibson, T.J., Karplus, K., Li, W., Lopez, R., McWilliam, H., Remmert, M., Soding, J., Thompson, J.D., Higgins, D.G., 2014. Fast, scalable generation of high-quality protein multiple sequence alignments using Clustal Omega. Mol. Syst. Biol. 7, 539–539. https://doi.org/10.1038/msb.2011.75

Sigrist, C.J.A., De Castro, E., Cerutti, L., Cuche, B.A., Hulo, N., Bridge, A., Bougueleret, L., Xenarios, I., 2013. New and continuing developments at PROSITE. Nucleic Acids Res. 41, 344–347. https://doi.org/10.1093/nar/gks1067

Sims, P.J., Wiedmer, T., 2001. Unraveling the mysteries of phospholipid scrambling.

Thromb. Haemost. 86, 266–275.

Sinton, L.W., Finlay, R.K., Lynch, P.A., 1999. Sunlight inactivation of fecal bacteriophages and bacteria in sewage- polluted seawater. Appl. Environ. Microbiol. 65, 3605–3613. https://doi.org/10.1373/clinchem.2008.112797

Sivagnanam, U., Palanirajan, S.K., Gummadi, S.N., 2017. The role of human phospholipid scramblases in apoptosis: An overview. Biochim. Biophys. Acta - Mol. Cell Res. 1864, 2261–2271. https://doi.org/10.1016/j.bbamcr.2017.08.008

Srinivasan, P.T., Basu, J., 1996. Altered membrane phospholipid organization and erythrophagocytosis in E??-thalassemia. Biochim. Biophys. Acta - Biomembr. 1285, 65–70. https://doi.org/10.1016/S0005-2736(96)00146-0

Talmud, P., Lins, L., Brasseur, R., 1996. Prediction of signal peptide functional properties : a study of the orientation and angle of insertion of yeast invertase mutants and human apolipoprotein B signal peptide variants 9, 317–321.

Tamura, K., Peterson, D., Peterson, N., Stecher, G., Nei, M., Kumar, S., 2011. MEGA5: Molecular evolutionary genetics analysis using maximum likelihood, evolutionary distance, and maximum parsimony methods. Mol. Biol. Evol. 28, 2731–2739. https://doi.org/10.1093/molbev/msr121

Tan, K.L., Board, P.G., 1996. Purification and characterization of a recombinant human Theta-class glutathione transferase (GSTT2-2). Biochem. J. 315, 727–32.

Tort, L., Balasch, J.C., Mackenzie, S., 2003. Fish immune system. A crossroads between innate and adaptive responses. Immunologia 22, 277–286. https://doi.org/10.1016/S1074-7613(04)00084-6

Tufail, Y., Cook, D., Fourgeaud, L., Powers, C.J., Merten, K., Clark, C.L., Hoffman, E., Ngo, A., Sekiguchi, K.J., O'Shea, C.C., Lemke, G., Nimmerjahn, A., 2017. Phosphatidylserine Exposure Controls Viral Innate Immune Responses by

Microglia. Neuron 93, 574–586.e8. https://doi.org/10.1016/j.neuron.2016.12.021

Umasuthan, N., Saranya Revathy, K., Lee, Y., Whang, I., Choi, C.Y., Lee, J., 2012. A novel molluscan sigma-like glutathione S-transferase from Manila clam, Ruditapes philippinarum: Cloning, characterization and transcriptional profiling. Comp. Biochem. Physiol. - C Toxicol. Pharmacol. 155, 539–550. https://doi.org/10.1016/j.cbpc.2012.01.001

Wan, Q., Whang, I., Lee, J., 2008a. Molecular cloning and characterization of three sigma glutathione S-transferases from disk abalone (Haliotis discus discus). Comp. Biochem. Physiol. - B Biochem. Mol. Biol. 151, 257–267. https://doi.org/10.1016/j.cbpb.2008.07.012

Wan, Q., Whang, I., Lee, J., 2008b. Molecular characterization of mu class glutathione-S-transferase from disk abalone (Haliotis discus discus), a potential biomarker of endocrine-disrupting chemicals. Comp. Biochem. Physiol. - B Biochem. Mol. Biol. 150, 187–199. https://doi.org/10.1016/j.cbpb.2008.03.002

Wang, L., Song, X., Song, L., 2017. The oyster immunity. Dev. Comp. Immunol. https://doi.org/10.1016/j.dci.2017.05.025

Wang, Y., Liu, L., Huang, J., Duan, Y., Wang, J., Fu, M., Lin, H., 2016. Response of a Mu-class glutathione S-transferase from black tiger shrimp Penaeus monodon to aflatoxin B1 exposure. Springerplus 5, 825. https://doi.org/10.1186/s40064-016-2381-4

Wei, J., Fan, S., Liu, B., Zhang, B., Su, J., Yu, D., 2017. Transcriptome analysis of the immune reaction of the pearl oyster Pinctada fucata to xenograft from Pinctada maxima. Fish Shellfish Immunol. 67, 331–345. https://doi.org/https://doi.org/10.1016/j.fsi.2017.06.030

Wiedmer, T., Zhao, J., Nanjundan, M., Sims, P.J., 2003. Palmitoylation of

phospholipid scramblase 1 controls its distribution between nucleus and plasma membrane. Biochemistry 42, 1227–1233. https://doi.org/10.1021/bi026679w

Wiedmer, T., Zhou, Q., Kwoh, D.Y., Sims, P.J., 2000. Identification of three new members of the phospholipid scramblase gene family. Biochim. Biophys. Acta - Biomembr. 1467, 244–253. https://doi.org/10.1016/S0005-2736(00)00236-4

Williamson, P., Schlegel, R.A., 2002. Transbilayer phospholipid movement and the clearance of apoptotic cells. Biochim. Biophys. Acta - Mol. Cell Biol. Lipids 1585, 53–63. https://doi.org/10.1016/S1388-1981(02)00324-4

Williamson, P., van den, E.S., Schlegel, R.A., 2001. Phosphatidylserine exposure and phagocytosis of apoptotic cells. Methods Cell Biol. 66, 339–364. https://doi.org/10.1016/S0091-679X(01)66016-3

Yamamoto, K., Zhang, P., Miake, F., Kashige, N., Aso, Y., 2005. Cloning , expression and characterization of theta-class glutathione S -transferase from the silkworm , Bombyx mori 141, 340–346. https://doi.org/10.1016/j.cbpc.2005.04.012

Yang, J., Wei, X., Xu, J., Yang, D., Liu, X., Yang, J., Fang, J., Hu, X., 2012. A sigma-class glutathione S-transferase from Solen grandis that responded to microorganism glycan and organic contaminants. Fish Shellfish Immunol. 32, 1198–1204. https://doi.org/10.1016/j.fsi.2012.03.010

Zhang, L., Qiu, L., Wu, H., Liu, X., You, L., Pei, D., Chen, L., Wang, Q., Zhao, J., 2012. Expression profiles of seven glutathione S-transferase (GST) genes from Venerupis philippinarum exposed to heavy metals and benzo[a]pyrene. Comp. Biochem. Physiol. - C Toxicol. Pharmacol. 155, 517–527. https://doi.org/10.1016/j.cbpc.2012.01.002

Zhou, L., Liu, M., Zhang, J., Chen, H., Dong, L.Q., Liu, F., 2010. Stress – Induced Adiponectin Downregulation 59. https://doi.org/10.2337/db10-0412.

Zhou, Q., Zhao, J., Al Zoghaibi, F., Zhou, A., Wiedmer, T., Silverman, R.H., Sims, P.J., 2000. Transcriptional control of the human plasma membrane phospholipid scramblase 1 gene is mediated by interferon-alpha. Blood 95, 2593–2599.

Zhou, Q., Zhao, J., Stout, J.G., Luhm, R.A., Wiedmer, T., Sims, P.J., 1997. Molecular cloning of human plasma membrane phospholipid scramblase. J. Biol. Chem. 272, 18240–18244.

Zorrilla, I., Arijo, S., Chabrillon, M., Diaz, P., Martinez-Manzanares, E., Balebona, M.C., Moriñigo, M.A., 2003. Vibrio species isolated from diseased farmed sole, Solea senegalensis (Kaup), and evaluation of the potential virulence role of their extracellular products. J. Fish Dis. 26, 103–108. https://doi.org/10.1046/j.1365-2761.2003.00437.x

Zwaal, R.F.., Comfurius, P., Bevers, E.M., 1998. Lipid–protein interactions in blood coagulation. Biochim. Biophys. Acta - Rev. Biomembr. 1376, 433–453. https://doi.org/10.1016/S0304-4157(98)00018-5